Synthesis of Novel Silanes with Functional Head Groups, Surface Modifications, and Characterization

Dissertation

Xiaosong Li

Geboren am 15-02-1979
in Peking, China

Mainz, 2008

Die vorliegende Arbeit wurde in der Zeit von 2005 bis 2008 im Max-Planck-Institut für Polymerforschung in Mainz unter der Anleitung von Herrn Prof. Dr. Wolfgang Knoll und Dr. Ulrich Jonas ausgeführt.

für

Yang Liu, meine Frau

für ihre Liebe

The deeper we look into nature, the more we recognize that it is full of life, and the more profoundly we know that all life is a secret and that we are united with all life that is in nature. Man can no longer live for himself alone. We realize that all life is valuable, and that we are united to all this life.

by Albert Schweitzer

Abstract (English):

The aim of this thesis was to investigate novel techniques to create complex hierarchical chemical patterns on silica or quartz surfaces with micro to nanometer sized features. These modified surfaces were used for functional group-selective surface reactions and site-selective assembly of colloidal particles. For this purpose, novel functionalized triethoxysilanes were synthesized by a modular convergent approach, coupling 3-aminopropyltriethoxysilane and an amino-reactive fragment. After deposition of these silanes as molecular layers onto planar silica and quartz surfaces, the functional groups of these silanes form new functional surfaces (by liquid- or vapor phase silanization) or even lateral functional patterns (by micro-contact printing or photolithography) that allow further chemical reactions at these surfaces.

By the above mentioned modular approach triethoxysilanes with terminal t-butyl-, maleimide-, succinimidyl-, and alkyne moieties were synthesized and surface layers were prepared with them. Kinetic experiments with varying hydrolysis- and incubation times were performed while monitoring changes in hydrophilicity of the functional surfaces and the layer thickness to study the efficiency of silanization process. From these results the hydrolysis conditions could be optimized in order to form uniform and well defined self-assembled surface layers. In model reactions it was shown that their head groups can further bind appropriate molecules due to their characteristic chemical reactivities.

Furthermore, a series of novel photosensitive silanes with 1-(4,5-dimethoxy-2-nitrophenyl)ethanol (CH_3-NVoc) protected -OH, -COOH and -NH_2 functionalities, and 3,5-dimethoxybenzoin (Bzn)-protected -NH_2 group were synthesized and characterized. UV-Vis spectra of both CH_3-NVoc and Bzn silanes were recorded in solution phase and as SAMs on quartz surfaces for different irradiation times at the respective deprotection wavelengths to optimize the photodeprotection step. By irradiation through a gold mask in a UV mask aligner (365 nm) or a crosslinker (254 nm), both CH_3-NVoc and Bzn SAMs could be patterned with functional (photodeprotected / irradiated) and protected

(unirradiated) regions, respectively. The obtained functional pattern could be visualized by site-selective staining with fluorescent probes. Furthermore, site-selective colloid absorption could be observed on the photosensitive silane layer patterns after local deprotection with light.

Abstract (Deutsch):

Synthese neuartiger Silane mit funktionalisierten Kopfgruppen, Oberflächen-modifizierung und Charakterisierung

Ziel dieser Arbeit war die Anwendung und Untersuchung neuer Techniken zur Herstellung komplexer chemischer Strukturen mit Abmessungen im Mikro- bis Nanometerbereich auf Silicium- oder Quarzoberflächen. Diese modifizierten Oberflächen wurden für selektive Oberflächenreaktionen der funktionellen Gruppen sowie Seiten-selektiver Selbstorganisation kolloidaler Partikel benutzt. Zu diesem Zwecke wurden neue funktionalisierte Triethoxysilane konvergent baukastenartig synthetisiert, was durch eine Kupplung von 3-Aminopropyltriethoxysilan mit einem für Amine reaktiven Fragment gelang. Nach Aufbringung dieser Silane als molekulare Schicht auf Quarz- und Silicumoberflächen, bilden die funktionellen Gruppen der Silane neue funktionalisierte Oberflächen (durch Flüssig- oder Gasphasensilanisierung) oder sogar seitliche funktionalisierte Strukturen (durch Mikrokontanktdrucken oder Photolithographie), was weitere chemische Reaktionen an diesen Oberflächen ermöglichen.

Das Baukastenprinzip wurde verwendet um Triethoxysilane mit terminalen t-Butyl-, Maleinimid-, Succinimidyl- und Alkinreste zu synthetisieren und Oberflächenschichten mit ihnen herzustellen. Um die Effizienz des Silanisierungsprozesses zu bestimmen wurden Kinetik-Experimente mit unterschiedlicher Hydrolyse- und Inkubationszeit durch Messung der Schichtdicke und der Hydrophilie der funktionalisierten Oberflächen durchgeführt. Mit den Ergebnissen konnten optimierte Hydrolysebedingungen geschaffen werden, um einheitliche und wohl definierte selbstangeordnete Oberflächenschichten zu bilden. In Modellversuchen wurde gezeigt, dass ihre Kopfgruppen durch ihre charakteristische chemische Reaktivität geeignete Moleküle binden können.

Weiterhin wurde eine Reihe neuer photosensitiver Silane mit 1-(4,5-dimethoxy-2-nitrophenyl)ethanol geschützten -OH, -COOH und -NH$_2$ – Gruppen sowie mit 3,5-dimethoxybenzoin (Bzn)-geschützten –NH$_2$-Gruppen synthetisiert und charakterisiert. Die UV-VIS Spektren der CH$_3$-NVoc- und Bzn-geschützten Silane wurde in Lösung und als SAMs auf einer Quartzoberfläche bei unterschiedlichen Bestrahlungsdauern und der jeweiligen Deprotektierungs-Wellenlänge aufgenommen, um die photoinduzierte Entschützung zu optimieren. Durch die Bestrahlung durch eine Goldmaske in einem UV Gerät (365 nm) oder einem Vernetzungsapparat (254 nm) konnten sowohl auf den CH$_3$-NVoc- als auch auf den Bzn- SAMs Muster mit funktionalisierten (photodeprotektierten/ bestrahlten) und geschützten (unbestrahlten) Regionen gebildet werden. Die erhaltenen funktionalisierten Muster konnten durch Seiten-selektive Anfärbung mit Fluoreszenzmarkenr visualisiert werden. Weiterhin konnte nach lokaler Bestrahlung mit Licht colloidale Seiten-selektive Absorption auf der photosensitiven Silanoberfläche beobachtet werden.

Contents

III

Abbreviations and Acronyms

2-D	Two dimensional
3-D	Three dimensional
AFM	Atomic force microscopy
APTE	Aminopropyltriethoxysilane
Ar	Argon
t-Bu	tert-Butyl
Bzn	Benzoin
CCD	Charged-coupled device
CH_2Cl_2	Dichloromethane
DCC	Dicyclohexylcarbodiimide
DIC	Differential interference contrast
DNA	Deoxynucleic acid
DMAP	4-Dimethylaminopyridine
EPR	Electron paramagnetic resonance
ESR	Electron spin resonance
Et	Ethyl
EtOH	Ethanol
HMDS	Hexamethyldisilazane
MBAAm	Methylenebisacrylamide
Mili-Q	Deionised water
n-BuLi	n-Butyl lithium
NIPAAm	N-isopropylacrylamide
NMR	Nuclear magnetic resonance
NVoc	Nitroveratryloxycarbonyl
OTE	Octadecyltriethoxysilane
PDMS	Polymethyldisiloxane
Piranha	Solution of conc. $H_2SO_4/30\% H_2O_2$ (7:3 v/v)

PMMA	Polymethylmethacrylate
PS	Polystyrene
PTFE	Polytetrafloroethylene
Rf	Retention factor
RMS	Root mean square
RNA	Ribonucleic acid
SA	Sodium acrylate
SAMs	Self-assembled monolayers
THF	Tetrahydrofuran
TLC	Thin layer chromatography

Chapter 1

Introduction

The first concepts in nanotechnology was in "There's plenty of room at the bottom," a talk given by physicist Richard Feynman at an American Physical Society meeting in 1959. Feynman described a process by which the ability to manipulate individual atoms and molecules might be developed, using one set of precise tools to build and operate another proportionally smaller set, so on down to the needed scale. Then in 1974, Professor Norio Taniguchi from Tokyo Science University first defined the term "Nano-technology" as: "Nano-technology consists of the processing of separation, consolidation, and deformation of materials by one atom or by one molecule." [Taniguchi 1974]

Two main approaches are used in nanotechnology. In the "top-down" approach, nano-objects are constructed from larger entities without atomic-level control. It is based on miniaturization of macroscale components down to nanometer level. In the last decades great improvements have already been achieved in this aspect (e.g. lithography

patterning of surfaces with the photoresist technology). However, top down techniques usually suffer from limitation in the degree of miniaturization, which in most cases lies above 100nm (e.g. the minimum feature size in photolithography is limited by the diffraction limit of the irradiation wavelength). [Xia 1998]

In the "bottom-up" approach, materials and devices are built from molecular components which assemble themselves chemically by principles of molecular recognition. Molecular assemblies on the substrate surface, called self-assembled monolayers (SAMs), form the basis for these interactions by defining the chemistry on the surface. In a so-called self-organization process, micro- to nanoscaled objects can spontaneously organized and aggregate into stable, well-defined structures on SAMs, due to favorable interactions between the chemical groups located at their outmost surface layer. [Jonas 2002a]

The site-selective adsorption of molecules and mesoscopic objects at predefined positions on solid surfaces is a key fabrication step and a major challenge in many applications, such as multifunctional biosensors and novel electronic, mechanical, and photonic devices [del Campo 2005]. In this context, this thesis aims at the development of novel surface functionalization procedures as a basis for further surface reactions or the assembly of nano-scaled objects onto planar surfaces, which have been modified with specific chemical functional patterns of silane layers. The functional patterns, that define the site-selective adsorption, were obtained by a photolithographic process using photo-reactive silane layers or micro-contact printing with PDMS stamps.
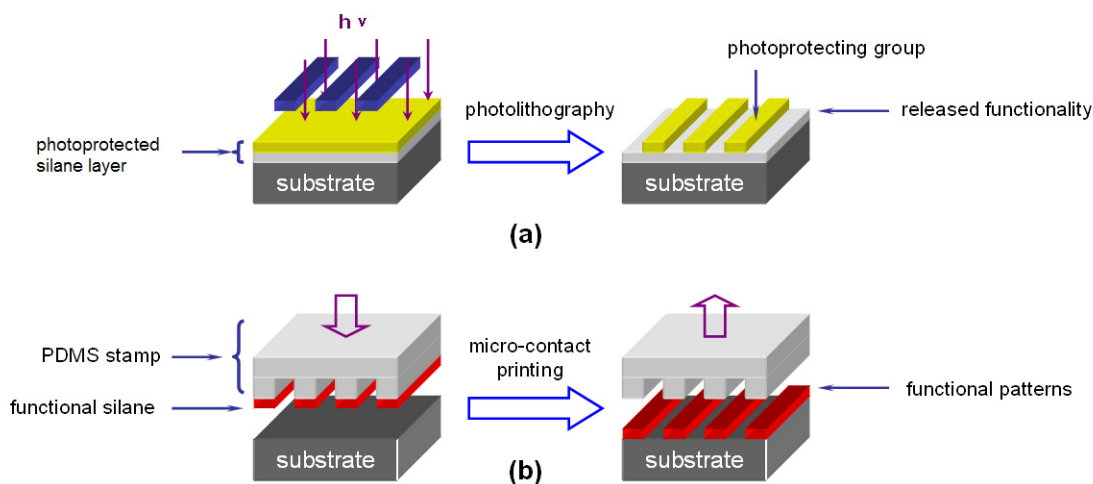
Figure 1.1: (a) Schematic illustration of a silane layer on a silica substrate bearing photoprotecting groups. Upon irradiation through a mask, a photochemical reaction is induced on the surface, which liberates new functional groups on the photoactivated regions. (b) Schematic illustration of the micro-contact printing process with a PDMS stamp soaked with a functional silane, which forms after the stamping the new functional patterns on the silica substrate surface.

The characteristic features of silica surfaces, their surface modification and patterning are viewed in **Chapter 2**. Special emphasis is placed on the alkoxysilane chemistry, due to the process of hydrolysis and condensation in solution and adsorption onto the surface. The photolithographic technique and micro-contact printing are presented.

After introducing the main characterization techniques used for this thesis in **Chapter 3**, modifications of different functionalized surfaces and the corresponding surface chemical reactions are described in **Chapter 4**. There, silanization techniques are introduced. Hydrolysis and condensation mechanisms in solution are investigated by ^{1}H NMR, AFM, and ellipsometry. Finally a modular synthesis approach and details are presented.

Synthesis approaches for novel photoprotecting silanes bearing 4,5-dimethoxy-2-

3

nitrophenyl and 3',5'-dimethoxybenzoinyl photoprotecting groups for chemical patterning are introduced in **Chapter 5**. For these silanes UV-Vis measurements both in solution phase and solid state are carried out for optimizing the irradiation time for silane activations. Colloidal assembly and fluorescent dye labeling are performed on the patterned surfaces modified with these molecules by subsequent irradiation.

Finally, **Chapter 6** presents the experimental details of the modifications of the substrate surfaces, including solution and vapor phase silanization, micro-contact printing, and photolithography. Details for the techniques of fluorescence labeling, colloidal assembly, and synthesis details are also reported.

Chapter 2

Principles of Patterned Silane Layers on Substrate Surfaces

Self-assembly is the fundamental concept which generates structural organizations on all scales, from molecules even to galaxies. In modern technology, the application of self-assembly in the bottom up approach is often based on the formation of self-assembled monolayers (SAMs) of molecules which adsorb to a surface and aggregate into a dense monolayer, often they are covalently bound to the substrate surfaces. The newly formed functional surfaces provide the possibilities to manufacture and attach mesoscale objects onto these surfaces, based on attractive interactions between the outmost surface molecules on the substrate and the objects. This approach potentially provides a new fabrication method in the quest for miniaturization, which may lead to smaller and lighter devices especially in microelectronics, optics, and sensors.

Rather than having to use a technique such as chemical vapor deposition or molecular beam epitaxy to add molecules to a surface (often with poor control over the

thickness of the molecular layer), self-assembled monolayers can be prepared simply by adding a solution of the desired molecule onto the substrate surface and washing off the excess. This simple process makes SAMs inherently manufacturable and technologically attractive for building superlattices and for surface engineering.

SAMs can range from disordered to highly ordered and oriented layer structures and can incorporate a wide range of groups both in the alkyl chain and at the terminal functionality. Therefore, a variety of surfaces with specific interactions can be produced with fine chemical control. Due to their dense and stable structure, SAMs provide an ideal platform in the bottom up approach.

(a)   **(b)**   **(c)**
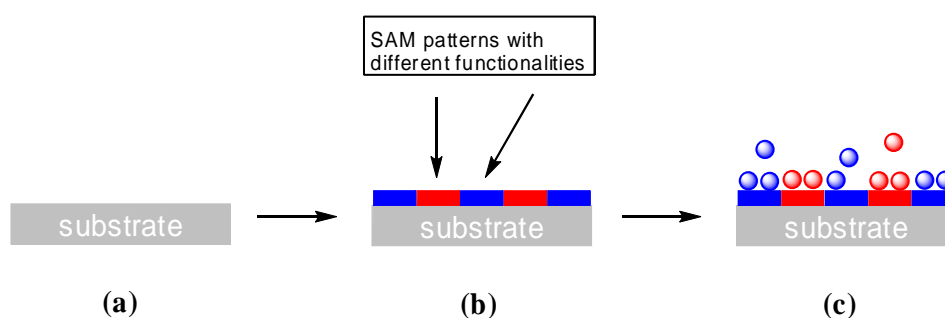
Figure 2.1: (a) A substrate to be modified by SAM; (b) SAM on the substrate surface with lateral functionalized patterns; (c) formation of a complex structure via self-assembly due to different attractive forces between the surface and the mesoscale objects.

When SAMs are combined with photolithography or micro-contact printing as "top-down" technique, lateral functionalized patterns onto the planar substrate with micro to nanometer dimensions can be created. These patterns can define the spatial location of attracted corresponding objects (Figure 2.1). For instance, in the 1990s Hammond and co-workers managed to self-assemble polyelectrolytes on laterally modified thiol substrates on gold whereas Vossmeyer and co-workers self-assembled gold nano-crystals on patterned silicon oxide surfaces [Chen 2000, Vossmeyer 1998]. Even though Hammond was using a metal and Vossmeyer with an oxide surface, both groups had modified their patterned surfaces with self-assembled monolayers (SAMs). Patterns of oxidized SAMs (or random copolymers) on silica are also reported being produced by

using extreme ultraviolet interferometric lithography [Gates 2005]. Most often SAMs are monolayers of either thiol or disulfide groups on gold or silane layers on silicon oxide surfaces that can chemically modify the surface of the substrate.

Other oxide surfaces, such as Al_2O_3, ZrO_2, SnO_2, TiO_2 or NbO_2, are generally modified with carboxylic acids or phosphonic acid, but some times also with chloro- or alkoxy silanes. Since precious metal surfaces, such as gold, may be mainly of academic interest and somewhat limited to a restricted number of technical applications this dissertation will only deal with silanes on silicon oxide surfaces, since it is more relevant for a wider range of potential applications (like many inorganic oxidic surfaces and oxidized polymer surfaces, e.g.).

2.1 Introduction to Silanes

Modifications of hydrophilic substrates by grafting organic chains with specific molecules are of great importance for both science and industry. Organosilanes with particular functional groups are used extensively for generating organic monolayers on silica substrates. They provide a wide field of applications from biosensors for antibody immobilization to lubricants.

The word "silane" comes from the combination of "silicon + methane", the silicon analogue of methane. More generally, a silane is any analogue of organic compounds (in particular hydrocarbons) with the silicon centre replacing a carbon atom. The surface-active silane molecule, which could form SAMs on silicon oxide surfaces spontaneously, should have an anchor group, suitable for strong interactions or even chemical bond with the substrate surface, a mesogenic or spacer group responsible for the two-dimensional packing by favourable lateral interactions between adjacent SAM molecules, and a head group determining the properties of the newly formed surface.

Such silanes that form the monolayers possess either a chloro- or alkoxy silane

anchor group that can interact with the silicon surface via physisorption or chemisorption. Alkoxy silanes are often preferred since they are less reactive and therefore much easier to handle under ambient laboratory conditions. In addition, they can be purified by passivating the silica gel column first with hydrophobic silane such as hexamethlydisilazane (HMDS). The very high reactivity of the chlorosilanes makes it difficult to handle them under regular laboratory conditions (e.g. H_2O in air). Furthermore, chlorosilanes produce HCl during hydrolysis which auto-catalyses the hydrolysis reaction and silanol condensation. An alkyl spacer separates then the anchor group from the functional head groups, which define the surface properties of the substrate and control the interaction with complementary objects.
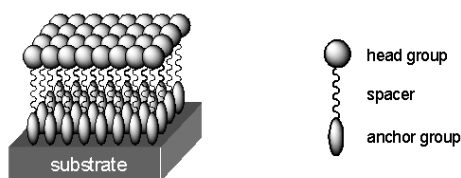
Figure 2.2: Cartoon of a surface-active molecule and the profile of a fragment of a self-assembled mono-layer.

Monolayers with a thickness of up to 10nm possess only molecular dimensions and they are therefore also referred to ultra-thin films. Depending on their functionalities, these films can substantially alter the properties of the surface, such as friction, adhesion, chemical resistance, wettability, etc. [Xia 2000].

2.2 Property of Silica Substrate Surfaces

Silicon dioxide (SiO_2) is a hard inorganic solid where Si atoms in the lattice are sp^3-hybridised and bound to four oxygen atoms in a 3-dimensional tetrahedral network. Because of the interaction between the free p-electron pairs of the oxygen and the empty d-orbitals of silicon, the bonding energy of the Si-O bond in general is very high. When silica and silicon wafers with oxide layer are immersed into water, they are known to

acquire a negative surface charge, primarily through the dissociation of terminal silanol groups (pK_A of Si-OH is ca. 7.5). Figure 2.3 shows the lattice of silicon dioxide.

graphic by
Ravi Laxman

Oxygen
Silicon

(a)　　　　　　　　(b)

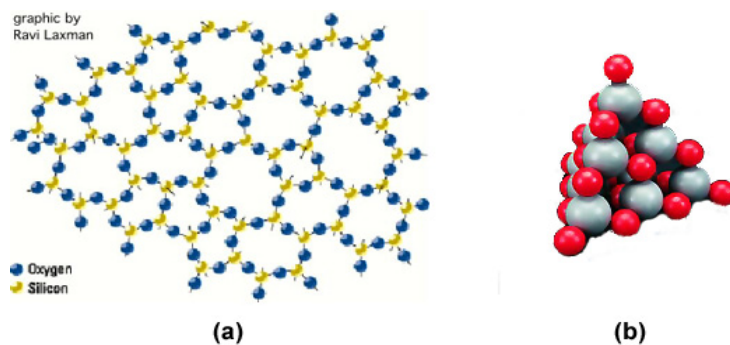**Figure 2.4** Silicon dioxide structure: (a) disordered surface structure; (b) bulk crystal lattice (white: silicon, red: oxygen) [Dobkin web resource].

Upon reaction with a strong acid such as Piranha solution (which is a mixture of conc. H_2SO_4 / 30%H_2O_2, 7:3 v/v), coordinated SiO_2 surface bonds can be broken, thus generating more "reactive" surfaces with hydroxyl groups. The concentration of Si-OH group on a pre-cleaned silica substrate surface is reported to be $\sim 5 \times 10^{14}$ groups / cm^2 [Zhuravlev 1987]. The high polarity of the hydroxyl groups gives the reactivity to the surface with the anchor groups of silanes.

2.3 Silanization of Silica Substrate Surfaces

Surface modification can occur by physisorption, due to attractive forces between the surface and the organo silane, or they can be chemisorbed via formation of covalent bonds between the silane and the silanol groups on the surface (Figure 2.5). Chemisorbed layers are more versatile and stable due to the stronger interaction with the surface compared to those with the physisorbed films [Fadeev 1999].

The first step in the silanization process is the hydrolysis of the alkoxysilanes to give hydroxyl silanes that can then interact with the silicon dioxide surface and further

condensate to form covalent bonds. Another possibility is that the hydroxyl silanes first condensate and then adsorb onto the surface when the anchor groups bear more than one functional group, such as di- or tri-functionalised alkoxysilanes. Condensation of these groups and the formation of a pre-polymer leads to aggregates of polymerised silanes which, when adsorbed onto the surface, may form an inhomogeneous layer. Extended silane condensation (forming large polymers) prior to adsorption to the surface has to be prevented so that a homogeneous coating can form via surface diffusion of physisorbed silanes [Ishida 1984].
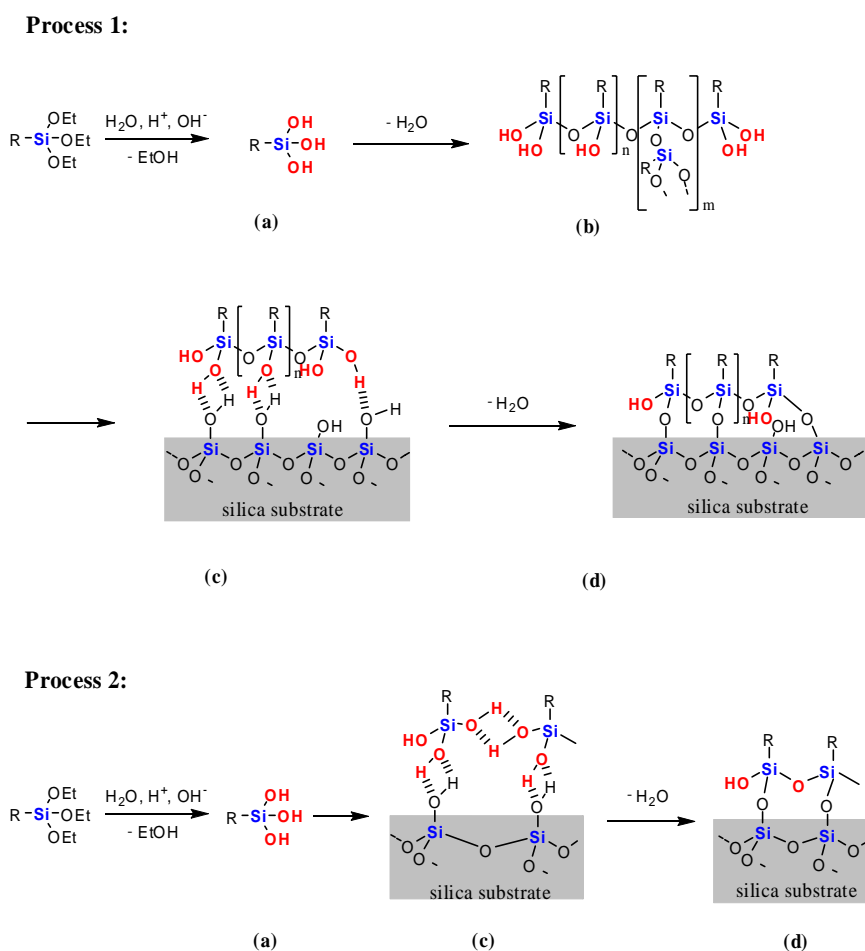
Process 1:

Process 2:

Figure 2.5: (a) Hydrolysis of the alkoxy silane in solution; (b) pre-polymeric condensation in solution; (c) physisorption of hydrolyzed alkoxy silane or polymerized silane aggregates onto silica substrate surface; (d) condensation of a silane with the surface and formation of a silane layer. Process 1 and 2 are competing with each other.

2.4 Micro-contact Printing

Microcontact printing uses a polydimethylsiloxane (PDMS) stamp to deposit molecules on surfaces. The stamp is first "inked" with a solution of molecules, often proteins or thiols that can either coat the stamp or, in the case of small molecules, are absorbed onto the PDMS in the form of a solid solution. The stamp is dried and pressed onto the surface to be patterned. The soft PDMS stamp makes conformal contact with the surface and molecules are transferred directly from the stamp to the surface in the space of a short time scale, usually a few seconds.

The stamps for microcontact printing are made using topgraphically patterned substrates, the so-called masters. This substrates form a mould in which liquid PDMS is crosslinked. On demoulding, a flexible transparent stamp is obtained, with structures that can be as small as 100nm and in extreme cases even below.
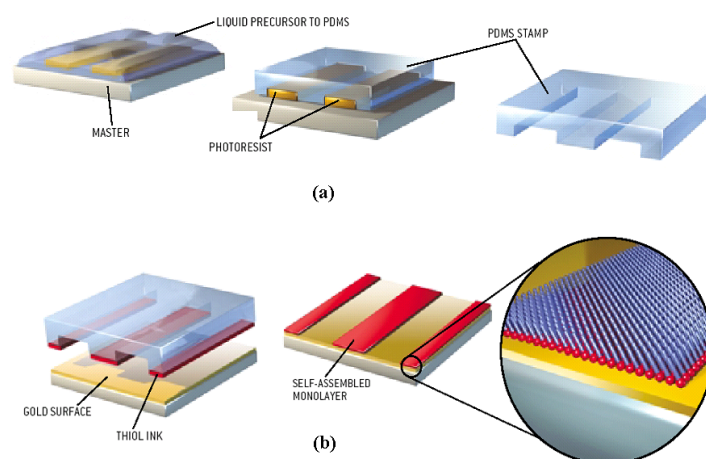

Figure 2.6: (a) Fabrication of a PDMS stamp by the polymerization of PDMS on a patterned master; (b) micro-contact print of thiol molecules on a gold surface and the formation of a patterned thiol SAM [Whitesides 2001].

Microcontact printing is a very powerful method for surface structuring. Patterns

can be made on many different materials and on flat or curved surfaces. Repeated printing using different stamps can be used to make complex surface patterns of more than one kind of molecule. Besides molecules, nanoscale objects such as colloidal particles can also be patterned using microcontact printing.

In this thesis, microcontact printing is used to pattern silica substrate surfaces with silanes: a stamp is used to apply a silane to certain areas of a silica surface. Additionally, after the transfer is complete, the silica substrate may be briefly dipped into a solution of a second silane, which fills the remaining bare areas. If suitable functional silanes are chosen, marked contrasts in properties such as hydrophilicity or protein binding may be obtained.

2.5 Photolithography

Photolithography has been the major tool for micro-fabrication in the semiconductor industry since the 1950s. Its basis is in an optical projection system in which the image of a reticle is reduced and projected onto a thin film of photoresist that is spin-coated on a wafer, through a high numerical aperture lens system. Contact lithography is the most common technique used to produce high resolution patterns. It refers to the fact that the radiation mask is placed right on top of the photoresist wafer to be patterned, so the mask features are reproduced without size reduction and need for a complex optical system. The irradiated parts of the resist undergo a chemical transformation and thus can be removed in an alkaline developer solution in the case of a positive-tone resist.
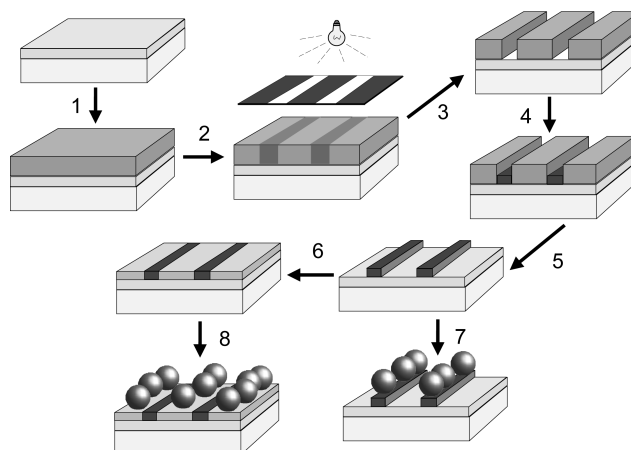
Figure 2.7: General outline of the fabrication process for patterned silane layers and the colloid assembly method: (1) spincoating of the photoresist film on a silicon substrate with oxide layer; (2) irradiation of resist coat through a mask; (3) developing of the exposed photoresist to generate the Si-OH pattern; (4) deposition of a silane monolayer at the free silica surface; (5) removal of photoresist coat leading to a silane A / Si-OH pattern; (6) deposition of a second silane monolayer at the Si-OH regions leading to an alternating silane A / silane B pattern; (7) selective colloid assembly on the silane A / Si-OH pattern; (8) selective colloid assembly on the silane A / silane B pattern [Jonas 2002b].

The first step in a general photolithography process (Figure 2.7) is to spin on the photoresist onto the silicon substrates, which have been cleaned in a Piranha solution in advance. They are then irradiated through a gold mask with UV light for an appropriate time. The irradiated areas of the resist are then washed off in a developer solution and rinsed gently with Milli-Q water. It is possible to modify these areas with the desired alkoxysilanes and then remove the remaining photoresist afterwards. The remaining free Si-OH surface can then subsequently react with another silane, bearing, for example a different charge or polarity. As a final step complementary functionalized objects, such as colloidal particles, can be assembled under conditions that allow specific interaction between the silane surface and the colloid.

In this case the photoresist is called a positive "tone" (+) resist whereas a negative "tone" (-) photoresist can also be used to remove the non-irradiated parts of the photoresist after irradiation. Negative photoresists form a 3D crosslinked polymer network upon irradiation that is not soluble anymore, hence the non-irradiated parts are

removed. The most common (+) photoresist system is the diazonaphthoquinon-Novolak-sytem, which is comprised of 3 major components; namely naphthoquinone as the photoactive component, a Novolak resin and a developer. The resin is a condensation product of phenol and/or cresol and formaldehyde that does not change upon irradiation. However, the diazonaphthoquinon (DNQ) is transformed into an indene carbonic acid during irradiation via a Wolff rearrangement and can be washed off afterwards with an aqueous basic developer.

Photolithographic methods using electromagnetic radiation such as UV can usually create the feature sizes of around 90nm. To go even further down with the resolution is a goal that scientists are very eager to achieve. Energetic particles, (i.e. electrons and ions) are an attractive means since their de Broglie wavelengths (which depend on the velocity of the electrons) are less than 0.1nm, which minimizes the effects of diffraction that limit many photolithographic processes [Xia 1999].

Comparing to the conventional photolithography, this thesis will present an alternative technique, termed direct monolayer lithography, that requires less process steps and makes use of a silane monolayer that carries photo-reactive groups as the protecting groups, which forms the lateral functional patterns on the surface by photo-deprotection process when the substrate are irradiated through a mask.

Chapter 3

Principles of Characterizations

3.1 Contact Angle Measurement

Contact angle measurement of a liquid droplet (usually water) on a planar substrate surface is a popular and uncomplicated means to characterise the hydrophobicity or hydrophilicity of this surface [Ulman 1991]. The shape of a droplet resting on a surface depends on the material properties of the liquid, the air (or vapour) around it, and the surface on which it is placed. The measurement is performed at the base of the droplet, in contact with the surface. Figure 3.1 illustrates such contact angle measurement.
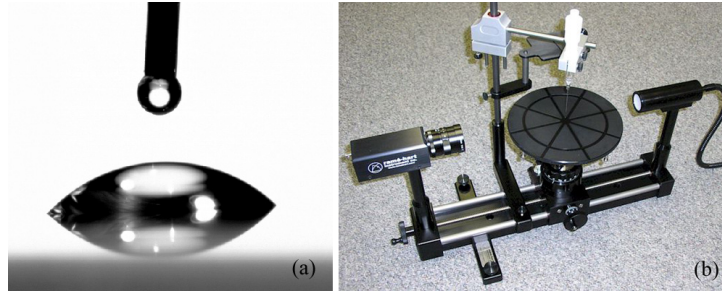
Figure 3.1: (a) Image from a video contact angle device: water drop on glass; (b) Image of Ramé-Hart contact angle goniometer.

According to the interfacial energy given by Young's equation (3.1), the contact angle can be traced to the balance of forces at the liquid-solid boundary, which is due to the interfacial and surface energies of the 3-phase-system (air-liquid-substrate).

$$\gamma_{sg} = \gamma_{ls} + \gamma_{gl} \cdot \cos\theta \tag{3.1}$$

Where γ_{sg}, γ_{ls}, and γ_{gl} are the interfacial energies between the solid and the gas, the liquid and the solid, and the gas and the liquid, respectively. And θ is the static contact angle between the droplet side profile and the substrate surface. Normally, the interfacial energies are described as forces per unit length and from the one-dimensional force balance along the x axis (refer to Figure 3.2), Young's equation is derived [Tadmor 2004].
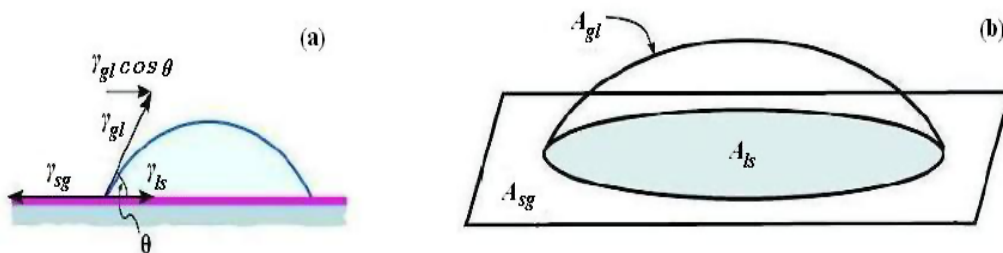
Figure 3.2: (a) Two-dimensional representation of a droplet on a substrate surface describing interfacial energies as forces balanced along the x axis which results in equation (3.1). Here, the contact line is viewed as a point object for which the force balance is provided. (b) There-dimensional representation of a droplet on a substrate surface. The surface tensions can be viewed as surface energies per area. The Young's equation can be obtained from surface minimization.

From Equation (3.1) it appears that there is only one thermodynamic contact angle (θ). However, our daily experience shows that droplets can show a series of contact angles ranging from the so-called advancing contact angle (θ_A) with the water droplet spreading on the surface, up to the so-called receding contact angle (θ_R) with the water droplet retracting from the surface, which are the maximum and minimum values the contact angle can obtain. This difference between advancing and receding contact angles is referred to as contact angle hysteresis. Surface imperfections, such as contamination, can lead to contact angle hysteresis and removing of such anomalies can greatly reduce the hysteresis. Consequently, most descriptions assume that the contact angle hysteresis is caused by surface flaws. However, even molecularly smooth and homogeneous surfaces can also show hysteresis. Anyway, contact angle hysteresis should be considered as a source of information on the behavior of liquid-solid interfaces: large hysteresis leads to pinning of a droplet and lower tendency for dewetting, small hysteresis leads to effective dewetting [Oener 2000].

The contact angle is very sensitive to the chemical composition and the values can range from about 0° (very hydrophilic, e.g. pure SiO_2 surface) to 120° (very hydrophobic, e.g. methylene head groups on self-assembled monolayers). Thus the contact angle measurement is well suited for monitoring the deposition of silanes onto the silica surface [Boos 2004].

3.2 Atomic Force Microscopy

The atomic force microscope (AFM), sometimes also called scanning force microscope (SFM), was invented by Gerd Binig, Calvin Quate and Christoph Gerber in 1986. With the AFM both, conductor as well as insulators can be imaged at molecular resolution. Thomas Albrecht and Calvin Quate were the first who imaged an insulator, boron nitride, and could see the periodic structure at atomic resolution. AFM can be operated in vacuum, air or liquids including water. This opened a wide range of applications for this technique at the molecular or atomic scale.

The AFM measures the surface topography of a sample with a sharp stylus, called a "tip". The tip is a few microns long and located at the end of a cantilever that is 100 to 200μm long. It is usually made of Si or Si_3N_4 and is capable of measuring forces between 10^{-8} to 10^{-6} N. Forces between the tip and the sample surface cause the cantilever to bend and deflect [Ulman 1991].

A laser beam is reflected from the backside of the cantilever and is focused on a photodiode sensor. When the cantilever is deflected, the position of the laser spot on the detector changes. The force acting on the cantilever is proportional to the deflection. Therefore by adjusting a force setpoint, the force between tip and sample is also adjusted. This results in a signal, which is recorded in a computer (Figure 3.3). The feedback of the computer controls the z translator (called piezoelectric scanner) to adjust the tip or sample up or down in order to restore the tip to its original deflection. The sample is scanned in the x, y-plane and the computer stores the vertical position of the z translator at each point and assembles the 3-D image.
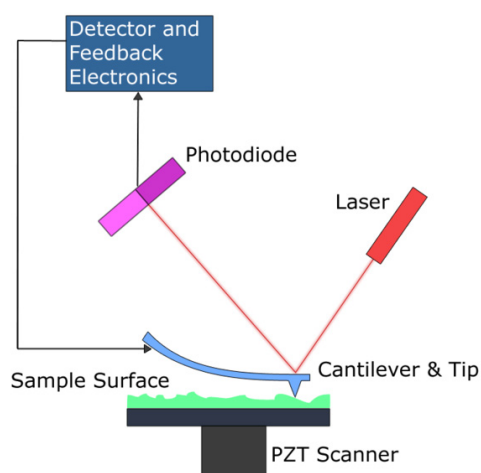

Figure 3.3: The sample is placed on the piezoelectric scanner, which can move in xyz. The photo-detector measures the vertical deflection of the cantilever with a resolution smaller than 10Å. The feedback of the computer controls the vertical position with respect to the corresponding (x, y) coordinates, which is translated into a 3-D map of the measured surface property.

Three fundamental operating techniques are usually performed with AFM, namely contact mode, non-contact mode, and intermittent contact mode (also referred to as tapping mode). In the contact mode, where the tip makes soft "physical contact" with the sample, the tip is attached to the end of a cantilever with a low spring constant (lower than the effective spring constant holding the atoms of the sample together). The contact force causes the cantilever to bend to accommodate changes in topography. Usually the cantilever is in strong contact with the sample surface and the force between the cantilever and the sample is repulsive. In the non-contact mode, the cantilever is held on the order of tens to hundreds of angstroms from the sample surface. Due to the long-range van der Waals interactions the force between the cantilever and the sample is attractive. In the tapping mode, the tip is periodically oscillated over the sample and changes in the oscillation frequency or amplitude by interaction of the tip with surface features are detected (Figure 3.4).
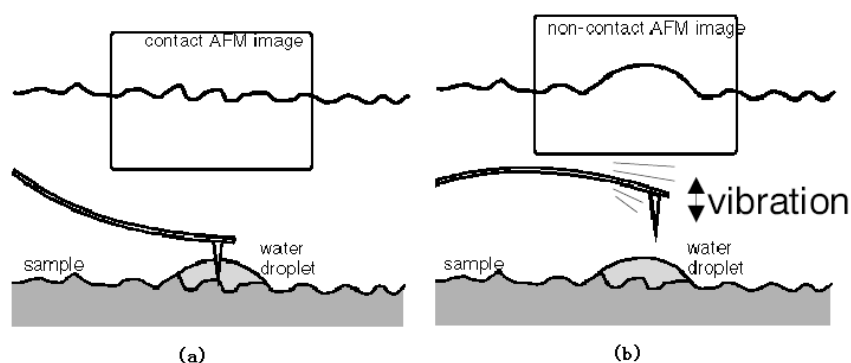
Figure 3.4: (a) Illustration of contact mode; (b) illustration of non-contact mode [Howland 1996].

Once the AFM has detected the cantilever deflection, it can generate the topographic data set by operating in two modes: constant height mode and constant force mode. In constant height mode, the spatial variation of the cantilever deflection can be used directly to generate the topographic data set since the height of the scanner is fixed when it scans. In constant force mode, the deflection of the cantilever can be used as an input to a feedback circuit that moves the scanner up and down in z direction, responding to the topography by keeping the cantilever deflection constant. By doing so the image is generated from the scanner's motion. With the cantilever deflection being held constant,

the total force applied to the sample is constant [Boos 2004].

Contact mode is usually applied to "hard" materials where the rather large force won't damage the surface. For "soft" materials, such as colloids, non-contact or inter-mittent contact mode is applied to avoid the damage of the samples.

3.3 Ellipsometry

Ellipsometry measures the change of polarization upon reflection or transmission. Typically, ellipsometry is done only in the reflection setup. The exact nature of the polarization change is determined by the sample's properties (thickness, complex refractive index or dielectric function tensor). Although optical techniques are inherently diffraction limited, ellipsometry exploits phase information and the polarization state of light, and can achieve angstrom resolution. In its simplest form, the technique is applicable to thin films with thickness less than a nanometer to several micrometers. The sample must be composed of a small number of discrete, well-defined layers that are optically homogeneous, isotropic, and non-absorbing.

Experimental Setup

Electromagnetic radiation is emitted by a light source and linearly polarized by a polarizer, it can pass an optional compensator (retarder, quarter wave plate), and falls onto the sample. After reflection the radiation passes a compensator (optional) and a second polarizer, which is called analyzer, and falls into the detector. Instead of the compensators some ellipsometers use a phase-modulator in the path of the incident light beam (Figure 3.5). Ellipsometry is a specular optical technique (the angle of incidence equals the angle of reflection). The incident and the reflected beam span the plane of incidence. Light, which is polarized parallel or perpendicular to the plane of incidence, is called p or s polarized, respectively.
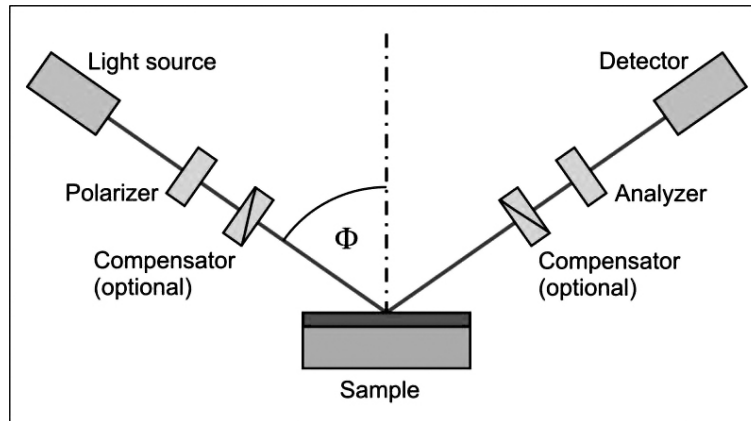
Figure 3.5 Schematic setup of an ellipsometry experiment.

Data Acquisition

Standard ellipsometry measures two of the four Stokes parameters, which are conventionally denoted by Ψ and Δ. The polarization state of the light incident upon the sample may be decomposed into an *s* and a *p* component (the *s* component is oscillating perpendicular to the plane of incidence and parallel to the sample surface, and the *p* component is oscillating parallel to the plane of incidence). The amplitudes of the *s* and *p* components, after reflection and normalized to their initial value, are denoted by r_s and r_p, respectively. Ellipsometry measures the ratio of r_s and r_p, which is described by the fundamental equation of ellipsometry:

$$\rho = r_p / r_s = \tan (\Psi)\, e^{i\Delta} \tag{3.2}$$

Thus, $\tan\Psi$ is the amplitude ratio upon reflection, and Δ is the phase shift (difference). Since ellipsometry is measuring the ratio (or difference) of two values (rather than the absolute value of either), it is very robust, accurate, and reproducible. For instance, it is relatively insensitive to scatter and fluctuations, and requires no standard sample or reference beam.

21

Data Analysis

Ellipsometry is an indirect method, i.e. in general the measured Ψ and Δ cannot be converted directly into the optical constants of the sample. Normally, a model analysis must be performed. Direct inversion of Ψ and Δ is only possible in very simple cases of isotropic, homogeneous and infinitely thick films. In all other cases a layer model must be established, which considers the optical constants (refractive index or dielectric function tensor) and thickness parameters of all individual layers of the sample including the correct layer sequence. Using an iterative procedure (least-squares minimization) unknown optical constants and/or thickness parameters are varied, and Ψ and Δ values are calculated using the Fresnel equations. The calculated Ψ and Δ values, which match the experimental data best, provide the optical constants and thickness parameters of the sample.

3.4 UV-Vis Spectroscopy

Ultraviolet-visible spectroscopy involves the absorption of ultraviolet or visible light by a molecule causing the promotion of an electron from a ground electronic state to an excited electronic state. The absorption spectra, which are due to the light absorption, are then measured. The spectra range from 200 to 800nm, where the quantitative absorption is defined by Lambert-Beer's law (3.5), which is based on a beam of light passing through a solution of known thickness b and concentration c of the adsorbing species depicted by the transmittance T

$$T = P/P_0 \, , \tag{3.3}$$

where P_0 is the intensity of the incident beam and P the resulting intensity of the beam after absorption by the solution. Upon transmittance the photons interact with the molecules in solution. The absorbance A of the solution is then defined as

$A = - \log_{10} T = \log (P_0 /P)$. $\hspace{8cm}$ (3.4)

Absorbance is directly proportional to the path length b and concentration c of the solution, which can be described by Lambert-Beer's law:

$A = \varepsilon bc$ $\hspace{10cm}$ (3.5)

where ε is a proportionality constant called "molar absorptivity" with unit of $Lmol^{-1}$ cm^{-1}. The linear relationship in Beer's law only holds for dilute solutions. With higher concentrated solutions (>0.01M) the distance between neighbouring species is reduced leading to interactions that change the ability to absorb at a given wavelength, which causes deviation from the linear relationship between absorbance and concentration.

3.5 Confocal Microscopy

Confocal microscopy is an imaging technique used to increase micrograph contrast and/or to reconstruct three-dimensional images by using a spatial pinhole to eliminate out-of-focus light or flare in specimens that are thicker than the focal plane. In confocal microscopy, a laser beam is used as the excitation light. After reflecting on a dichroic mirror the laser hits two xy galvanometric scanners; these mirrors scan the laser across the sample. Dye in the sample fluoresces and the emitted light gets descanned by the same scanners that are used to scan the excitation light from the laser. The emitted light is through the dichroic mirror and is focused onto the pinhole plane. The light that passes through the pinhole is measured by a detector, i.e. a photomultiplier tube.

The confocal aperture (pinhole) is placed in front of the photodetector, such that the fluorescent light from points on the sample that are not within the focal plane will be obstructed by the pinhole. In this way, out-of-focus information (both above and below the focal plane) is greatly reduced (Fig.3.6). Light excited in the sample in the focal point of the lens is precisely imaged in the opening of the detector pinhole. In this way, a single

point anywhere in a 3D sample can be accurately imaged with a resolution of >1μm. By scanning this point laterally through the focal plane, a 2D image of a slice parallel to the sample surface can be made. As the laser scans across the sample with the help of mirrors, the analog light signal, detected by the photomultiplier, is converted into a digital signal, contributing to a computer monitor attached to the confocal microscope.
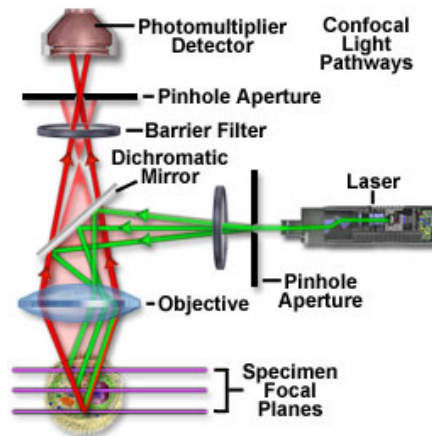
Figure 3.6: Confocal principle: laser light (green) reflects on dichroic mirror and is emitted at the focal point in the focal plane (red light). The emitted light is then passed through the dichroic mirror and focused onto the pinhole by a microscope objective. Light emitted out-of-focus (faint red light) is not focused on the pinhole [Olympus Web Resouce].

The advantage of using a confocal microscope is that it is really efficient at rejecting out of focus fluorescent light. The best horizontal resolution of a confocal micro-scope is about 0.2 microns, and the best vertical resolution is about 0.5 microns. [Wilhelm 1998]

3.6 Optical Microscopy

Optical Microscopy is a widely used method to visually magnify small objects by the use of light, with the resolution around half the wavelength of light (practically around 0.5μm for separated points). There are two modes for the illumination:

transmission mode, where the light source is on the opposite side of the specimen with respect to the eyepieces (partially transparent samples required), and reflection mode, where the illumination comes from the same side as the eyepieces, and the reflected light is observed (non-transparent samples can be investigated). Figure 3.7 shows the light paths of the two modes.
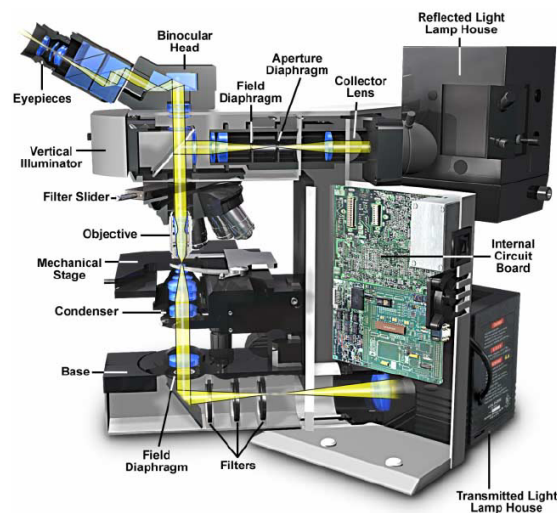

Figure 3.7 Scheme of an optical microscope and light paths for transmission mode and reflection mode [Davidson 1999].

When the light from a microscope lamp passes through a condenser and then either through or around the sample, some of it passes without disturbance of its path and some is attenuated. The decreased intensity of light passing through the sample can be due to absorption or diffraction and deflection. The term Brightfield Microscopy is applied when direct light is projected straightly on our retina and the brightest light we observe is where there is no object. Thus, the background is brighter than the specimen. Weakly absorbing samples often require to be stained. Darkfield microscopy, on the other hand, only allows diffracted rays to pass to the eyepiece so that the scattering specimen appears as bright object on a dark background (Figure 3.8).
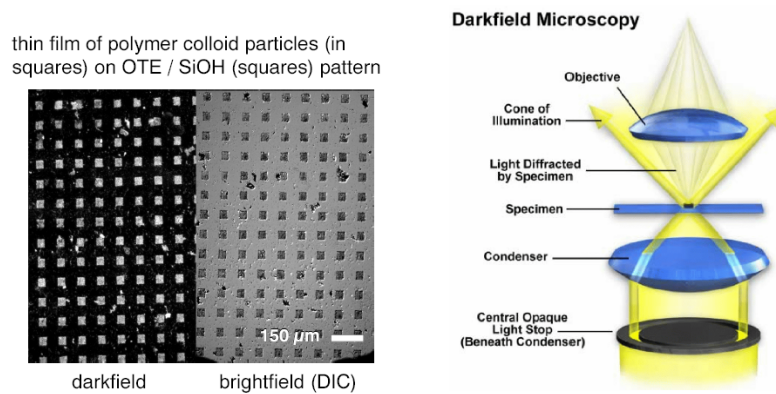
Figure 3.8 Illustrations of darkfield and brightfield methods [Davidson 1999, Krüger 2001].

Another microscopy technique often being used is differential interference contrast (DIC): light from an incandescent source is passed through a linear polariser, so that the electric field vectors of all transmitted light are parallel. The light then passes through a prism where it is split in two beams that pass through the condenser lens as parallel beams with perpendicular polarization. They then pass through the specimen and in any part of the specimen in which adjacent regions differ in refractive index, the two beams are delayed or refracted. When they are combined again by a second Wollaston prism before the objective lens, an interference contrast is created that can be observed as differences in intensity and color whose shadow effects lead to a kind of 3-D appearance of the specimen (Figure 3.9) [Davidson 1999].

Chapter 4

Novel Silanes for Chemical Modifications on Silica Surfaces

The aim of this chapter is to describe how different ω-functionalized triethoxy silanes were synthesized by modular approaches. From these silanes new functional surface layers and the lateral functional patterns were obtained by using surface modification methods and standard micro-contact printing technique. The resulting silane layers could be further modified by reactive species and corresponding surface chemical reactions occurred between the functionalities of the chemical or biological substances and the newly formed functional surfaces.

4.1 Introduction

Independent control of surface structure and chemical properties and the resulting structures-property relationships are both scientifically interesting and technologically

important. For many applications, controlling the properties of interfaces (or surfaces) is very important. It ultimately defines how this interface interacts with its environment through its surface chemistry and physical topography, for example the dewetting of a water droplet on a plant leaf.

Since chemical surface properties are generally considered to be controlled by the outmost 5-10Å at a substrate surface, surface properties of substrates depend critically upon the chemical and physical details of molecular structure on the surface of the substrates. A practical technique to modify the surfaces with desired properties is the deposition of ultrathin molecular films to screen the substrate surfaces.

Silane SAMs are especially suitable for the studies of surface phenomena due to ease of preparation, type of functional groups, mixtures, and the control over the surface functional group concentration. These surfaces can be produced to have surface energies which span the range from very high energy surfaces (metal surfaces (e.g. copper: 2000 mJ·m^{-2}, 300K) or pure silicon dioxide surface, -surface –OH groups (1400 mJ·m^{-2}, 300K)) to "Teflon-like" surfaces (surface –CF$_3$ groups: 18.3 mJ·m^{-2}, 300K) [Israelachvili 2002]. By choosing different head groups for the surface active silane molecules, special chemical properties can be introduce to the substrate surfaces and achieve the desired functions for the substrate. For example, silane SAMs with succinimidyl ester as the head group can be used to immobilize amino groups, such as protein adsorption [Ulman 1996].

In the work of this chapter, we designed and synthesized the following triethoxy silanes with specific head groups to modify the silica substrate surfaces and achieved the surface chemical reactions on these surfaces to show the characteristic reactivity (Figure 4.1). Tert-butyl ester in 11-triethoxysilanyl-undecanoic acid tert-butyl ester (a) acts as protecting group, which can be deprotected by trifluoroacetic acid (TFA).

compound 2:
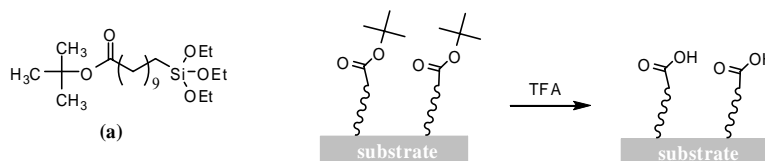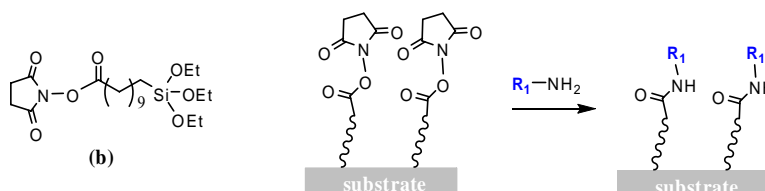
compound 4:

compound 6 & 8:
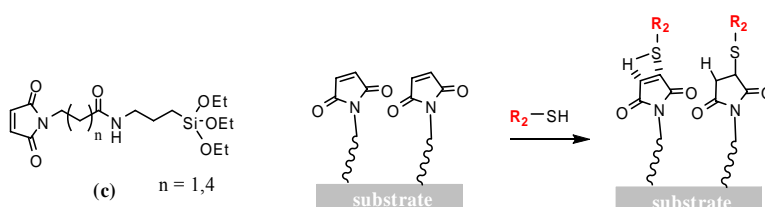
compound 10:
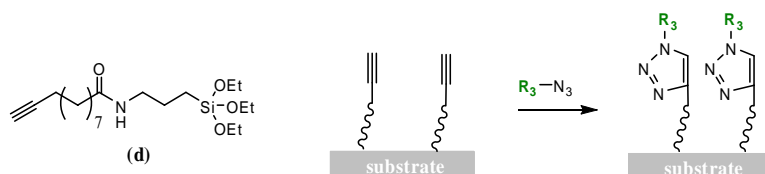
Figure 4.1: (a) tert-butyl 11-(triethoxysilyl)undecanoate; (b) 2,5-dioxopyrrolidin-1-yl 11-(triethoxysilyl)undecanoate; (c) 3-(2,5-dioxo-2,5-dihydro-1H-pyrrol-1-yl)-N-(3-(triethoxysilyl)propyl) propanamide and 6-(2,5-dioxo-2,5-dihydro-1H-pyrrol-1-yl)-N-(3-(triethoxysilyl)propyl)hexanamide; (d) N-(3-(triethoxysilyl)propyl)undec-10-ynamide.

The silica surface modified with tert-butyl ester can be functionally patterned by micro-contact printing with a TFA-soaked PDMS stamp in several minutes. For 11-triethoxysilanyl-undecanoic acid-2,5-dioxo-pyrrolidin-1-yl ester (b), the succinimidyl group is an activated ester, which has high reactivity with amino group to form amide bonds. Thus the surface modified with silane (b) can capture chemical or biological amino components (e.g. peptides and proteins). The maleimide surfaces modified by silane (c) can couple to thiol groups by an addition reaction on the double bond in the

maleimide ring. Thus, the modification of substrate surfaces with maleimide silane (c) provides a basic for thiol immobilization and investigation. For silane (d), the terminal alkyne group can couple with azide groups to yield 1,2,3-triazoles via a Huisgen 1, 3-dipolar cycloaddition reaction. The unique properties of this reaction in solution (high selectivity, quantitative yields, no byproducts, simple reaction conditions) could provide access to a range of novel, functionalized surfaces by analogy to the Sharpless click chemistry concept for solution phase synthesis [Lummerstorfer 2004].

4.2 Synthesis Approach

The synthetic strategy applied in this work is aiming at an easy route to introduce many different functional groups by a simple and modular synthesis concept. In these compounds, one end, the anchor group, is a triethoxysilyl group for the reaction with the hydroxylated silica surface, whereas the other end has a functional head group suitable for the newly desired substrate surface. In between, the spacer should have chain lengths suitable for the formation of self-assembled monolayers by the lateral interactions between two adjacent silane molecules.
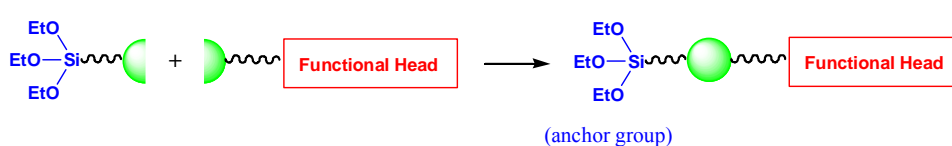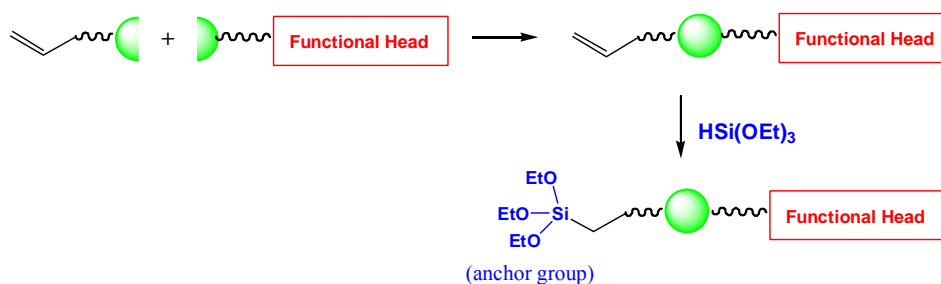
Two modular approaches were applied in the present work. The first approach based on the bond formation between two molecules carrying anchor group (triethoxysilyl) and head group, respectively. The second one was applied for the synthesis of silane molecules carrying complex head groups which need more steps to achieve. Due to the instability of triethoxysilyl group, it is introduced as the anchor group at the last step, called hydrosilylation to avoid the decomposition.

4.2.1 Modular Approach A

The modular approach starts from the commercially available aminopropyl-triethoxysilane (APTE) and couples a variety of functional groups to the amino function via amide bond formation.

Modular approach A:
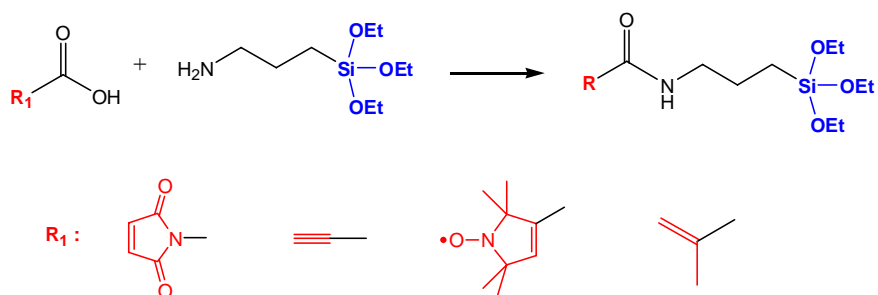
N-hydroxysuccinimide (NHS) is widely used for synthesizing various amide derivatives. NHS can form an activated ester with a carboxylic acid by activation with a carbodiimide, which has a high affinity for the nucleophilic attack of amines, because the electron-withdrawing group (imide unit) enhances the electrophilic character of the carbonyl group in the acid. Figure 4.2 shows the mechanism of the route via the activated NHS ester.
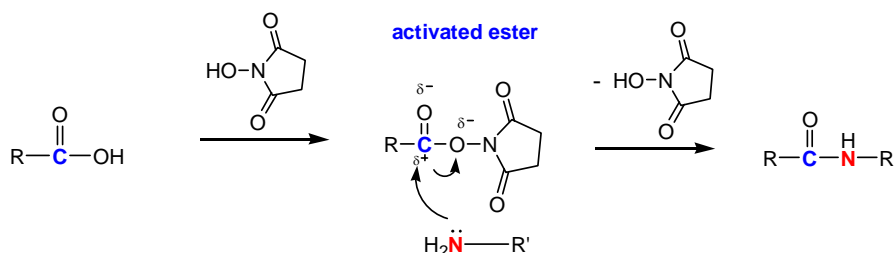
Figure 4.2: The mechanism of amide bond formation via a NHS activated ester derivative.

For the preparation of the activated NHS ester, the carboxylic acid was reacted with NHS in the presence of N,N'-dicyclohexylcarbodiimide (DCC). Carbodiimide esterification occurs between equal molar mixtures of acids and alcohols. The condensation is driven by the formal addition of water (the condensation product from the esterification) across the carbodiimide group to produce the stable dicyclohexyl urea (DCU) as byproduct. It bears advantage of avoiding the need to prepare and handle preactivated and labile acid derivatives such as acid chlorides. Figure 4.3 shows the mechanism of DCC esterification.
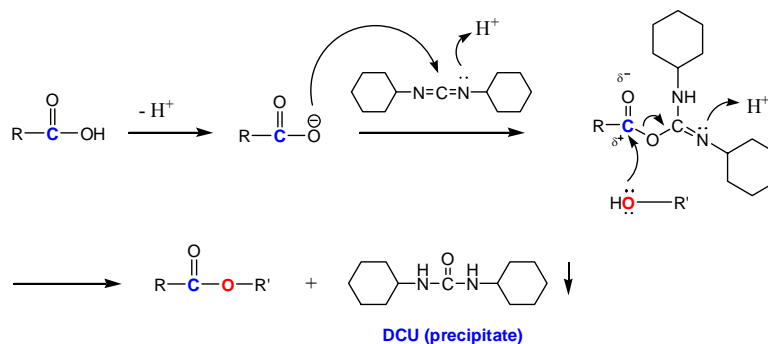
Figure 4.3: The mechanism of the DCC esterification.

4.2.2 Modular Approach B

The second modular approach for the strategy is based on a commercially available

1-carboxylic acid with a terminal ethylene group. In this carboxylic acid molecule, the carboxy group can react for example with an alcohol molecule, which contains the desired functional group, by the formation of an ester bond. At the other end, the terminal ethylene group can couple to triethoxysilane with platinum catalyst, in a so-called "hydrosilylation" reaction.

Modular approach B:
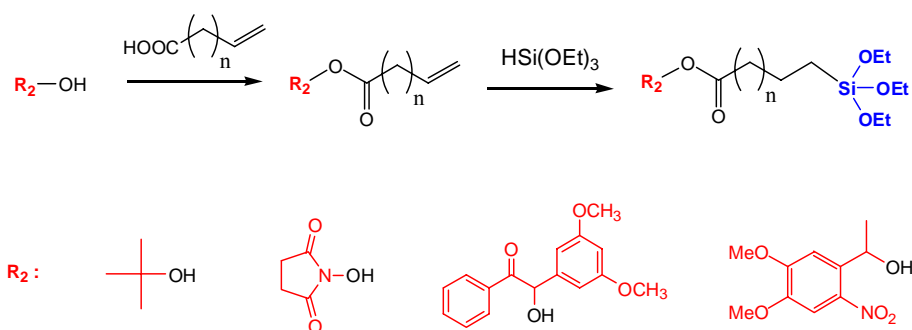
A transition metal complex, ML_n (L = ligand), especially an electron-rich complex of a late transition metal such as Co(I), Rh(I), Ni(0), Pd(0), or Pt(0) as a pre-catalyst, activates both hydrosilanes, $HSiR_3$, and a variety of substrates, typically alkenes. A catalytic cycle is considered to involve further two steps as depicted in Figure 4.4. The conventional hydrosilylation of alkenes catalyzed by $H_2PtCl_6 \cdot 6H_2O$/ *i*-PrOH (called the Speier catalyst) is generally assumed to proceed by the Chalk-Harrod mechanism (Figure 4.4, cycle A). Oxidative addition of a hydrosilane gives a hydrido-silyl complex (I) which is coordinated with the substrate alkene (extremely rarely isolated at this stage). The complex I undergoes migratory insertion of the alkene into the M-H bond (hydrometallation) to give the alkyl-silyl species (II). Reductive elimination of the alkyl and silyl ligands from II forms the hydrosilylation product.

Although the Chalk-Harrod mechanism accounts for an alkene isomerization, an H-D exchange between deuteriosilanes and alkenes, as well as the observed regioselectivity always associated with the catalytic hydrosilylation, an alternative mechanism has been proposed which involves preferentially an alkene insertion into the M-Si bond

(silylmetallation) by using Rh(I) or Co(III) catalyst precursor to form the β-silylalkyl-hydrido intermediate (III), followed by reductive elimination to complete the hydrosilylation (Figure 4.4,cycle B). [Hayashi 1999]
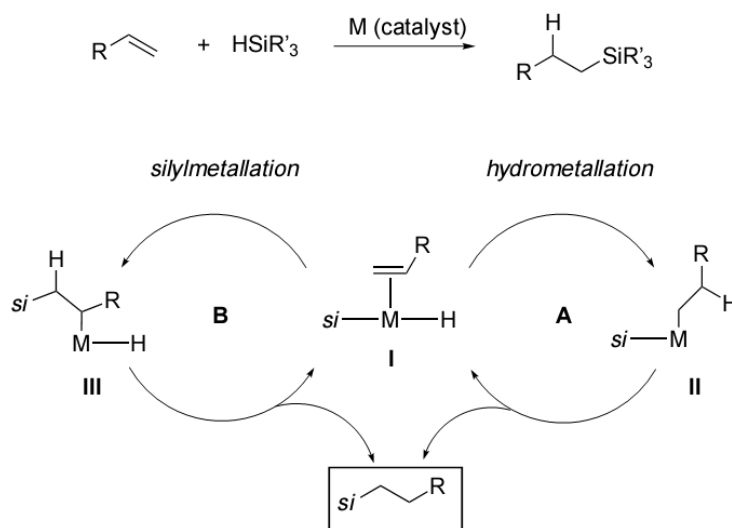
Figure 4.4: Mechanism of hydrosilylation of olefins catalyzed by transition metal complexes.

The alkene chain of the carboxylic acid should have an efficient length that can supply enough lateral interaction between two adjacent molecules in order to form the self-assemblies.

4.3 Surface Modification and Characterization

4.3.1 Formation of Functional Surfaces

For the preparation of the silane monolayers two general techniques are used, namely adsorption from a silane solution and deposition of the silane from the vapor phase.

Solution Phase Silanization

Solution phase silanization is a common technique where the substrate is immersed into a 0.5-2% solution of the silane in an appropriate solvent (Figure 4.5). This method also allows controlled hydrolysis of the silane prior or during substrate immersion. During hydrolysis of the triethoxysilane anchor group and adsorption onto the surface, different chemical and physical processes occur simultaneously (e.g. hydrolytic cleavage of alkoxysilyl bonds, silanol condensation in solution, adsorption of monomeric and oligomeric species to the surface, silanol condensation at the substrate surface, and chemical bonding of the molecule to the Si-OH groups on the substrate surface).
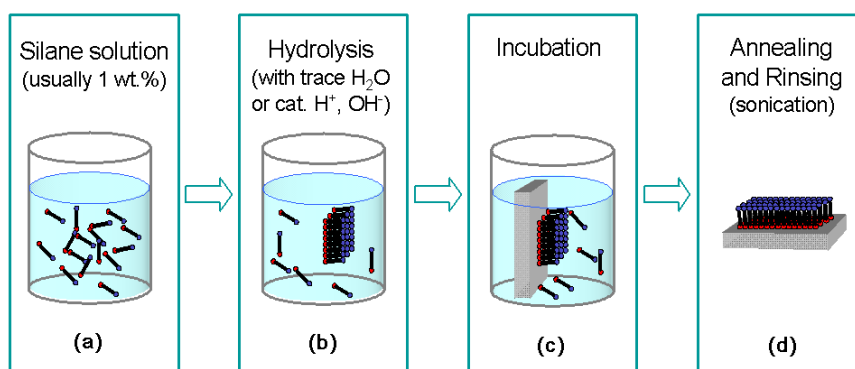
Figure 4.5: Cartoon of solution phase deposition: **(a)** the silane molecules are hydrolyzed in a solvent; **(b)** the hydrolyzed silane molecules form layer structure by adsorption and lateral interactions; **(c)** the silane anchor groups chemisorbs onto the silica surface; **(d)** the SAM is generated.

The reaction conditions thus have to be carefully optimized for each silane derivative in order to prevent undesired three-dimensional aggregation in solution. This is particularly important for ω-functionalized silanes (with C3 and C4 alkyl chains), since the ω-functionality can substantially influence the hydrolysis and condensation behavior due to hypervalent interaction with the silicon center (as seen by solution NMR). In this thesis work, all the synthesized functional silanes were deposited on silica substrate surfaces by solution phase silanization.

Vapor Phase Silanization

If the boiling point of the silane is low enough at a given pressure, another silanization technique could be applied: vapor phase silanization. The setup is shown as Figure 4.6. Compared to solution phase deposition, vapor phase deposition should lead to a more defined monolayer since hydrolysis, condensation and covalent bonding occur exclusively at the substrate surface.
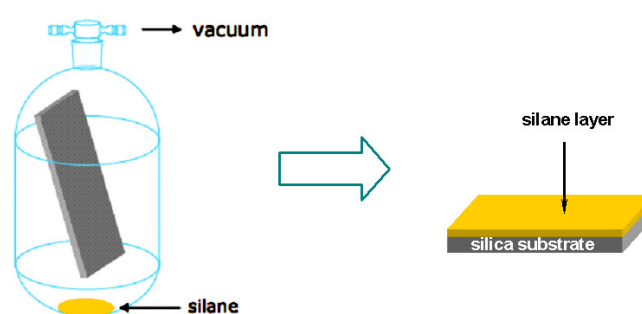
Figure 4.6: Vapor phase deposition in a closed vessel containing only the substrate and the pure silane.

In this thesis, vapor phase silanization was used for the passivating processes of the glasswares with hexamethyldisilazane (HMDS). The mechanism of this reaction is shown in Figure 4.7.
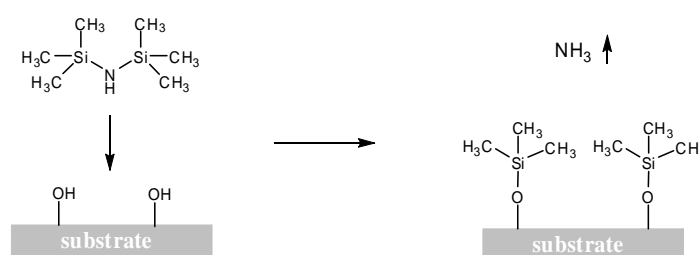
Figure 4.7: Reaction of HMDS at the Si-OH surface.

Upon the reaction with silanol groups at the silica surface, the HMDS molecule is cleaved, and trimethylsilyl groups are covalently bound to the surface, with ammonia as a

side product. HMDS has a reasonably low boiling point and a high vapor pressure (129°C, 1024mbar). It is thus possible to perform the vapor phase silanization at room temperature and ambient pressure for 30 minutes. The resulting contact angle was 74°, which is characteristic for non-polar, hydrophobic trimethylsilyl groups at the silica surface [Fadeev 1999].

4.3.2 Kinetic Investigation of the Hydrolysis Process

In order to anchor triethoxy silane to the silanol groups on the silica substrate surface, its ethoxy groups have to be hydrolyzed in solution to the more active silanol groups that can bind covalently to the silica surface. In order to investigate the kinetics of hydrolysis, ^{1}H NMR spectra of the solution were recorded at different reaction times. Since hydrolysis results in the formation of three hydroxyl groups attached to the silicon atom and 3 molar equivalents of ethanol, the decrease of the ethoxy methyl and methylene groups and the increase of the ethanol methyl and methylene groups in the ^{1}H NMR spectra can be used to quantitatively follow the process (Figure 4.8b).

To find the optimum reaction conditions for obtaining a smooth surface layer, contact angle measurement, atomic force microscopy (AFM), and ellipsometry analysis were used to monitor the quality of the final surface after surface modification under different conditions.

(a)   (b)
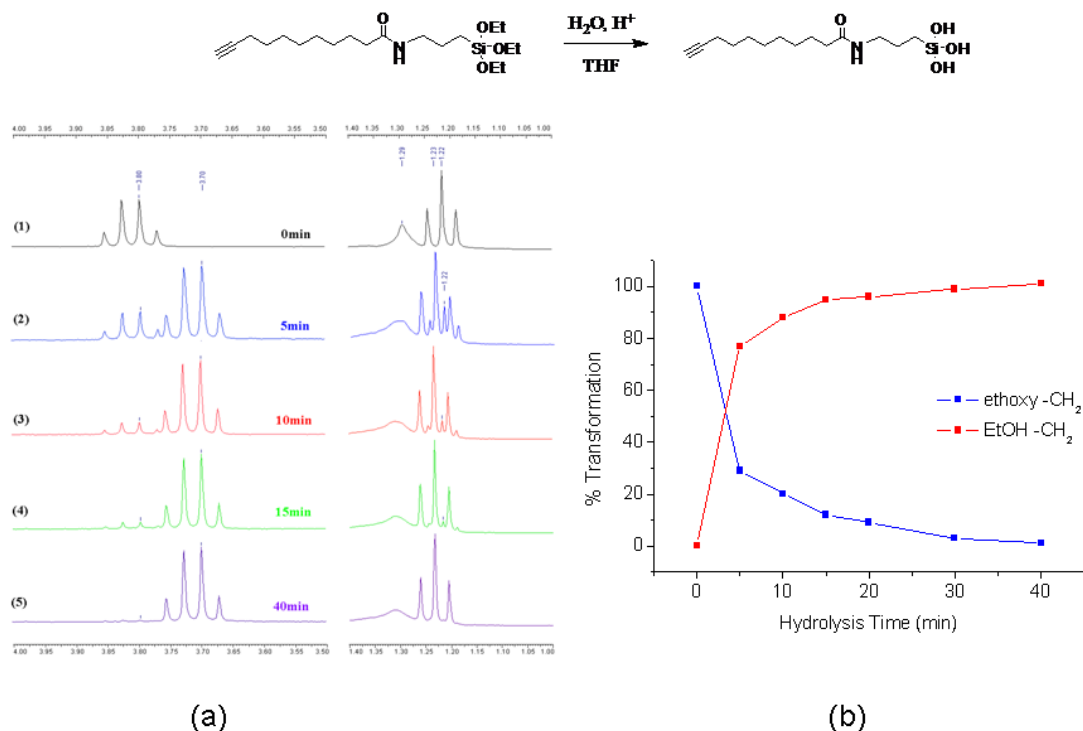
Figure 4.8: Hydrolysis of triethoxysilane into trihydroxysilan; (a) ^{1}H NMR spectra of hydrolysis: decrease of ethoxy –CH$_2$ at 3.80ppm, increase of EtOH –CH$_2$ at 3.70ppm, decrease of ethoxy –CH$_3$ at 1.22ppm, and increase of EtOH –CH$_3$ at 1.23ppm; (b) Kinetic plot for monitoring the hydrolysis of alkyne triethoxysilane using 1μL 1N HCl as a catalyst in a 1mL d$_8$-THF silane solution (0.103mol/L). The calculations of the transformation percentage were based on the increase of EtOH –CH$_2$ and the decrease of ethoxy –CH$_2$.

The ^{1}H NMR kinetic experiments for the hydrolysis in solution were carried out using 1mL of 1% (w/w %) solution of undec-10-ynoic acid (triethoxysilanyl-propyl)-amide in deuterated THF with 1μL 1N HCl as catalyst. More ethanol was present in the hydrolysis system than ethoxy groups after 5 minutes. And after about 40 minutes nearly all ethoxy groups had been hydrolyzed. That means the solution was appropriate for the incubation of the silica substrates in the next silanization step.

4.3.3 Silane Deposition on Silica Surfaces

Chemisorption on silica surfaces occurs when the silicon or quartz wafers are immersed into the hydrolyzed silane solution. The optimum time for the surface reaction

can be monitored by placing the silicon wafers into the hydrolyzing solution at different hydrolysis times and measuring the contact angle of the resulting layers. The contact angle increases with time from less than 10°, which is the contact angle of the pure silica surface (hardly to measure the accurate degree due to the complete wetting behavior), to a steady value of a characteristic degree which depends on the polarity of the newly formed surface.

When the contact angle remains constant, the functional silane monolayer formation is completed, possibly followed by a multilayer formation after longer adsorption time. The layer thickness measured by ellipsometer can be used to investigate a proper adsorption time for silanization of different silanes.

t-Butyl Functional Silane

The water contact angle analysis shows a kinetic process of the polarity change of the silica surfaces by the formation of t-butyl-functional silane layer in Figure 4.9. In the hydrolysis dependence measurement (Figure 4.9b), all the samples were prepared in t-butyl silane solution (1% w/w, THF) with different hydrolysis times and 1 hour of incubation. The result shows that the hydrophobicity increased with a longer hydrolysis time, due to a more complete coverage of the substrate surface with the silane molecules. After about 50 minutes, the value of the water contact angle reached a maximum plateau. This can be explained as the bare hydrophilic silica substrate surface was completely covered by hydrophobic t-butyl functionalities. According to the findings in the incubation dependence measurements and in agreement with the NMR hydrolysis experiments, we chose 1 hour of hydrolysis for the following samples.

The substrate samples with 10 min, 20 min and 40 min of incubation in the silane solution with 1 hour of hydrolysis process have been analyzed by water contact angle. The data were totally unproductable, which could due to the silane layer formation was not homogeneous and complete. Thus we optimized the incubation time up to more than 1 hour.

compound 2:

(a)

(b)

(c)

Figure 4.9: (a) Reaction scheme of the hydrolysis of t-butyl silane in the presence of a catalytic amount of acid or base; (b) increase of hydrophobicity as a function of hydrolysis time of the silane solution and visualized by an increase of contact angle (incubation time was fixed as 60 minutes); (c) water contact angle analysis of the incubation time dependence of the surface layer formation (each samples were immersed into the silanization solution with a fixed hydrolysis time of 60 minutes).

The result in Figure 4.9c shows only a weak change in water contact angles and their hysteresis with the increase of the incubation time. From this result it was concluded that the number of t-butyl functionalities does not change after immersing the substrates into the silanization solution for an efficient time period. The constance of the contact angle hysteresis shows the roughness and heterogeneity of the functional surface had not changed in 6 hours of incubation.

Qualitative roughness values of the functional silane layer surface with different incubation times were measured by AFM (tapping mode). On each t-butyl surface sample,

four different positions were chosen to average the measurements. In Figure 4.10a, the root mean squared roughness varied from 0.4nm to 0.8nm (0.3nm for a bare silica surface) with the incubation time increasing from 1 hour to 5 hours. The results show that the roughness remained essentially constant during 5 hours of the incubation time. This behavior would explain the observation that the hysteresis is independent of the incubation time.

(a)   (b)

Figure 4.10: Incubation dependence measurements of (a) surface roughness and (b) layer thickness by atomic force microscopy and ellipsometry, respectively. 0.6nm of RMS roughness and 1.2nm of thickness shows a well defined self-assembled t-butyl monolayer.

Figure 4.10b shows the layer thickness increasing with incubation time. At 1 hour of incubation, the layer thickness (1.2nm ± 0.15nm) was measured, which increased to 1.8nm as the incubation time went up to 5 hours. This could be explained as longer the incubation, the more silane molecules could accumulate at the substrate surface. Due to polymerization of the trifunctional silane anchor groups by covalent bonds, the formed multilayer structure would not be destroyed and rinsed off by sonication. But the constant water contact angle shows that the overall surface density of the exposed t-butyl functionalities stays constant even on the multilayer structure.

In summary, the optimal parameters for the modification with the t-butyl functional silane are 1 hour of prehydrolysis of the silane solution and 1 hour of incubation time, which will lead to a uniform and well defined monolayer on silica surfaces.

41

Succinimidyl Functional Silane

Similar, the triethoxy silane with a succinimidyl head group was investigated in the same ways.
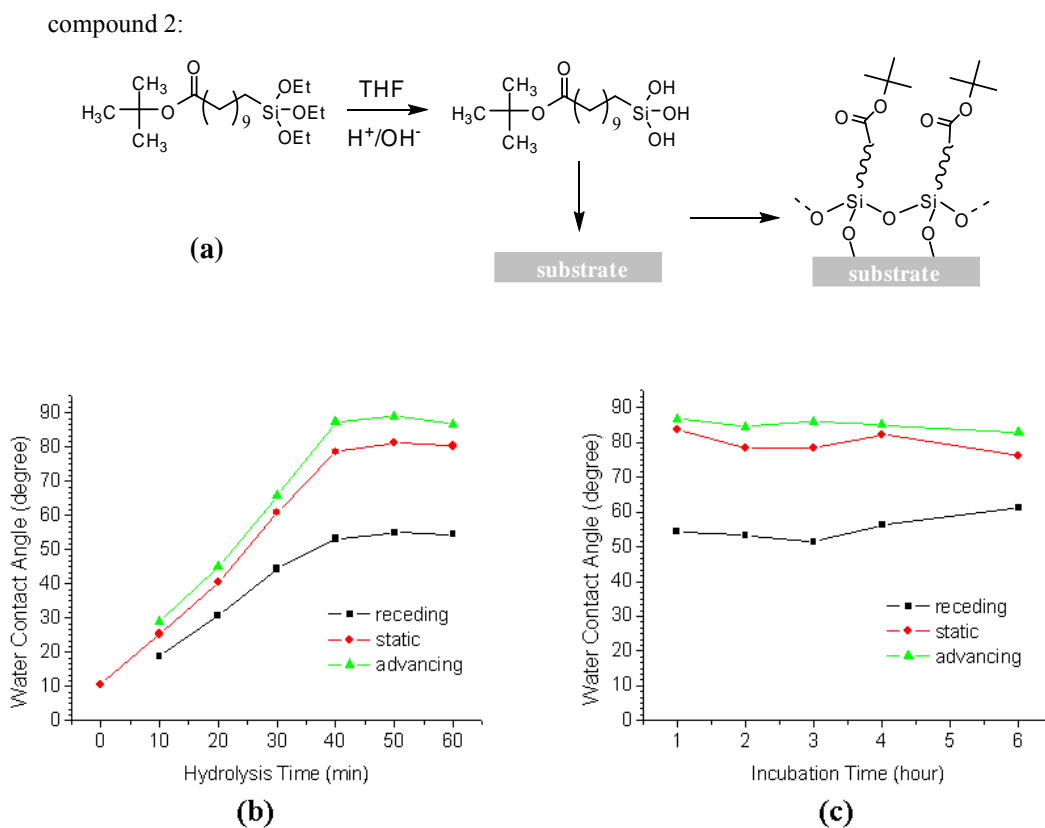
compound 4:
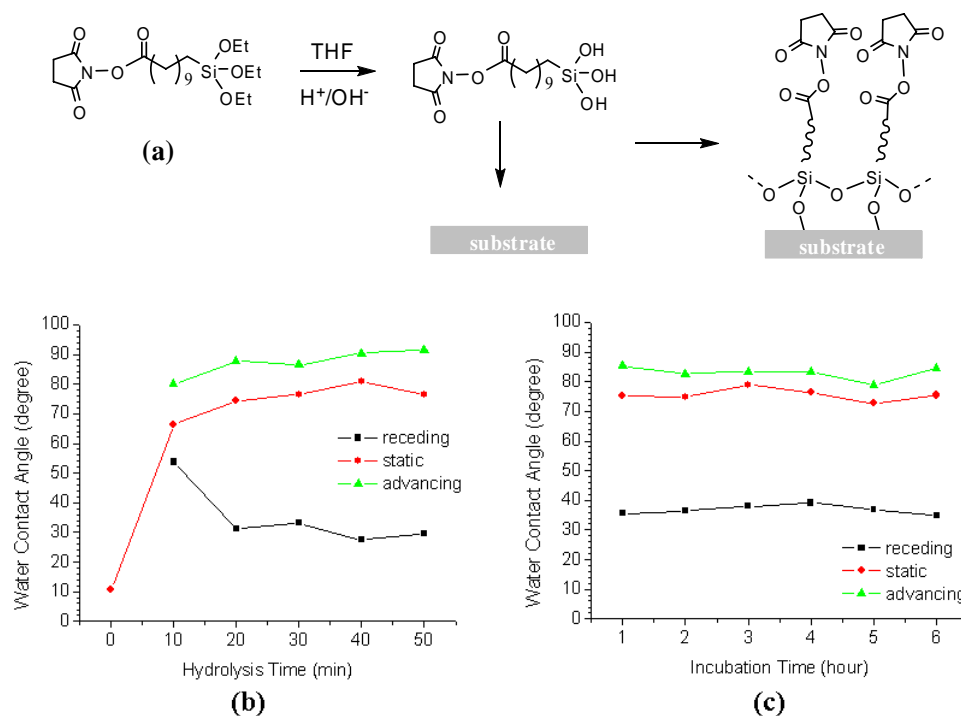
Figure 4.11: (a) Reaction scheme of the hydrolysis of succinimidyl silane in presence of catalytic amounts of acid or base; (b) increase of hydrophobicity as a function of hydrolysis time of the silane solution and visible as increase of contact angle (incubation time was fixed as 60 minutes); (c) water contact angle analysis of the incubation time dependence of the surface layer formation (each sample was immersed into the silanization solution with a fixed hydrolysis time of 60 minutes).

In hydrolysis dependence research, succinimidyl silane molecules were dissolved in THF and stirred for 10 minutes up to 50 minutes. The silica substrates were immersed into the corresponding hydrolysis solution for 1 hour. In Figure 4.11b, the static water contact angle reached to the most hydrophobic value with 40 minutes of hydrolysis time. This indicates that after 40 minutes, the succinimidyl silane molecules had been hydrolyzed efficiently to deposit on silica surface and trihydroxysilanyl anchor groups

had reacted with all the available Si-OH groups covalently. The hysteresis is smallest at 10 minutes indicates a smoother surface, but the static water contact angle has not reach its maximum, which means the succinimidyl functionality has not been deposited on the surface completely. Thus a longer hydrolysis time is necessary.

In incubation time dependence research, the silane solution was hydrolyzed for 40 minutes (due to the previous hydrolysis dependence research, 40 minutes of hydrolysis time is efficient) to incubate the silica substrates for corresponding time. The measurement result shows there were no obvious change of the water contact angles and their hysteresis. We can conclude that a longer incubation time (up to 5 hours) did not influence the concentration of succinimidyl functional groups on silica surface. The constant contact angle hysteresis can be explained with the results showing in Figure 4.12a. The root mean square roughness varied in a relatively small range from 1.1nm to 1.7nm. This slight change of the surface roughness is not enough to change the hysteresis.
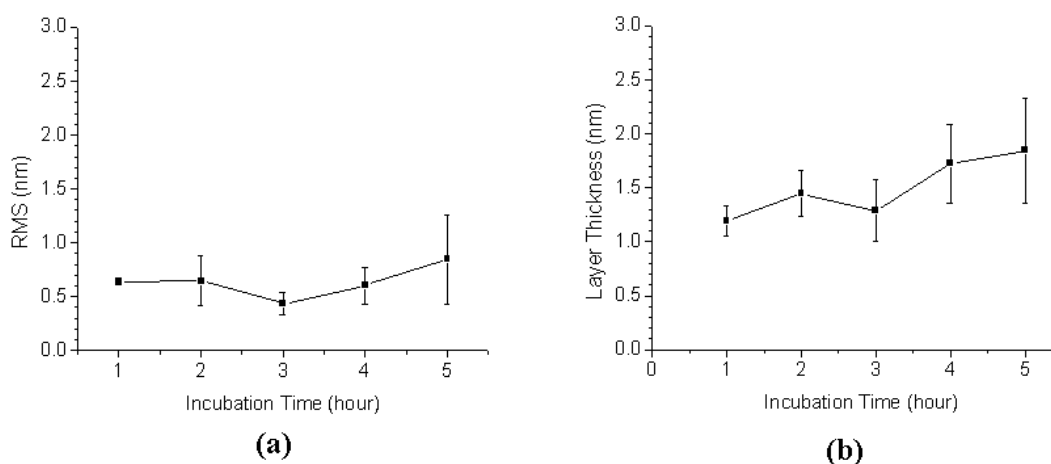

Figure 4.12: Incubation dependence investigation of (a) surface roughness and (b) layer thickness by atomic force microscopy and ellipsometry, respectively.

The increase of succinimidyl functional layer thickness showing in Figure 4.12b means that the layer thickness increases during the incubation process. The surface absorbs increasing amounts of silane molecules to form a multilayer structure while it is immersed in the solution. Thus in order to form a uniform succinimidyl functional

surface, we optimized the hydrolysis as 40 minutes and incubation time as 1 hour, respectively.

Maleimide Functional Surface

As in the cases described above, the formation of the functional layer on silica surface by maleimide functional silane molecules was characterized by water contact angle measurement, AFM, and ellipsometry (Figure 4.13 and 4.14).

Figure 4.13: (a) Reaction scheme of the hydrolysis of triethoxy silane with maleimide head group in presence of catalytic amounts of acid or base; (b) increase of hydrophobicity as a function of hydrolysis time of the silane solution and visible as increase of contact angle (incubation time was fixed at 60 minutes); (c) water contact angle analysis of the incubation time dependence of the surface layer formation (each samples were immersed into the silanization solution with fixed hydrolysis time at 60 minutes).

The static water contact angle reached its maximum with 60 minutes for hydrolysis

and 1 hour for the incubation process. The surface polarity and roughness did not change with longer incubation time, as confirmed by the constant water contact angle values and hysteresis. From root mean square roughness analysis by AFM, the roughness did not change obviously (ave. is 1.9 nm), which is reflected by a constant contact angle hysteresis. And comparing with the t-butyl surface (RMS roughness = 0.8nm, contact angle hysteresis = 30°), the rougher maleimide surface causes a larger contact angle hysteresis (c.a. 40°).
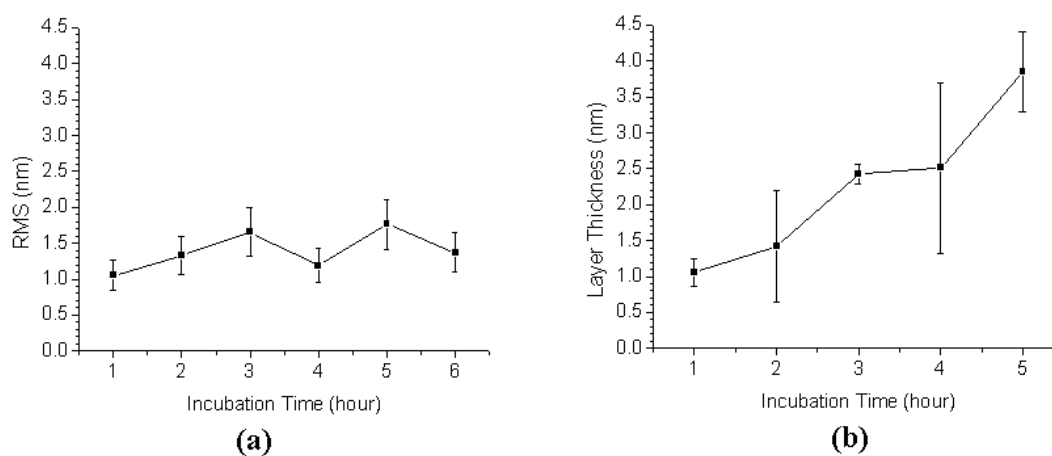

Figure 4.14: Incubation dependence measurements of (a) surface roughness and (b) layer thickness by atomic force microscopy and ellipsometry, respectively.

After 3 hours of incubation the maleimide surface layer thickness increased rapidly, indicating a multilayer structure had been achieved. Thus the surface modification condition for maleimide functional silane can be optimized as 1 hour of hydrolysis and 1 hour of incubation in analogy to the previously described t-butyl- and succinimidyl functional silanes.

Alkyne Functional Silane

As seen in the ^{1}H NMR kinetic experiment discussed above, after about 40 minutes hydrolysis nearly all ethoxy groups of the alkyne silane molecules had been hydrolyzed. The same conditions were used in the hydrolysis kinetic experiment measured by water

contact angle, which is alkyne triethoxy silane dissolved in THF (1%, w/w) in the presence of catalyst amount of 1N HCl. The static contact angle reached the highest value after 40 minutes, indicating that the alkyne terminal functional groups had completely covered the silica surface (Figure 4.15b). In the first 3 hours of incubation process, the static contact angels and hysteresis stayed constant, which indicates the surface polarity and roughness did not change on the corresponding silica substrates. As the incubation time increases from 3 hours up to 5 hours, an increase of advancing contact angles and hysteresis was observed.
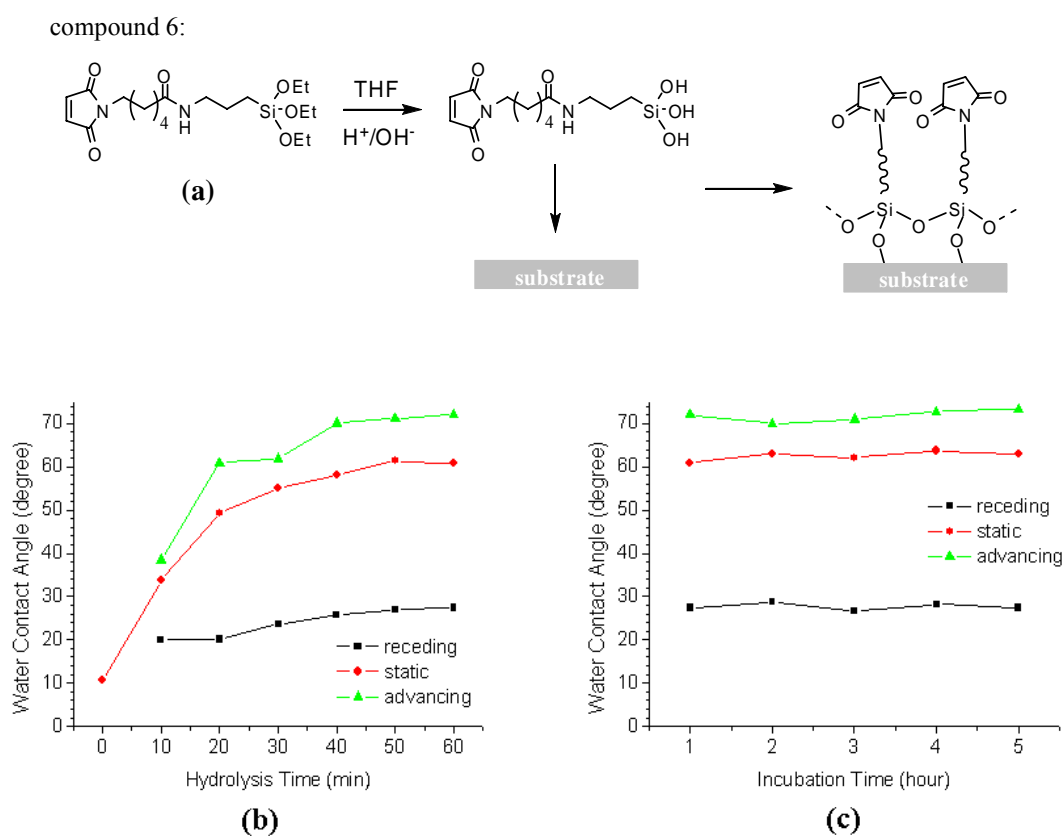
compound 10:

(a)

(b)

(c)
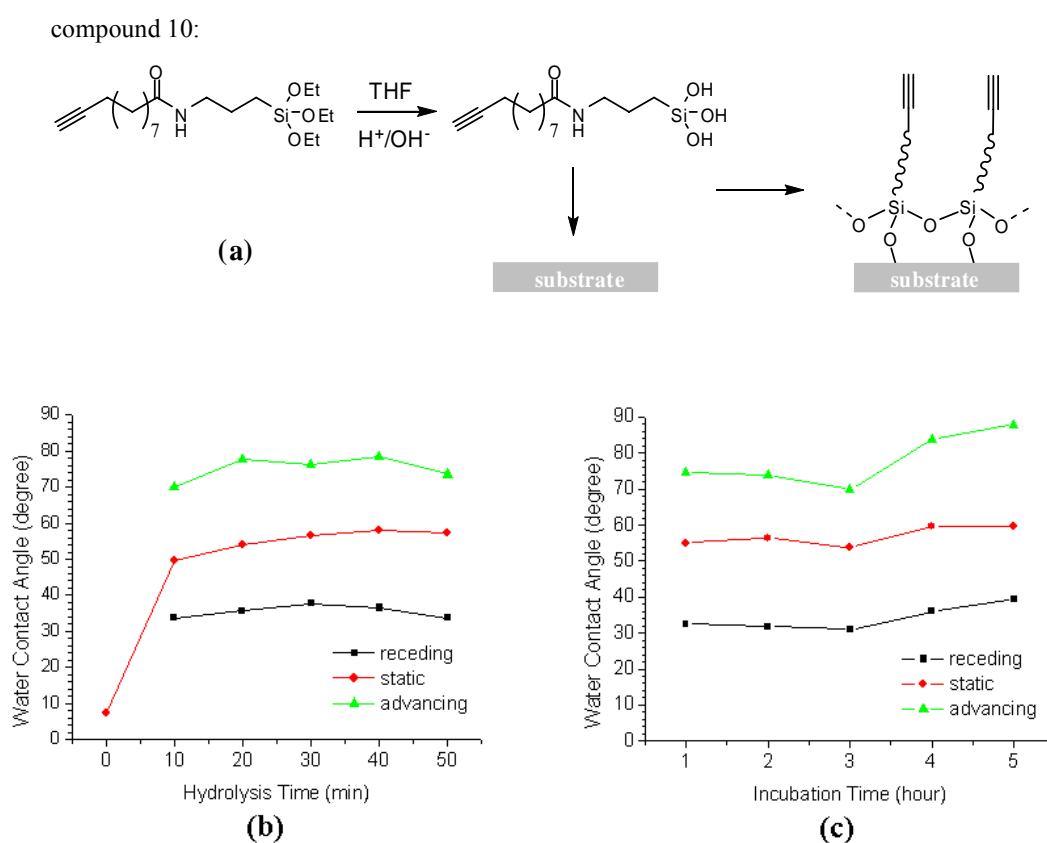
Figure 4.15: (a) Reaction scheme of the hydrolysis of triethoxy silane with alkyne head group in presence of catalytic amounts of acid or base; (b) increase of hydrophobicity as a function of hydrolysis time of the silane solution and visible as increase of contact angles (incubation time was fixed at 60 minutes); (c) water contact angle analysis of the incubation time dependence of the surface layer formation (each sample was immersed into the silanization solution with a fixed hydrolysis time of 60 minutes).

This increase can be explained in Figure 4.16, which shows an increase of the root

mean square roughness after 3 hours. This rougher surface layer could be caused by 3D aggregates of silane molecules depositing on the silica substrates and forming inhomogeneous multilayer structures. This multilayer formation could also be seen by the increase of the layer thickness by ellipsometry (Figure 4.16b).
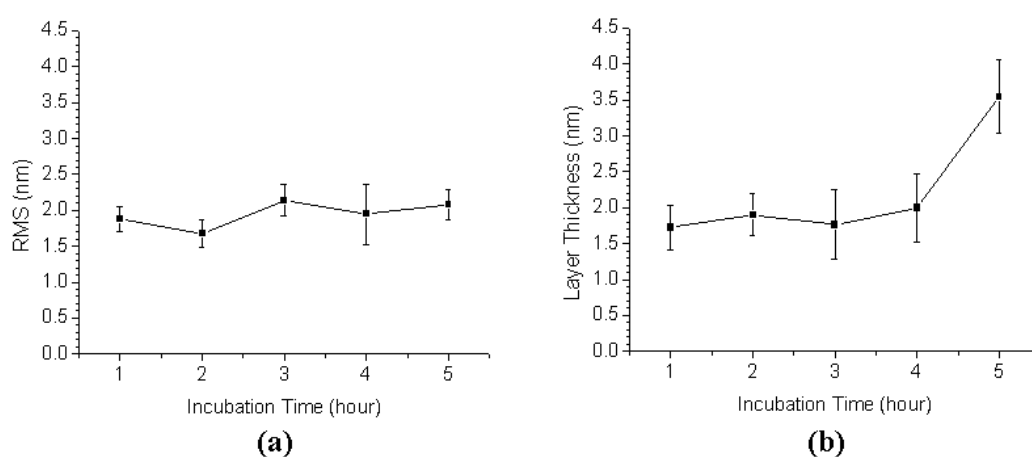

(a) **(b)**
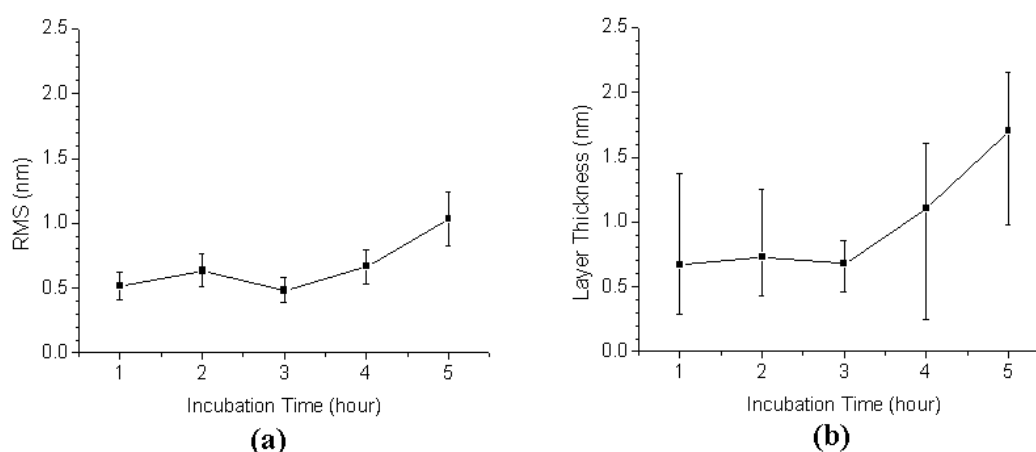
Figure 4.16: Incubation dependence measurements of (a) surface roughness and (b) layer thickness by atomic force microscopy and ellipsometry, respectively.

Thus the surface modification condition for alkyne functional silane are optimal as 1 hour of hydrolysis (in the presence of catalytic amounts of 1N HCl) and 1 hour of incubation, which leads to a uniform and well defined alkyne functional layer with 0.7nm thickness.

In summary, the modular approaches of silane synthesis can be used generally to introduce functional head groups on silane molecules. The deposition of triethoxysilanes is a fast process, the silanes were covalently bound to substrate surfaces within 1 hour of hydrolysis and 1 hour of incubation. The silanization process introduces newly formed silane layers to the surfaces with functional head groups. The change of polarity, surface roughness and layer thickness can be monitored by water contact angle, AFM and ellipsometry. The new chemical properties will be monitored in the following.

4.4 Surface Chemical Reactions on Modified Silica Surfaces

The modified silica substrates with t-butyl, succinimidyl, maleimide, and alkyne functional silanes were studied in the corresponding surface chemical reactions in order to investigate possible applications.

(a)

(b)

(c)

(d)
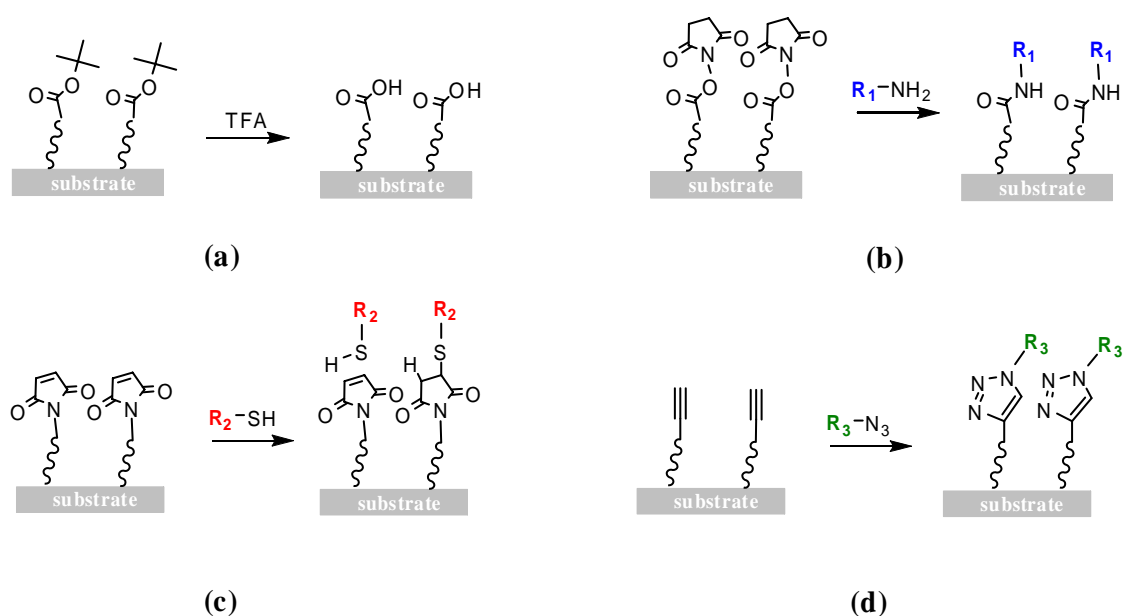
Figure 4.17: Surface chemical reactions tested with the modified silane surfaces (a) the t-butyl ester surface being deprotected by trifluoroacetic acid (TFA) to obtain a carboxylic surface, not accessible by direct silanization; (b) the surface with succinimidyl activated ester being coupled with an amino group to yield an amide (R_1: HO-CH$_2$CH$_2$-); (c) the surface with maleimide groups being coupled with a thiol by an addition reaction (R_2: n-octanyl); (d) the surface with terminal alkyne groups being coupled with azide groups by Huisgen 1, 3-cycloaddition reaction in the presence of Cu(I) as catalyst (R_3-N$_3$: bisazido tetraethylene glycol).

4.4.1 Deprotection of t-Butyl Ester Surface

Carboxylic groups on substrate surfaces are very attractive in the field of surface chemistry, since the surface could be modified, for example by esterification with an

alcohol derivative or it could be negatively charged by adjusting the surface environment to basic conditions. A major problem consists of the fact that triethoxy silanes carrying carboxylic groups are not stable in their free form. The acid group will catalyze the hydrolysis of ethoxy groups into silanol groups and accelerate the silane condensation beyond control. Thus the carboxylic groups were protected during the synthesis and silanization by the formation of t-butyl ester. Then the protecting groups can be deprotected by TFA under quick and mild conditions to yield carboxylic surfaces. [Greene 1999]

The silica substrates with t-butyl ester layers were developed in the solution of TFA / CH_2Cl_2 (90%, v/v) for 1 minute, 5 minutes, and 10 minutes. Then the substrates were rinsed with dichloromethane, THF, and Mili-Q water, and dried in a stream of nitrogen. The change of the water contact angles and layer thickness were measured for different developing times (Figure 4.17).

(a)

(b)

(c)
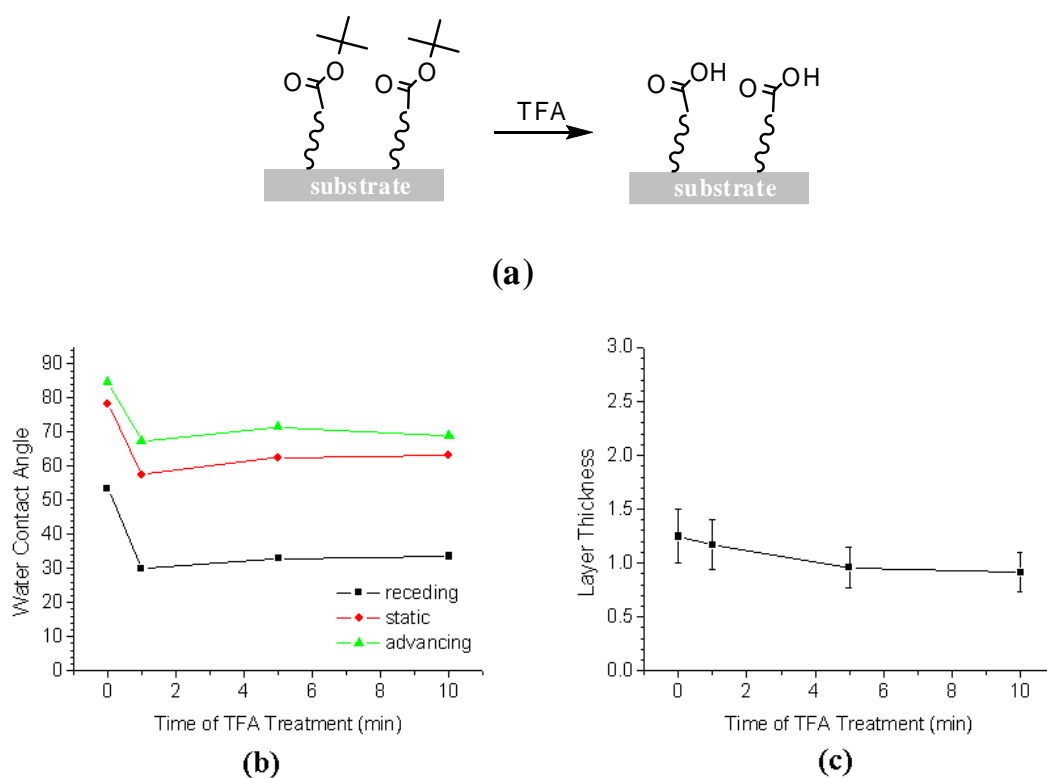
Figure 4.17: (a) Reaction scheme of t-butyl ester surface being deprotected by trifluoroacetic acid (TFA) to

achieve carboxylic surface; (b) water contact angles dropped about 25 degrees after the t-butyl ester surfaces were developed in TFA / CH$_2$Cl$_2$ (90%, v/v) solution; (c) the layer thickness decreased about 0.2 nm after the substrates were deprotected by TFA.

It was found that the water contact angle dropped about 25 degree after 1 minute of treatment by TFA solution due to the formation of free carboxylic acid groups after deprotection. While the t-butyl protecting groups were released, the layer thickness decreased by about 0.2 nm.

4.4.2 Succinimidyl Surface with Amino Groups

The development of strategies to immobilize groups of biopolymers to substrates has given rise the field pf biochips and has dramatically increased the rate and scope of discoveries in basic and applied science. Examples include the development of DNA chips for genome analysis, the preparation of protein chips for evaluation of protein-substrate interactions, and the construction of peptide and carbohydrate chips for the evaluation of ligand-receptor interactions and enzymatic activities. A key challenge in biochip technology has been the development of reliable and reproducible chemicals for the immobilization of ligands to a single substrate. [Houseman 2003]

The N-succinimidyl activated ester has been used extensively to promote the coupling of carboxylic acids and amines for carbodiimide-mediated aminolysis. The high selectivity toward amines has been attributed to stabilization of the transition state by hydrogen bonding between the amine and the succinimidyl carbonyl group. Thus activated ester-modified surfaces could be coupled to biologically relevant molecules using approaches developed for solid phase synthesis. In this section, we report the activity of succinimidyl surface with amines and provide a potentially new route for the immobilization of biomolecules. [Wojtyk 2002]

(a)   **(b)**
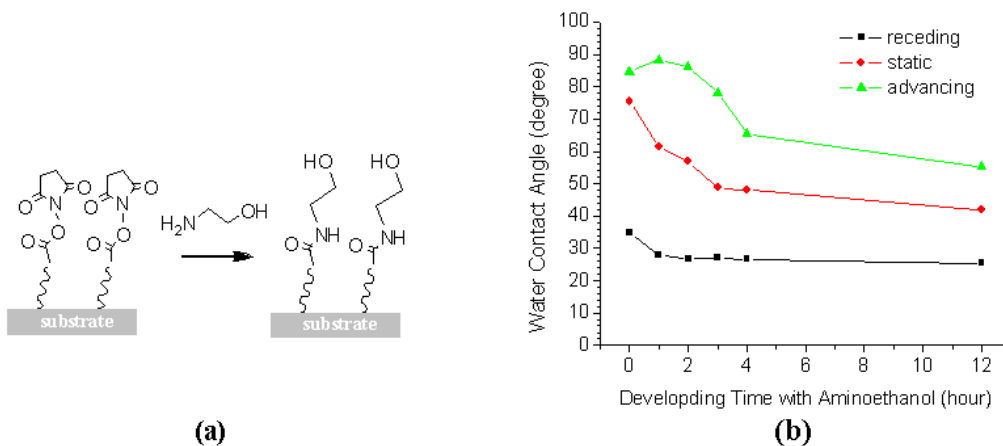
Figure 4.18: (a) Reaction scheme of N-succinimidyl activated surface with aminoethanol to yield a hydrophilic hydroxyl surface; (b) water contact angle dropped to about 45 degree with 12 hours exposure to aminoethanol solution.

Two kinds of 1.0×10^{-3} mol/L of aminoehtanol and octylamine solutions were made up in the mixture of phosphate-buffered saline (PBS) solution (pH = 7.4) and ethanol (8:2, v/v). The silica substrates with N-succinimidyl silane layer were immersed in these two kinds of solutions for 12 hours. The samples were taken out of the amine solution when they needed to be characterized, rinsed with dichloromethane and Mili-Q water and dried in the stream of nitrogen. Aminoethanol molecules were coupled to the activated surfaces and yield a hydrophilic surface by the hydroxyl groups. The process can be monitored in Figure 4.18b. On the contrary, octylamine kept the hydrophobicity of the surface, which could hardly be distinguished by water contact angle measurement. But the increase of the layer thickness can be monitored by ellipsometry. The calculated alkyl chain of octylamine is about 1nm, which matches the increase of the layer thickness from 1.5 nm to about 3.0 nm.

(a)   (b)
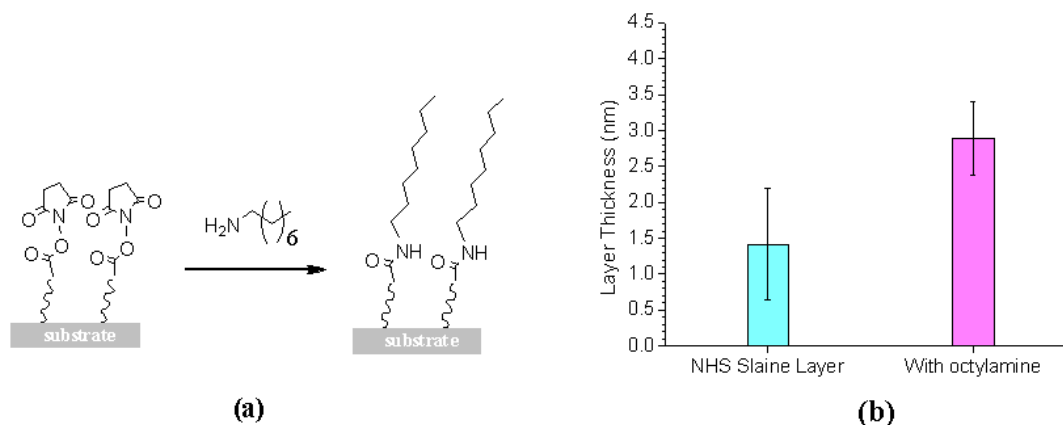
Figure 4.19: (a) Reaction scheme of N-succinimidyl activated surface with octylamine; (b) layer thickness increased about 1.5 nm with 12 hours exposure to octylamine solution.

4.4.3 Maleimide Surface with Thiol Groups

In the application of a wide variety of biochips, an immobilization reaction should have several characteristics. First, the reaction should occur rapidly and therefore allow the use of low concentrations of reagents for immobilization. Second, the immobilization process should occur selectively in the presence of common functional groups, including amine, thiols, carboxylic acid, etc. The reaction should ensure that ligands are immobilized in an oriented and homogeneous manner. Several groups have reported immobilization chemistry between maleimide and thiols that possess the above features. Scheiber and co-workers, for example, used the reaction between thiols and surface-bound maleimide groups to immobilize several small molecules to glass slides. [MacBeath 1999]

We simplified the surface modification protocol with only one step of silanization with maleic functional silanes. Comparing with the 2-step-protocol (first modifying the surface with aminopropyltriethoxysilane, second coupling with a maleimide-NHS activated ester to transform amino to maleimide), our approach is simpler to supply an uniform monolayer.

(a)

(b)

(c)
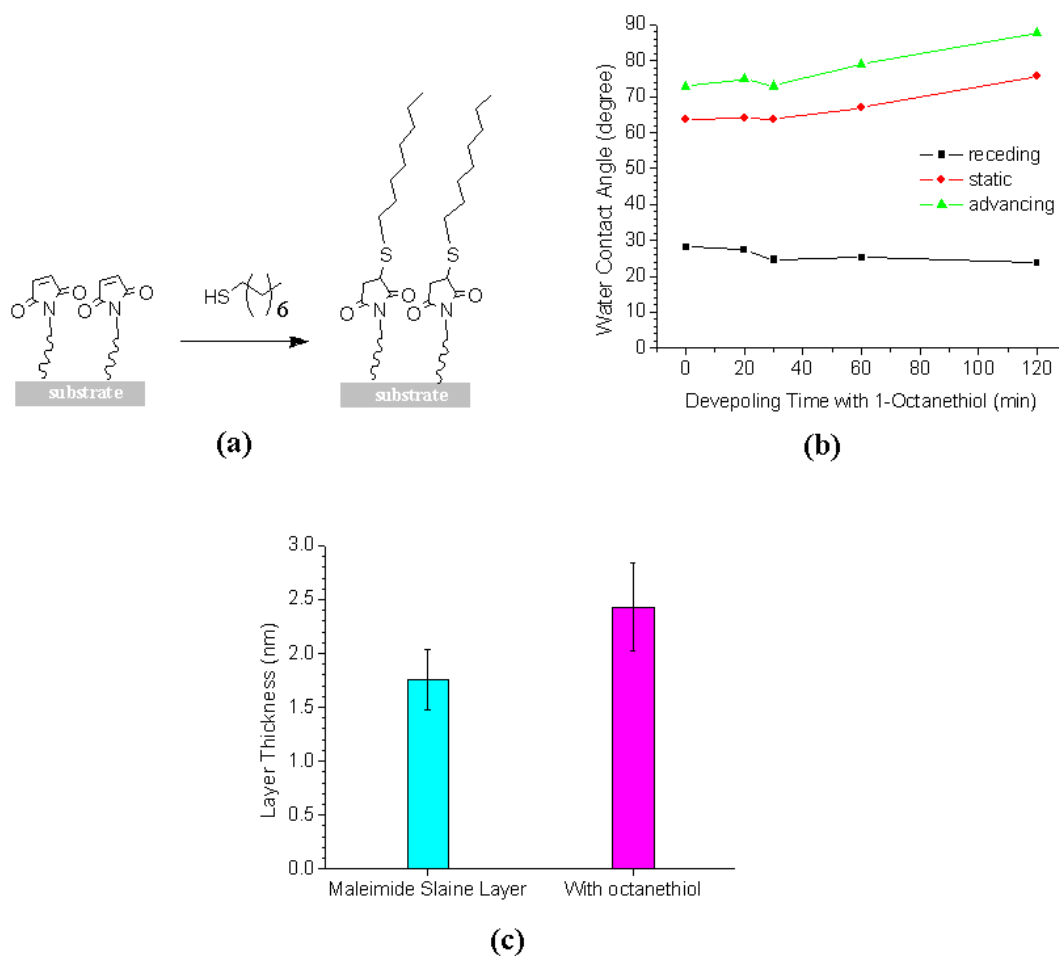
Figure 4.20: (a) Reaction scheme of maleimide functioanl surface with octanethiol to yield a hydrophobic alkyl surface; (b) water contact angle increased to about 70 degree with 120 minutes exposure to octanethiol solution; (c) layer thickness increased about 0.7nm with 120 minutes exposure to octanethiol solution.

Silica substrates with maleimide silane layer were immersed into a 1.0×10^{-3}mol/L solution of octanethiol in ethanol for 2 hours. The samples were taken out of the thiol solution when they needed to be characterized, rinsed with dichloromethane and Mili-Q water and dried in the stream of nitrogen. Octanethiol molecules were coupled to the double bonds of maleimide and yield a hydrophobic surface by the alkyl chains. The process can be monitored in Figure 4.20b. And the increase of the layer thickness can be monitored by ellipsometry. The calculated alkyl chain of octanethiol is about 1nm, which matches the increase of the layer thickness from 1.7 nm to about 2.4 nm.

53

4.4.4 Huisgen 1, 3-Cycloaddition on Alkyne Surface

"Click chemistry" is a chemical philosophy introduced by K. Barry Sharpless in 2001 and describes chemistry tailored to generate substances quickly and reliably by joining small units together. This is inspired by the fact that nature also generates substances by joining small modular units. [Kolb 2001] The modular approach for click chemistry is based on a few highly selective and quantitative couping reactions for the assembly of new molecules from individual "building blocks". The Azide-Alkyne Huisgen Cycloaddition is a 1, 3-dipolar cycloaddition between an azide and a terminal or internal alkyne to give a 1, 2, 3-triazole. Huisgen was the first to understand the scope of this organic reaction. [Lummerstorfer 2004] The mechanism of Huisgen reaction can be shown as Figure 4.21.
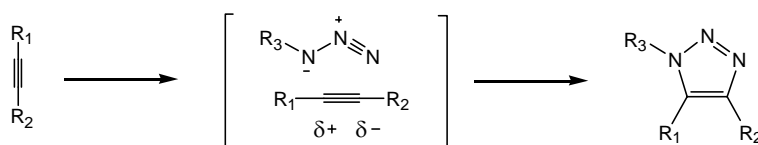
Figure 4.21: Mechanism of Huisgen 1, 3-dipolar cycloaddition.

In our work, we modified the surface with terminal alkyne silanes and monitored the activity of Huisgen reaction on the alkyne surface with bisazido tetraethylene glycol.

Lateral patterns transformation by micro-contact printing:

PDMS stamp was inked with the alkyne silane solution (0.5% wt. conc. in THF, hydrolyzed for 1 hour) and evaporated to dryness at room temperature. Then the stamp was pressed against a silica substrate for 2 minutes, and the substrate was backed at 70°C for 1 hour and sonicated in THF for 10 minutes. The silane molecules formed a self-assembled layer on the silica surface that reproduced the stamp's pattern.
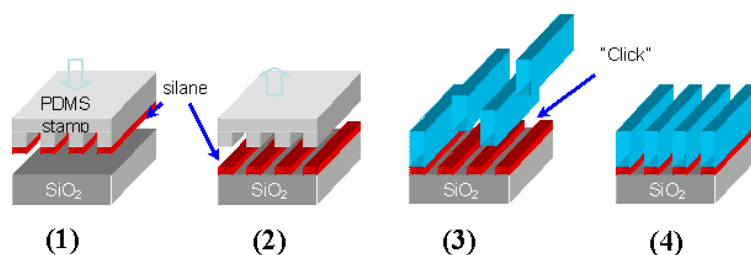
Figure 4.22: Transformation of the silane as patterned layers on silica substrates and the corresponding surface click chemistry reactions.

Huisgen 1, 3-cycloaddition reaction on substrate surfaces:

Both fully alkyne-funtionalized and micro-contact printed silica wafers were dipped into 10mL of aqueous solution of bisazido tetraethylene glycol (conc. wt. 5%, t-Bu / H_2O = 1:1) with 0.05g of CuCl as catalyst for 24 hours at room temperature. Afterward, the wafers were rinsed with toluene, acetone, and ethanol. Finally, they were sonicated in ethanol for 10 minutes and blow-dried in nitrogen.

Figure 4.23 shows the change of water contact angle and layer thickness and indicates the Huisgen 1, 3-cycloaddition reaction took place on the alkyne-functionalized surface. A higher hysteresis indicates a change in surface chemistry. From the data, we can conclude that the new layer surface formed by azide coupling is rougher than the silane monolayer. And a smaller layer thickness value hints the molecules are not standing straight upward on the substrate surface.
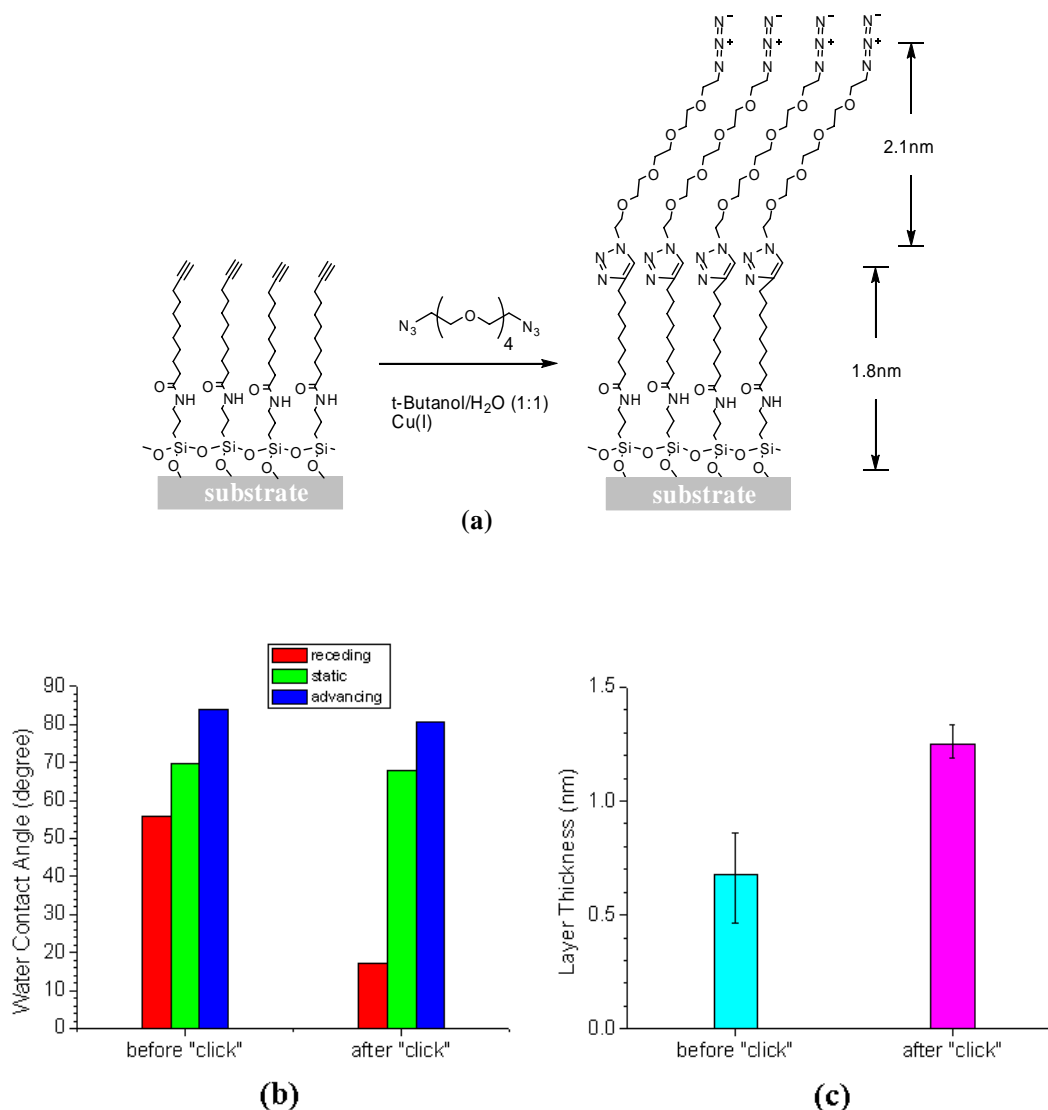
Figure 4.23: (a) scheme of the Huisgen 1, 3-cycloaddition reaction on alkyne-functionalized surface and calculated thicknesses of the silane monolayer and the layer after the surface reaction with assumption all the molecules standing straight up; (b), (c) changing of water contact angle and layer thickness after the surface click chemistry reaction, respectively.

Alkyne functional patterns were also introduced to silica surface by microcontact printing. And by using the same condition for click chemistry as previously, bisazido tetraethylene glycol was reacted on the functional patterns and enhance the thickness of the reacting regions. From Figure 4.24a, we can observe that the self-assembled silane patterns have a thickness of 50 nm as in average. And after the reaction, the thickness of

the patterns comes up to 100 nm. From the section analysis pictures, we can also see that the topology of the pattern surface turned to less defined. From the height data we can conclude, that the microcontact stamping does not produce a thin silane monolayer, but rather a 3D structure of a functional silane network.
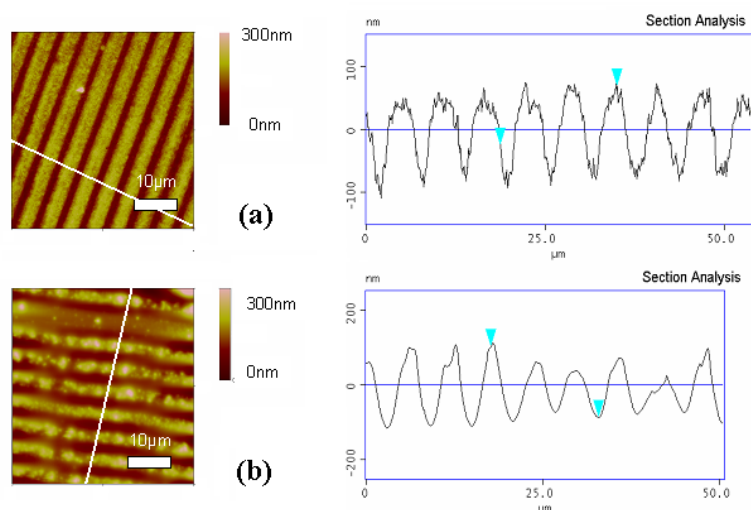
Figure 4.24: (a) section analysis of microcontact printed sample only with silane functional patterns shows the average height of the patterns is 50nm; (b) after the azide coupling, the height comes 100nm in average and the patterns were less defined.

In summary, we have found out the condition to make alkyne-functional silane self-assembled monolayers on silica substrates and modified active surfaces for Huisgen 1, 3-cycloaddition reaction. And we have shown this reaction provide a simple and convenient way for surface modification.

4.5 Summary

It has been possible to synthesis the silane compounds with designed functionalities, which can be used to modify silica substrate surfaces due to their triethoxysilane anchor groups. There head groups can further react with corresponding functional groups due to their characteristic chemical reactivities. Hydrolysis conditions were optimized in order to form uniform and well defined self-assembled layer surfaces, arising from the reactive

alkoxysilanes group. Kinetic experiments with varying hydrolysis time and incubation time were performed to study the efficiency of silanization. The changes in hydrophilicity of functional surfaces and their layer thickness were clearly visible in the surface reactions, which imply the surfaces were functionalized as we had expected.

Chapter 5

Patterning of Photoprotected Silane Layers

5.1 Introduction

When functional silanes carrying a photoprotecting group are combined with the photolithography technique, lateral functionalized patterns onto the planar substrate with micro to nanometer dimensions can be created. These patterns can define the spatial location of attracted objects due to different polarity, charges, or chemical reactivity on different patterns (Figure 5.1).
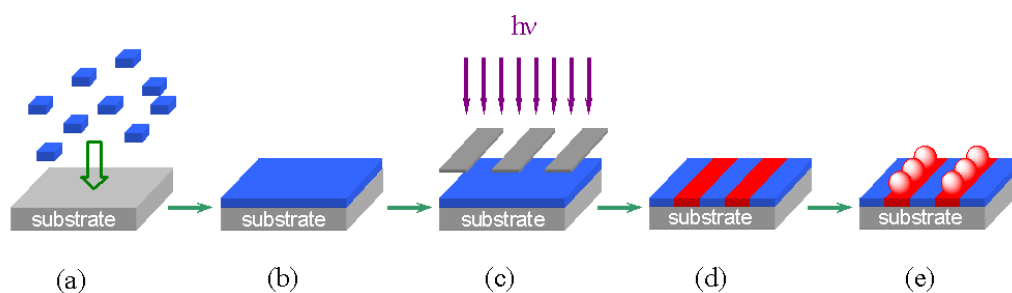
Figure 5.1: Illustration of the procedure of surface functional patterning by direct monolayer photolithography: (a) bare silica substrate; (b) formation of a photoprotected functional silane layer (blue

color representing the photoprotecting group, e.g. NVoc groups or benzoin derivatives); (c) irradiation of the photoprotected surface through a mask; (d) resulting chemical patterns on the substrate surface with the deprotected functionality in red (for instance, amino, hydroxyl, or carboxylic group) and the non-irradiated, protected regions in blue; (e) site-selective deposition of molecules or mesoscopic objects (red spheres) onto the irradiated regions.

Light directed chemical patterning has so far found many applications in medicinal-biological areas. For example, light directed synthesis of DNA arrays has emerged as a powerful tool for parallel hybridization-based analysis of DNA and RNA sequences and provides a versatile probe method for microfabricating probe arrays with densities of 1×10^7 unique sequences per cm^2 [McGall 1997]. In modern microelectronic industry, the use of semiconducting and metallic nano-particles is advancing rapidly. Vossmeyer and co-workers have developed a process for generating complex, spatially separated patterns of multiple types of these nano-particles by using lithographic patterning of organic monolayers that contain photo-labile groups and are covalently bound to the silica surface [Vossmeyer 1998]. This concept could be further expanded towards the control of mesoscale assembly as demonstrated by regioselective colloid assembly after direct monolayer patterning with light [Jonas 2002a].

The requirement for a photoprotected silane is that the photoprotecting group should be sensitive to light but relatively stable to all chemical reagents encountered during the whole layer preparation and modification process in the ground state manifold [Pillai 1980]. The wavelength of the light chosen should be that it will only be absorbed by the protecting group and will not affect other parts of the silane molecule. Moreover, photo-deprotection should not harm the protected functionality and the resulting photoproduct should be easily removed. Another factor of great importance is the lifetime of the excited state, which is responsible for the deprotection reaction. That means, the longer the excited state before cleavage occurs, the more the chances are for undesirable quenching processes to arise, which in turn reduces the efficiency of the cleavage reaction. This of course, would hinder the removal of the photo-protecting group and might labilise the quenching species [Becker 1991].

The common procedure to introduce photosensitive moieties onto a substrate involves first the modification of a surface to introduce functional groups (e. g. amino, carboxyl, hydroxyl groups), which then react in a second step with the photosensitive protecting groups. Since all of the chemical reactions occur at the surface, the disadvantage of this approach lies in the limited control over the reaction yield, layer composition and analysis of the product. Nevertheless, many scientists have used this technique in the past for post-modification of functionalized gold or silica surfaces [Vossmeyer 1997, Stenger 1992, Elender 1996]. The approach taken in this section is based on a surface modification process that uses functionalized alkoxysilanes, carrying covalently attached photoprotecting groups. These silanes are synthesized prior to deposition onto the surface. The advantage of synthesizing a silane that directly incorporates a photoprotecting group versus post-modification of a surface lies in the specific preparation of a well defined molecular structure and the possibility to prepare mixed monolayers. By this approach, the photo-reactive silane can be fully characterized by NMR and mass spectrometry prior to deposition, which is much more difficult after bonding to a surface. By this method, the highly defined, quantitative reactions of the protected surface functionalities and full control over the layer preparation process can be achieved due to synthesis and purification prior to layer fabrication. Patterning of the adsorbed silane layer can be achieved in the same way as in conventional photolithography by irradiation through a mask.

One of the most popular carbamate protecting group is the nitroveratryloxycarbonyl group (NVoc) used for protection of the amine group, which upon deprotection decarboxylates to give an aldehyde, the free amine and CO_2. However, NVoc protection can also be used for photoprotection of alcohols and carboxylic acids leading to the corresponding NVoc ester and carbonates [del Campo 2005].
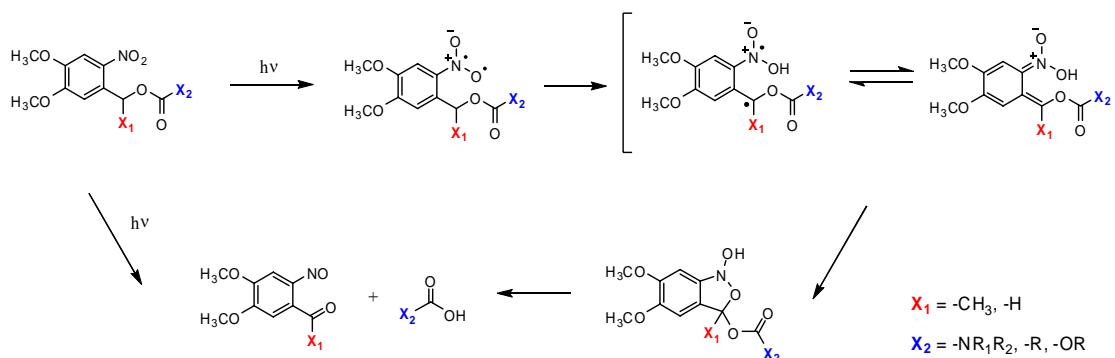
Figure 5.2: Mechanism of the photolytic cleavage of NVoc-protected carbonyl compounds.

The mechanism of NVoc photo-deprotection is shown in Figure 5.2, where the nitro group is firstly excited by irradiation to produce a diradical, then the primary photochemical process is an intramolecular hydrogen-abstraction from the benzyl C-H bond in ortho-position by the excited nitro group. An electron distribution then follows to form an azinic acid (aci-nitro group), which rearranges to the nitroso group. The only problem associated with the NVoc group is the potential side reaction of the formed aldehyde photoproduct with the released amine group to give an imine [Cameron 1991]. This problem can be addressed by the introduction of a methyl group at the benzylic position, as discussed further below.

Benzoin esters (Bzn) have also become very popular as photoprotecting groups due to their excellent photosensitivity. In 1964 Sheehan and co-workers showed that it was possible to cyclize benzoin acetate into 2-substituted benzofuran and to release the carboxylic acid group by irradiation at 366 nm with a high pressure mercury lamp with a Pyrex filter [Sheehan 1964, Sheehan 1971]. The carboxylic acid was thereby released with a high quantum yield ($\Phi = 0.64$) thus making it attractive for the protection of carboxylic acids. They also found out that substitution of the benzylic ring can significantly increase the rate of the reaction and that 3',5'-dimethoxybenzoin led to a fast and smooth cyclization upon photolysis. The benzoin substituents play a major role in determining the photolysis mechanism. Whereas 4,4'-dimethoxybenzoin only gave trace amounts of benzofuran, 3',5'-dimethoxybenzoin leads to a very smooth cyclisation, with a high deprotection yield in the case of the acid moiety. On the other hand, if no

substituents are present the mechanism occurs via an α-cleavage of the diradical, resulting from the carbonyl excitation, which does not lead to the formation of benzofuran and the desired free acid moiety [Lewis 1975, Lipson 1996]. The dimethoxybenzyl moiety has also been used by other groups as a photo-protecting group [Cameron 1991, Chamberlin 1966, Bochet 2000] and they found that the deprotection reaction occurred within 10^{-10} second after the absorption of a photon. The benzofuran photoproduct is non-polar and inert and can therefore be readily separated from the liberated acid or other polar compounds. The mechanism of photocleavage of a benzoin derivative via a diradical process is shown in Figure 5.3. In our case, group X would be the triethoxysilanyl imide to yield an amino functionality after photocleavage.
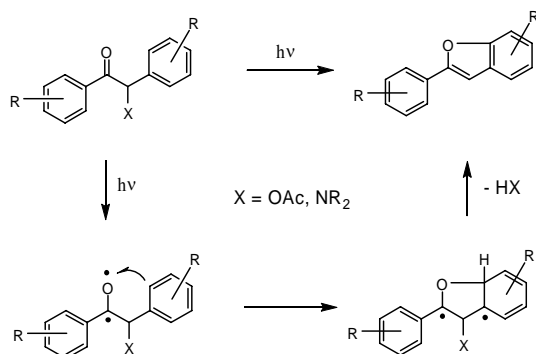
Figure 5.3: Photolytic cleavage of a benzoin ester via a diradical mechanism in the presence of substituents to yield benzofuran and the liberated fragment HX.

NVoc-protected amino- and Bzn-protected carboxyl silanes were previously synthesized and the possibility of creating photopatterned structures was demonstrated for each of them. Even orthogonal photopattering by depositing a mixture of these silanes (1:1, molar ratio) on a substrate was performed. For this purpose, the substrate was irradiated first at 411 nm to deprotect the NVoc group through a mask with alternating gold stripes and then the same mask was rotated at 90° and irradiated at 254 nm to deprotect the Bzn group, resulting in a square pattern (Figure 5.4) [del Campo 2005]. The resulting chemical contrast between exposed and non-irradiated regions was used to direct the assembly process of specific targets onto the activated areas.
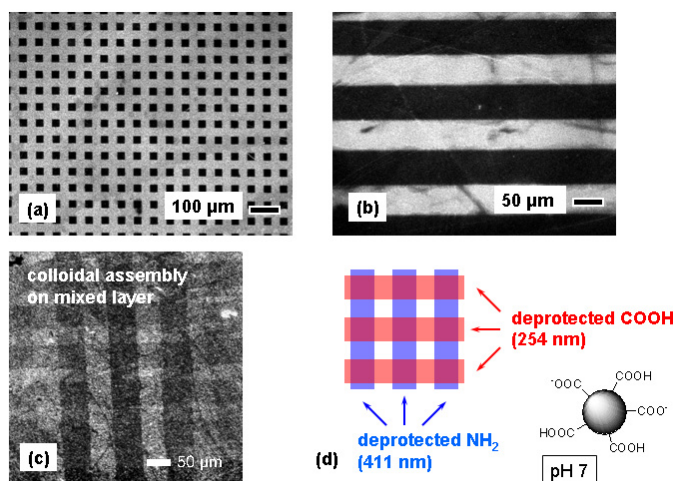
Figure 5.4: Optical micrographic images (dark field) of assembly patterns from carboxylated PBMA particles (diameter 183nm) adsorbed from aqueous suspension at pH=7 onto silane layers of (a) NVoc-protected NH_2 / NH_2; (b) Bzn-protected COOH / COOH irradiated through a mask; (c) shows a mixed layer of NVoc protected amino and Bzn protected carboxyl silane, irradiated at two different wavelengths (254nm and 411nm) through a 90°-rotated line masks for orthogonal deprotection (according to the color scheme in scheme d) [del Campo 2005].

Based on these methods, the synthesis procedures were modified to introduce an additional methyl group in the benzylic position (X_1 group in Figure 5.2, $X_1 = CH_3$) for the NVoc-protecting group. For convenience it is called here the CH_3-Nvoc group. As an electron-donating group, the methyl group activates the adjacent benzylic C atom for the formation of the 5 member ring. Furthermore, the benzyl ketone photoproduct is less reactive to imine formation than benzaldehyde, thus improving the yield of the liberated amine group and reducing the irradiation time with respect to the NVoc without the methyl group. In the present work, the protected functional groups are also extended to -NH_2, -COOH and -OH for the CH_3-NVoc group, and -NH_2 for the Bzn group.

The synthesis and characterizations of novel CH_3-NVoc and Bzn silanes is reported here. For this purpose, the possibility of using soft lithography for generating micro-scaled patterns of self-assembled monolayers (SAMs) by contact printing is explored. Efforts are being made to use direct monolayer photolithography [Ramrus 2004], which involves photo patterning of a light sensitive silane monolayer by irradiation of CH_3-

NVoc silanes through a mask at 411 nm using mask aligner, and of Bzn silane through a mask at 254 nm using a UV crosslinker.

5.2 Synthesis Approach

CH$_3$-NVoc:

Synthesis of CH$_3$-NVoc protected silanes with -NH$_2$, -COOH and -OH terminated groups was achieved in a four-step procedure (Figure 5.5). Commercially available 3,4-dimethoxy acetophenone was nitrated using standard nitration procedures. This was in turn converted to the corresponding alcohol in 96% yield. The unsaturated precursors with different length (n =1 or 9) of alkyl chains were obtained by chloroformylation, or Mitsunobu reaction. Further hydrosilylation of these precursors afforded the CH$_3$-NVoc protected -NH$_2$, -COOH and -OH silanes in around 60-70 % yield.
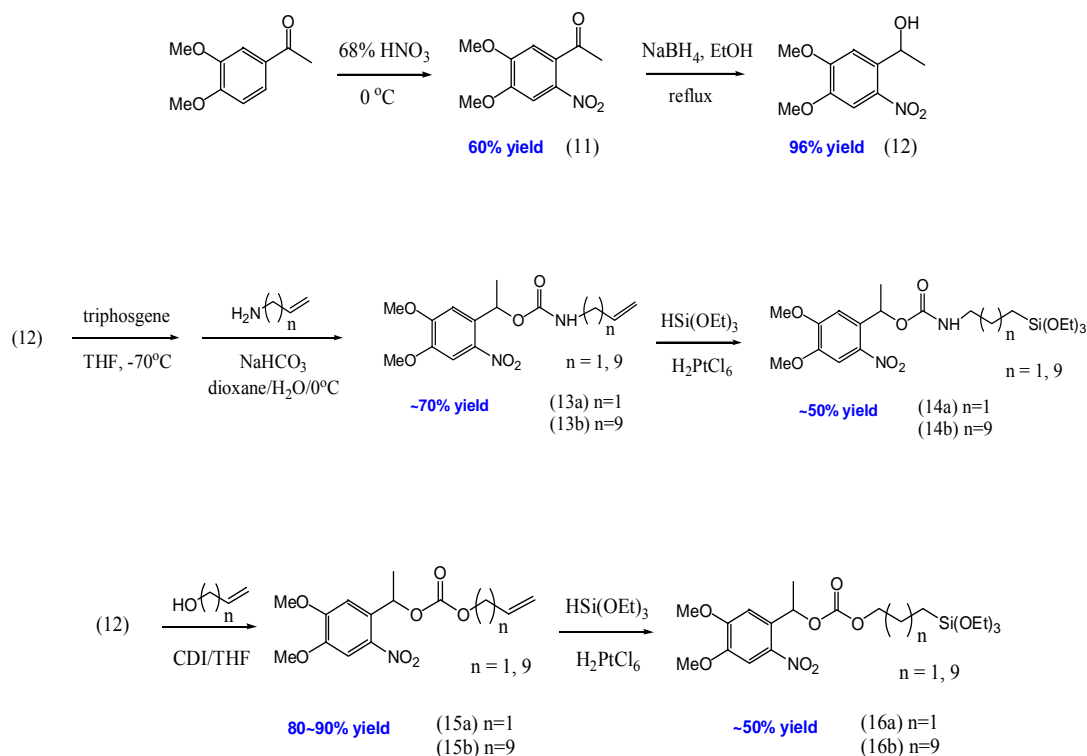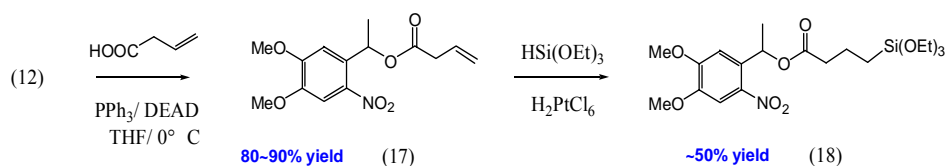
Figure 5.5: Synthesis of CH$_3$-NVoc protected -NH$_2$, -OH, and -COOH functional triethoxysilanes.

Benzoin:

The synthesis of the benzoin protected silane was carried out via a benzotriazole mediated conversion of benzaldehyde to a benzoin protected urethane bearing a double bond at the terminal position of the propyl chain for further hydrosilylation. This procedure involves first the activation of benzaldehyde with benzotriazole to yield an acyl anion equivalent **19** (Figure 5.6) that can then be easily lithiated and trapped with the electrophilic dimethoxybenzaldehyde during acid work-up [Katritzky 1995]. After chloroformylation of the aryl ketone, the last step involves the hydrosilylation of the double bond with triethoxysilane to yield the desired silane.
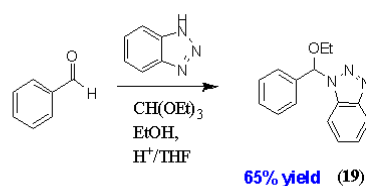
Figure 5.6: Synthesis of benzotriazole-activated benzaldehyde starting from benzaldehyde, benzotriazole, absolute ethanol, triethylorthoformate and catalytic amounts of sulfuric acid.

The next step was an benzoin condensation to yield the benzoin product (Fig. 5.7). In order for the condensation to occur lithiation of **19** with n-BuLi at -78°C and quenching with the electrophile had to be performed very fast in order to avoid partial decomposition of the resulting anion intermediate and hence low yields. Even though the product was stored under argon and below -10°C it was readily seen that its color had

changed from yellow to dark red. FD-mass spectrometry confirmed the decomposition of the product. Therefore the next reaction step had to be carried out as soon as the pure benzoin compound had been isolated. This step involved the urethane formation with the alcohol moiety **20** and allylamine (Fig. 5.7).
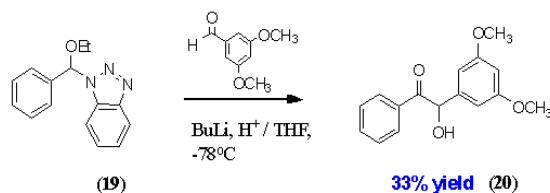
Figure 5.7: Synthesis of 3',5'-dimethoxybenzoin via lithiation of the benzotriazole derivate **19**.

Urethane formation of **20** was carried out by two steps, first chloroformylation of the hydroxyl group, followed by reaction with allylamine to obtain the urethane bearing a double bond at the terminal position of the propyl chain for further hydrosilylation (Figure 5.8a). Due to the highly toxic nature of phosgene gas, triphosgene was used as the substitute to perform the desired chemical transformation. The reaction requires only one third mole-equivalent of triphosgene compared to phosgene [Eckert 1987]. After purification by column chromatography in the dark, the pure compound of **21** was isolated and subjected to hydrosilylation with triethoxysilane to yield the desired photoprotected product (Figure 5.8b).

(a)

(b)
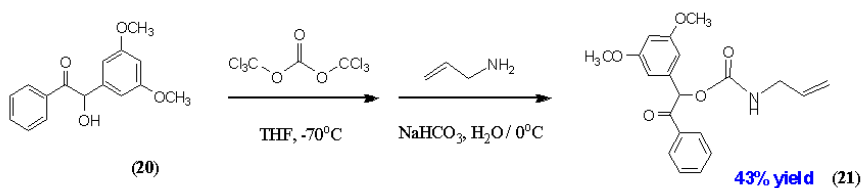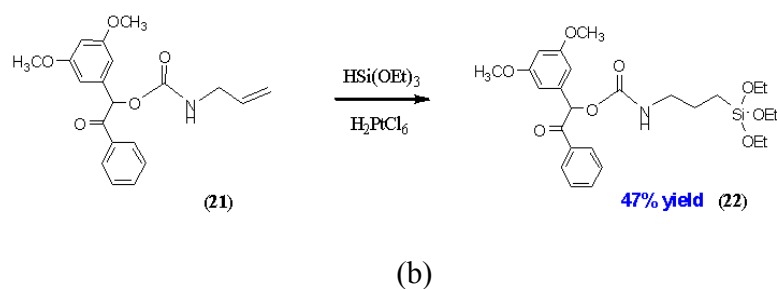
Figure 5.8: (a) Chloroformylation of the hydroxyl group by triphosgene, followed by reaction with allylamine to obtain the urethane bearing a double bond at the terminal position of the propyl chain; (b) Hydrosilylation with hexacholoroplatinic acid and triethoxysilane.

5.3 Time Dependent Irradiation and UV-Vis Measurement in Solution

In Figure 5.9 is presented the absorption spectrum of a 0.1 % solution of the R-CO-Me-NVoc compound in THF solution. This compound has an absorption maximum at ~280 nm corresponding to the carboxyl moiety and at ~350 nm due to the nitro group on the methoxy substituted benzene ring. For following the photocleavage process and its kinetics the solution was irradiated at 365 nm from a UV crosslinker and was monitored by UV-Vis spectroscopy. We observe that there is an increase of the absorbance for peak at ~265 nm and apperance of a new peak at ~390 nm. By UV irradiation, the nitro group is excited, intramolecular H abstraction occurs, and a nitroso derivative is formed [Ottl 1998] and these new absorption bands probably belong to the 3,4-dimethoxy-6-nitrosoacetophenone photoproduct [Braun 2003, Min 2005].
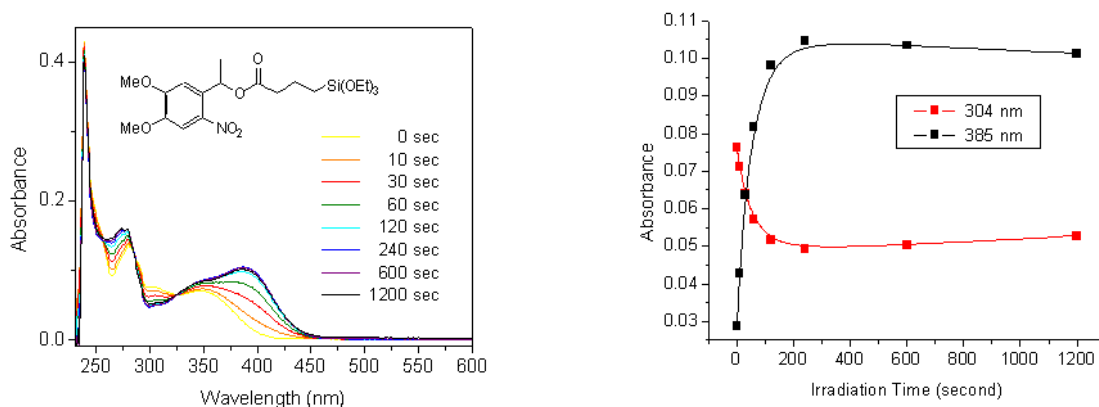
Figure 5.9: Kinetic research by UV-Vis spectroscopy of R-CO-Me-NVoc (CH$_3$-NVoc protected -COOH silane).

In Figure 5.10 is depicted the spectral evolution upon irradiation at 365 nm for the same compound in THF solution in acidic conditions (HCl) We also observe the appearance of a new peak at ~366 nm which is about 20 nm blue shifted with respect to the solution without catalyst. This might be due to the protonation of the photoproduct and thus not having exactly the same species in both cases. Besides this when comparing the absorbance evolution at the different pH it is observed that for the acidic conditions, the photoproduct is remarkably degraded after 20 minutes while for the other conditions after this irradiation time there is no significant evidence of degradation as it is extracted from the insets.
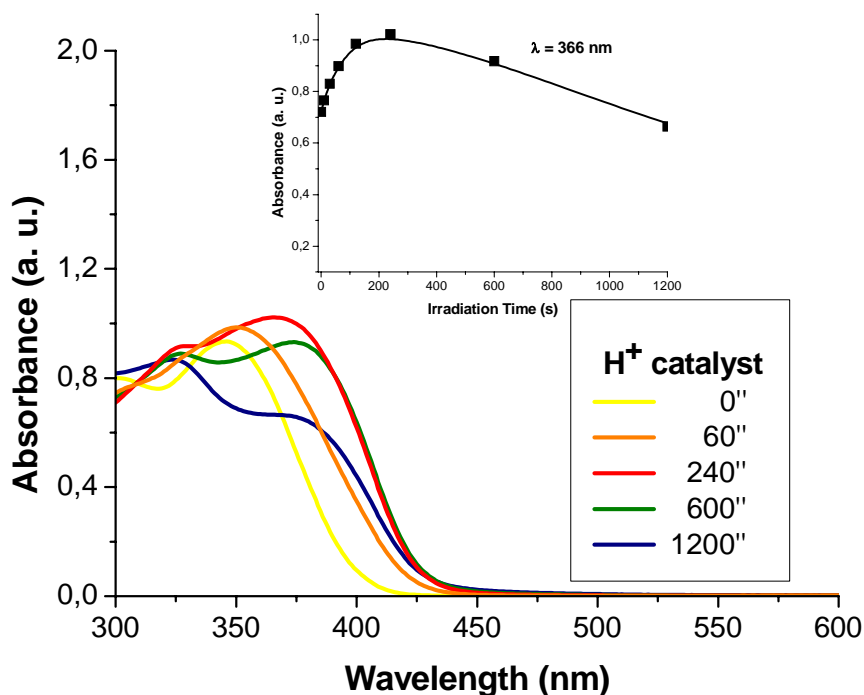
Figure 5.10: UV/VIS absorption spectra of the R-CO-Me-NVoc silane 0.1% wt solution in THF, irradiated at 365 nm with acidic catalyst.

In Figure 5.11 is presented the absorption spectrum of benzoin silane 0.1 % wt in THF solution. It has an absorption maximum at ~247 nm and at ~290 nm. The kinetics of the photocleavage of the benzoin silane upon irradiation of this solution at 254 nm from a UV crosslinker was monitored by UV-Vis spectroscopy. It shows a decrease at ~250 nm, an increase of the absorbance for the peak at ~290 nm and a new peak appears at ~304 nm corresponding to the photoproduct. This follows the same behaviour described in the literature for benzoin compounds [Sheehan 1971].
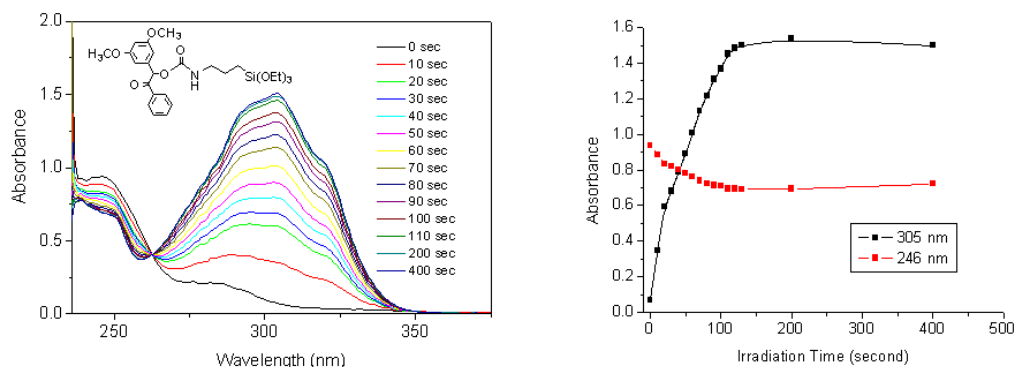
Figure 5.11: Kinetic research by UV-Vis spectroscopy of (a) CH₃-NVoc protected OH- silane; (b) benzoin protected amino silane in THF solution with the irradiation of 365nm and 254nm, respectively.

5.4 Surface Modifications and Characterizations

Bzn Protected NH₂ Silane:

Bzn silane was deposited onto silica and quartz substrates by solution phase silanization. The hydrolysis time for the triethoxysilanyl anchor group was optimized by measuring the water contact angle for each surface layer prepared after the given hydrolysis time. Figure 5.12a shows the time dependence of the water contact angle on Bzn silane surfaces. The samples were prepared in Bzn silane solution (1% w/w, THF) with different hydrolysis times and 1 hour of incubation. The result shows that the hydrophobicity increased with longer hydrolysis times, due to a more complete coverage of the substrate surface with the silane molecules. After about 120 minutes, the value of the water contact angle reached a maximum plateau, which indicates that the hydrophilic silica substrate surface was completely covered by hydrophobic Bzn functionalities. Figure 5.12b shows the layer thickness (~0.4 nm) of the Bzn SAM with 2 hours of prehydrolysis and 1 hour of incubation (investigated by ellipsometry), which fits well with the expected monolayer thickness. Further more, after the substrate was irradiated by UV light at 254 nm for 2 minutes and followed by sonication of 10 minutes in THF, the thickness reduced about 0.1 nm to 0.3 nm nominal thickness. This phenomenon could be explained by that the Bzn protecting groups were released from the surface.

(a)   **(b)**
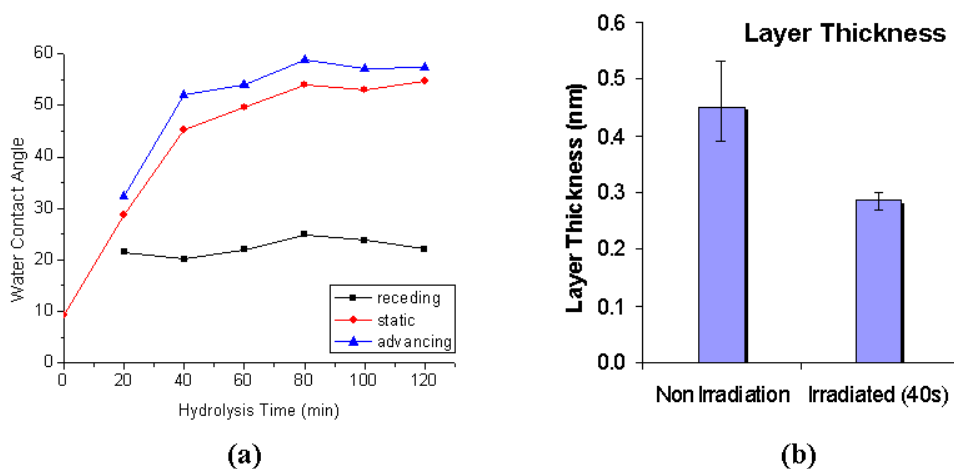
Figure 5.12: (a) Increase of hydrophobicity of Bzn silane modified surfaces as a function of hydrolysis time of the silane solution as visualized by an increase of the water contact angle (incubation time was fixed as 60 minutes); (b) layer thickness of the Bzn silane SAM before and after the irradiation at 254 nm.

CH$_3$-NVoc Protecting Silanes:

By the vapour phase deposition process, it is possible to obtain a monolayer of the CH$_3$-NVoc silanes on silica or quartz substrate. A covalent attachment of the silane to the substrate is achieved as the trimethoxysilane anchor groups hydrolyse directly at the substrate surface by interaction with surface OH-groups and residual trace of adsorbed water molecules, and form a siloxane network structure with the silanol groups from the substrate. In Figure 5.13 presents the spectrum of a SAM prepared by the vapor deposition procedure, after solvent rinsing before and after UV irradiation. It clearly shows that the deprotection also takes place with SAMs of the CH$_3$-NVoc silane on quartz similar to the solution photoreaction. Upon irradiation new bands appear in the spectrum at ~270 and ~380 nm, indicating also similar decomposition products of CH$_3$-NVoc in comparison with the liquid phase reaction.
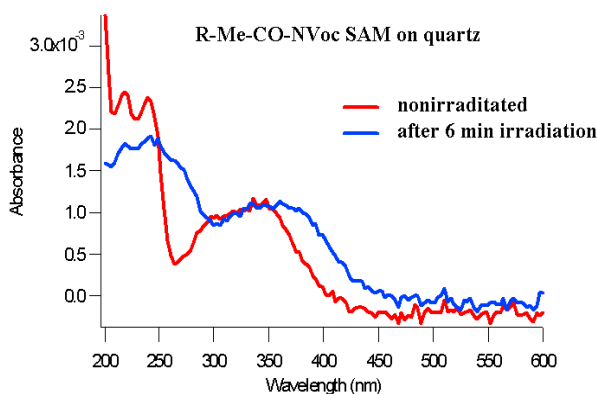
Figure 5.13: UV-Vis spectra of the R-CO-Me-NVoc silane monolayer on a quartz substrate before and after irradiation. Upon irradiation new peaks appear due to the formation of new species with the CH_3-NVoc deprotection.

To check the topography of the surfaces after the silane deposition, the films were characterised using AFM (tapping mode). As can be observed in Figure 5.14a (left), the substrate is covered by silane "islands", which are removed after rinsing several times with ethanol. After rinsing a smooth surface of silane monolayer is obtained (Figure 5.14a right), indicating that the silane aggregates weakly bound by physisorbtion on the SAM have been removed. To the same conclusion lead the absorption spectra depicted in Figure 5.14b, where the absorption decreases and it remains constant during several posterior rinsing steps.
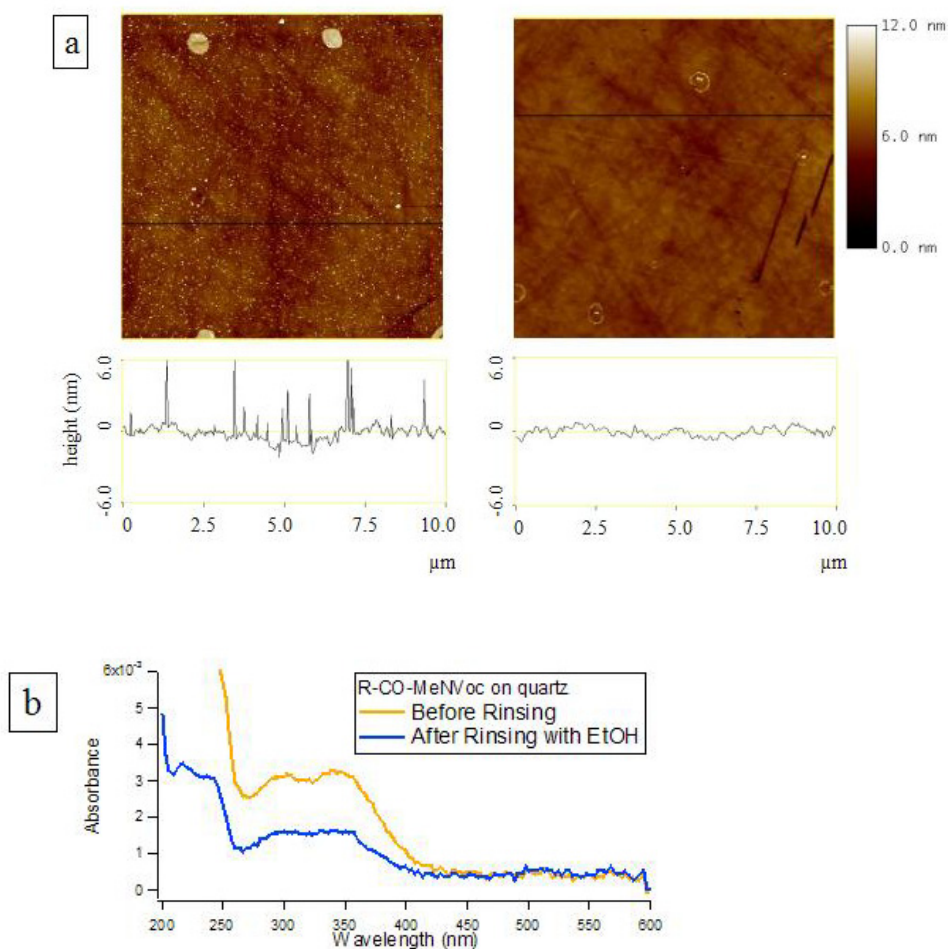
Figure 5.14: (a) Atomic force microscope images (10×10 μm^2) and height profiles (along the indicated horizontal line) of a silane vapor deposited sample before (left) and after (right) rinsing. (b) Absorption spectra of the film without and with rinsing treatment. After several rinsing steps the absorbance remains constant.

The thickness of each monolayer was measured by ellipsometric measurements and was found to be about 1.4 nm which is in complete accordance to the values found for these types of molecules [del Campo 2005]. The static water contact angle for the R-CO-Me-NVoc was around 65º for the NVoc surface. After deprotection and ethanol rinsing of the photoproduct, the value decreased slightly, indicating liberation of the more polar carboxyl groups.

5.5 Water Condensation Patterns on Site-selectively Irradiated Surfaces

Based on the proofs of photo-deprotection in solution phase, patterning of the CH_3-NVoc and Bzn modified surfaces were undertaken by photolithographic irradiation through gold masks at appropriate wavelengths. Due to the change of the contact angle by the photoreaction during the irradiation process (described above), it is possible to visualize the patterns by water condensation, as there are regions with different hydrophilicities. In Figure 5.15 represents the water condensation patterns for samples with CH_3-NVoc and Bzn protected -NH_2 monolayers. The samples were exhaled while cooling down with dry ice and immediately observed under an optical microscope. For the Me-NVoc silanes (figure 5.15a), the water tends to condense in the irradiated areas corresponding to the more hydrophilic groups. In the pattern for the sample with benzoin silane, regions with different droplet sizes appear. The bigger ones correspond to the more hydrophilic regions, i.e. irradiated areas (inset in figure 5.15b).

(a)   (b)
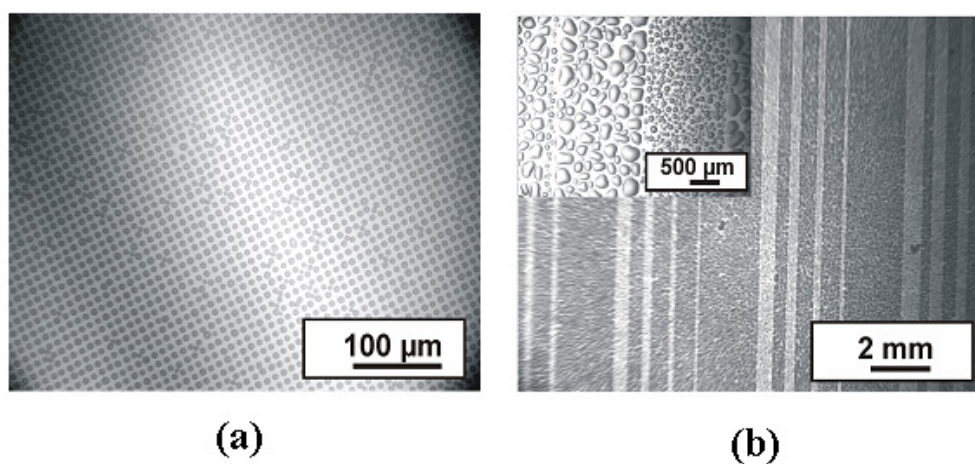
Figure 5.15: Optical microscope images of water condensation the SAM surfaces: (a) the sample of the CH_3-NVoc protected -NH_2 silane layer was irradiated with a mask aligner at 365 nm through a mask illuminating 5×5 μm^2 squares. The darker dots are the regions still covered by CH_3-NVoc groups. (b) The sample with the Bzn protected -NH_2 silane layer was irradiated with a crosslinker at 254 nm through a mask with alternating gold stripes. The darker stripe regions are non-irradiated.

5.6 Colloidal Assembly on Site-Selectively Irradiated Surfaces

By tailoring the surface functionalities, it allows colloidal particles to selectively self-assemble on silane layer patterns and thus study mesoscale assembly in a model system [Lee 2002, Tieke 2001]. Selective self-assembly of colloidal particles at surfaces due to attractive electrostatic interactions has become very popular in recent years. The ability to harness intrinsic interactions between surfaces leads to novel and elegant methods for self-organised deposition of colloidal particles, where the driving forces are electrostatic interactions, surface tension, Van del Waals forces, and capillary forces. These interactions between the particles and the surface can be tuned by modifying the pH conditions and the particle structure, and therefore it is possible to control the preferred region of colloidal deposition, so that 2D or even 3D structures can be created by controlling these forces [Im 2002, Burmeister 1999]. Hence, another approach to characterize the photopatterned silanes on quartz substrates in our work was by colloidal particle deposition.

For the particle assembly of the colloidal particles on the patterns, the substrates were completely immersed into a suspension with 1-3% solid content and were vertically lifted from the solution as shown in Figure 5.16 [Cheng 2006, Fustin 2003, Fustin 2004]. The patterns with the colloids were characterized by optical microscopy, scanning electron microscopy and atomic force microscopy.
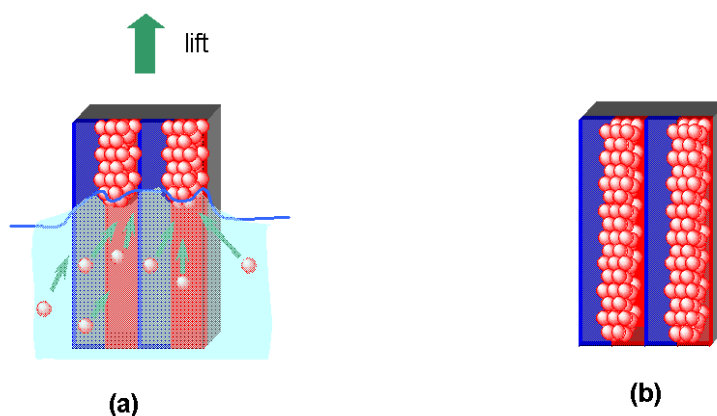
Figure 5.16: Fabrication scheme for the site-selective colloidal deposition: (a) after a photolithography process the substrate with a patterned silane layer is vertically lifted from a colloidal suspension, and the colloidal particles are preferrably to depositing on the photodeprotected region due to capillary forces and favourable interactions between the particles surface and the deprotected functional groups; (b) after the drying process, the colloidal particle patterns are obtained.

The influence of particle functionalities and pH effect on the assembly process on patterned R-CO-Me-NVoc (abbreviated term for Me-NVoc protected carboxylic silane) samples was studied by using PMMA-NH$_2$ (abbreviated term for amidine-modified polymethylmethacrylate particles) and PS-NH$_2$ particles (quaternary amine functionalised polystyrene amidine modified colloids) at pH 3/4 (respectively) and pH 6.

In the present work, amidine-modified polymethacrylate particles (PMMA-NH$_2$, ϕ = 250 nm) were obtained according to the procedure described in Cheng's article [Cheng 2006]. Quaternary amine functionalised polystyrene amidine terminated colloidal particles (PS-NH$_2$, ϕ = 130 nm) were prepared according to a modified synthesis of Vancso and coworkers [Dziomkina 2006]. Silica particles (ϕ = 15 nm) were purchased from Akzo Nobel. The patterns with the colloids were characterized by optical microscopy, scanning electron microscopy and atomic force microscopy.
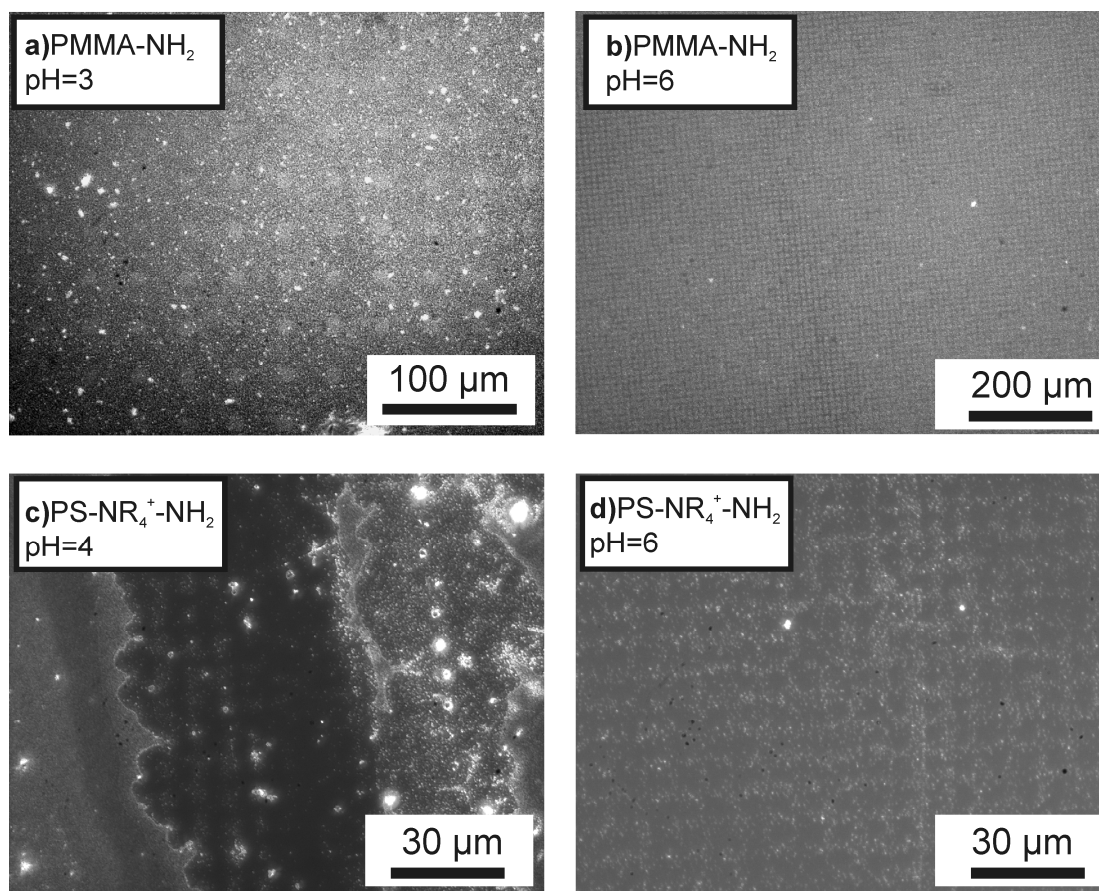
Figure 5.17: Dark field optical microscopy images of R-CO-Me-NVoc patterns with PMMA-NH$_2$ and PS-NH$_2$ colloids deposited by a vertical lifting deposition from aqueous solutions at pH ca 3.5 and pH 6.

PMMA-NH$_2$ colloids:

In Figure 5.17a and b are presented the dark field optical microscopy images for the patterned samples of R-CO-Me-NVoc decorated with PMMA-NH$_2$ particles at pH 3 and pH 6 respectively. The brighter squares that correspond to the irradiated areas (carboxyl groups) have a higher scattering density, indicating a much denser particle population for both pH conditions. The pattern obtained at pH 3 is more difficult to perceive due to the low contrast in particle density between both regions. The nature of the interactions between the carboxyl and the amidine groups in the colloidal particles are polar and hydrogen bonding interactions.

PS-NH$_2$ colloids:

The patterned R-CO-Me-NVoc samples with PS-NR$_4^+$-NH$_2$ particles are shown in

78

Figure 5.17c and d. At pH 4 the colloids go preferentially to the irradiated areas observed in the case of PMMA-NH$_2$. Surprisingly at higher pH (pH 6) the PS particles go to the protected NVoc regions, but for this behaviour we have currently no explanation.

Silica particles:

For checking if the characterisation of the patterns could also be done with much smaller particles, silica spheres of 15 nm of diameter were used. Silica particles close to neutral pH conditions usually carry hydroxyl surface group from the preparation process. The experiments were conducted for R-CO-Me-NVoc and R-NH-Me-NVoc patterned SAMs with aqueous silica solutions at pH ~6.5, and the experimental procedure for deposition was the same vertical lifting deposition method as described for the previous systems. For both kinds of silanes, the silica particles do attach with a high selectivity to the irradiated areas (pattern with R-NH-Me-NVoc shown in Figure 5.18). At the working pH the particles are not charged (pKa ~7.5) and therefore polar and hydrogen bond interactions would be the driving forces for the interactions.
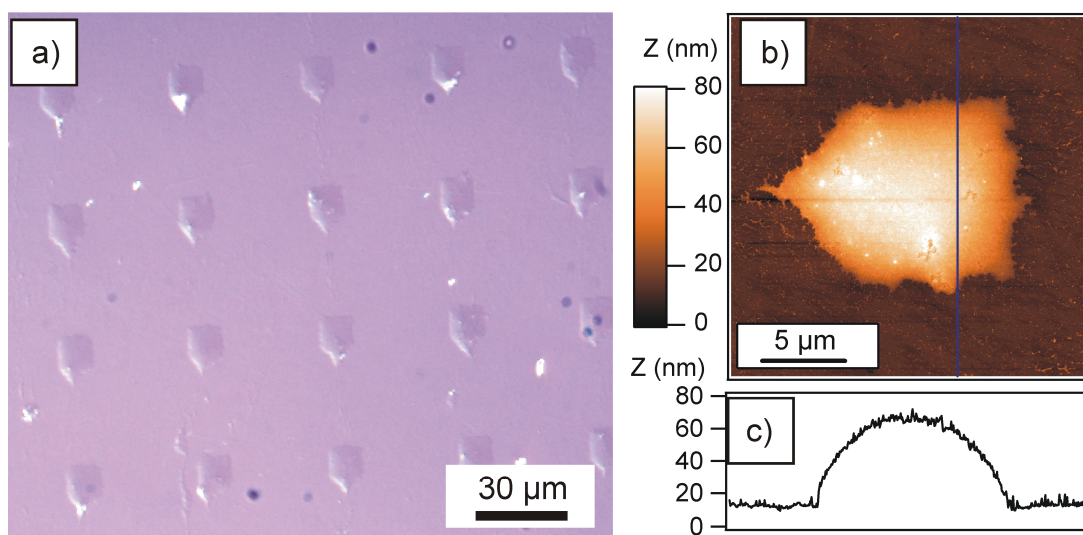
Figure 5.18: (a) Optical microscopy image of a patterned R-NH-Me-NVoc sample with silica particles (ϕ = 15 nm) deposited by a vertical lifting deposition at pH ~6.5; (b) AFM topography and (c) section profile of one of the squares with the silica particles.

In Figure 5.18, a new feature due to the colloidal deposition method can also be

observed: a "tail" in the square appears in the vertical lifting direction due to the fact that the water drop has this shape in the drying process.

5.7 Fluorescence Labelling of Silane Patterns

Since the irradiation experiments were supposed to yield active -COOH, -OH and -NH_2 groups, their presence had to be verified. A common and well known method is fluorescence staining by specific interaction or reaction with fluorophore dyes. The presence of a fluorescence pattern with the geometry of the irradiation mask would be indicative of the successful liberation of the expected functional group during photodeprotection.

5.7.1 Fluorescence Dyes

In order to visualize the patterns by means of fluorescent dyes, two different dye structures ATTO 635 and Alexa Fluor 488 (AF488) in aqueous solutions were used (as shown in Figure 5.19). The patterned SAM films were immersed in different dye solutions between 1 to 10 minutes, then washed intensively with the solvent and were visualized by confocal laser scanning fluorescence microscopy using the excitation lines of 488 nm for AF488 and 635 nm for ATTO635 according to the excitation maximum for each dye. In both cases the contrast has been adjusted to see the image better.

(a) ATTO 635   (b) Alexa Fluor 488
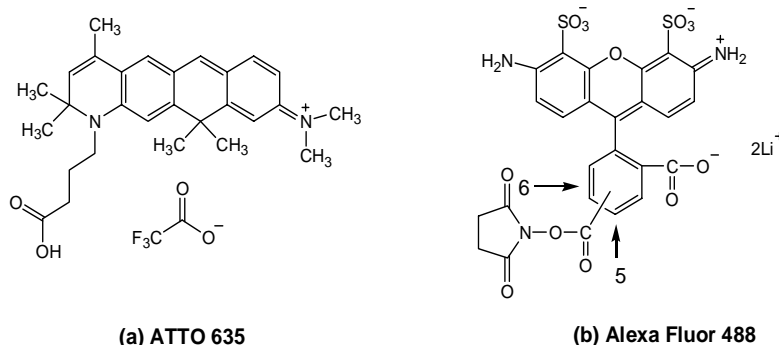
Figure 5.19: Structures of fluorescence dyes (a) ATTO 635; (b) Alexa Fluor 488 for carboxylic acid coupling.

5.7.2 Results

In Figure 5.20, the fluorescent patterns of the R-CO-Me-NVoc silane with the different dyes used are presented. The squares in both figures correspond to the regions that were irradiated with the mask aligner. The adsorption of the dyes to the carboxyl moieties (irradiated areas, the squares in the figures) or to the NVoc groups (non irradiated areas) can be controlled by playing with the dye structures. In the case of the sample decorated with ATTO 635 (Figure 5.20 left), the higher fluorescence signal corresponds to the irradiated areas, whereas for the sample decorated with AF488 (Figure 5.20 right), the higher intensity corresponds to non-illuminated regions. These results might mean that the main driving force in the process studied is the electrostatic interactions. When a dye with a positive core as ATTO 635 is used, it mainly directs to the negative parts of the monolayer, i.e. to the irradiated areas. When the chosen dye has a negative core, as in the case of Alexa Fluor 488, electrostatic repulsion with the carboxyl groups on the surface are present and there is a low amount of dye in the deprotected area. The presence of dye in the Me-NVoc domains indicates that there is non-specific adsorption due to polar and aromatic interactions.
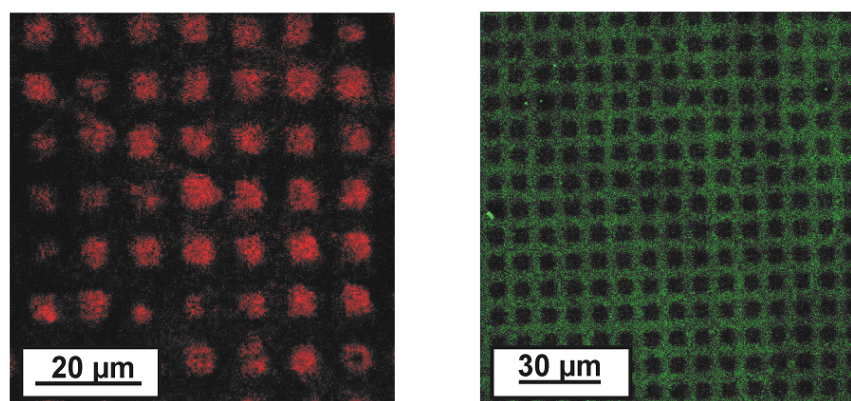
Figure 5.20: Fluorescence microscopy images of patterned SAMs of R-CO-Me-NVoc silane labelled with ATTO 635 (left), and Alexa Fluor 488 (right).

5.8 Discussion and Summary

In summary, the synthesis, characterization and surface modification of CH_3-NVoc silanes terminated with -OH, -COOH and -NH$_2$ functionalities, and a Bzn-protecting silane with a -NH$_2$ functional group is demonstrated. Selective adsorption of colloidal particles from colloidal suspensions onto the hydrophilic patterns in the deprotected regions after mask irradiation was possible due to the directing influence of the liberated functional groups. Particles of different diameters ranging from few hundred nanometers to smaller colloidal particles could be deposited by this method. Photodeprotection of CH_3-NVoc silane was possible at lower wavelengths than NVoc silanes previously reported [del Campo 2005] and less irradiation time required.

Chapter 6

Experimental Section

6.1 General

All chemicals and solvents were purchased from Acros Organics (B-2440 Geel), Fluka Chemie AG (D-82024 Taufkirchen), ABCR (D-76189 Karlsruhe), Fisher Scientific UK Ltd. (GB-Loughborough, Leics. LE11 5RG), Merck KGaA (D-64271 Darmstadt), Riedel-de-Haen (D-30926 Seelze) and Sigma-Aldrich Chemie GmbH (D-89555 Steinheim), with p.a. purity, and were used as received (unless stated otherwise). Solvents were dried over molecular sieves (4 Å) or with known literature procedures.

Chromatography:

Preparative column chromatography and flash column chromatography were carried out using Merck silica gel (63-200 μm) and (43-63 μm), respectively. Analytical thin layer chromatography was carried out using Merck silica gel G/UV$_{254}$ using a UV

lamp, potassium permanganate solution, and "Bromocresol Green" solution to visualize the components. Preparative thin layer chromatography was carried out with TLC plates (20cm×20cm, 2mm layer thickness, SIL G-200 UV_{254}) purchased from Macherey-Nagel, Germany.

"Bromocresol green solution": 0.04g of commercial "Bromocresol green" powder was dissolved into 100mL of ethanol. NaOH solution (0.1N) was added by titration till the solution turned to green.

Melting Point:

Melting points were measured with a semi-automatic melting point apparatus Büchi B-545.

Mass Spectra:

Mass spectra were recorded with Field Desorption (FD) using a ZAB 2-SE-FPD from VG-Instruments.

NMR Measurement:

Solution ^{1}H-NMR and ^{13}C-NMR spectra were measured on a Bruker Spectrospin 250. All measurements were done at room temperature, referenced to TMS (δ = 0ppm) and calibrated by the deuterated solvent. The chemical shifts are given in parts per million and the coupling constants in Hz. The following abbreviations are used in this thesis: s-singlet, t-triplet, q-quartet, m-multiplet, br-broad.

IR Spectra:

Infrared spectra were measured on a Perkin Elmer Paragon 1000 FT-IR spectrometer. The wavenumbers are given in cm^{-1} and the following abbreviations are

used: br-broad, s-strong, w-weak.

UV-Vis Spectra:

UV-Vis spectra were recorded on Perkin Elmer L9 UV-Vis NIR spectrometer, and the axes were denoted with wavelength (nm) and relative absorbance.

Contact Angle Microscopy:

For contact angle measurements a Drop Shape Analysis System DSA 10 by Kruess, Germany was used, combined with a CCD camera for image capturing.

Optical Microscopy:

Optical microscopy images were recorded on a Zeiss Axioscope with reflected light microscopy (HBO lamp) with a digital camera (Zeiss AxioCam), which was attached to the microscope.

Atomic Force Microscopy:

All the images in this thesis were recorded under ambient conditions by a MultiMode Atomic Force Microscope Dimension 3100 connected to a NanoScope IIIa controller. The microscope was operated in tapping mode. The substrates to be measured had a size of $2cm \times 1cm$ and were sucked onto the sample holder by vacuum.

Ellipsometry:

The thickness of the SAMs was measured on a Nanofilme Ellipsometer made by Nanofilm Technologie GmbH. The wavelength of the incidence laser beam was 532nm, with 70° as the incidence angle. The refracted indices of silicon substrate and the SiO_2 layer on the surface were assumed $n(Si) = 4.17$ and $n(SiO_2) = 1.46$, respectively.

Confocal Microscopy:

The microscope used was a commercial LSM setup manufactured by Carl Zeiss (Jena, Germany) consisting of the module LSM 510 and the inverted microscope model Axiovert 200. The types of laser included an Argon laser (457nm, 488nm, 514nm with an output power of 3mW, 10mW, and 15mW, respectively), a green He/Ne laser (543.5nm, 1mW) and a red He/Ne laser (632.8nm, 5mW). Two objective lenses were used; namely a ZEISS Plan-Neofluar (with $20\times$ magnification and a numerical aperture of 0.5), and a ZEISS C-Apochromat (with $40\times$ magnification and a numerical aperture of 1.2).

Kinetic Experiments:

The conditions in the NMR tube were the same as in a real hydrolysis experiment. This means that a 1% solution of the silane in deuterated THF was made up to which the catalyst was added just before the NMR measurement. It was thus possible to calculate from the liquid 1H-NMR spectrum the percentage of transformation of the ethoxy CH_2 and CH_3 peaks into free ethanolic CH_2 and CH_3 peaks, which were formed upon hydrolysis of the ethoxy substituents attached to the silicon atom.

6.2 Silane Deposition on Silica Substrate Surfaces

Silica wafers (2cm$\times$1cm), provided by Waker Siltronic with a 1.6 nm native oxide layer, were placed into a fresh Piranha solution (conc. H_2SO_4 / 30% H_2O_2 = 7:3 v/v) for 1 hour at 80°C for cleaning and then rinsed with copious amount of Mili-Q water (R = 18MΩ·cm), and were blow dried in a stream of nitrogen.

6.2.1 Solution Phase Silanization

Butyl silane (**2**), succinimidyl silane (**4**), maleimide silane (**6, 8**) were prehydrolised

as a 1 wt% solution in THF for 1 hour. Alkyne silane **(10)** was prehydrolised as a 1 wt% solution in THF with the presence of 0.1 wt% of 1N HCl for 1 hour. After filtration of the hydrolised solutions through 0.2μm PTFE (Teflon) filter, the clean substrates were then immersed into the silane solution for 1 hour. After deposition the substrates were gently rinsed with THF and then tempered at 80°C for 1 hour in a vacuum oven. They were sonicated in an ultrasonic bath in the sequence of dichloromethane, dichloromethane /methanol, and methanol for 10 minutes each to remove any unspecifically adsorbed silanes and then blown dry in nitrogen stream for further use.

3',5'-Dimethoxybenzoin silane **(22)** was prehydrolised as a 2 wt% solution in THF for 2 hours, and filtrated through a 0.2μm PTFE (Teflon) filter. The clean substrates were then immersed into the silane solution for 1 hour, then rinsed gently with THF, baked at 95°C for 1 hour in a vacuum oven. Finally the substrates were sonicated in the sequence of dichloromethane, dichloromethane/methanol, and methanol for 10 minutes each.

6.2.2 Vapor Phase Silanization

Monolayers of CH_3-NVoc silanes **(14a, b; 16a, b; and 18)** were obtained by vapor phase deposition technique. Clean substrates were exposed to vapors of silanes at room temperature using ambient pressure and afterwards baking at 100°C overnight, rinsed with ethanol and Milli-Q water and dried with a N_2 stream.

Passivation Process of Glassware

In this thesis, vapor phase silanization was used for the passivation processe of the glassware with hexamethyldisilazane (HMDS). The mechanism of this reaction is shown in figure 6.1.
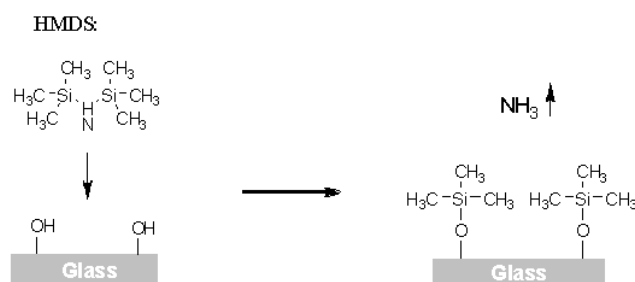
Figure 6.1 Reaction of HMDS at the glass surface.

Upon the reaction with the silanol groups at the glass surface, the HMDS molecule is cleaved, and trimethylsilyl groups are covalently bounded to the surface, with ammonia being released. HMDS has a reasonably low boiling point and a high vapor pressure (129°C, 1024 mbar; at room temperature 26.6 mbar). It is thus possible to perform the vapor phase silanization at room temperature and ambient pressure for 30 minutes. The resulting contact angle was 74°, which is characteristic for non-polar, hydrophobic trimethylsilyl groups at the silica surface [Fadeev 1999].

6.2.3 Micro-contact Printing

Preparation of PDMS stamps:

40g of Sylgard 184 (PDMS) was taken in a beaker. 4g of Sylgard 184 curing agent was added and stirred vigorously till bubbles rise. This mixture was then degassed by keeping it in a desiccator using argon/vacuum. It was left in the desiccator for 20 minutes till all the bubbles were gone. Masters for microcontact printing were taken in a petri dish and the above mixture was poured over it (approximately 2 mm above the master). It was then kept in the oven for curing overnight (for harder stamps) at 70°C.

After removing the masters with PDMS from the oven, they were separated by using a sharp scalpel. The stamps were cleaned with Milli-Q water, N_2 stream and then O_2 plasma for 1 minute (to avoid back pattern transfer). Stamps were dipped in the stamping solution or to be stamped was placed on the top of the stamp, when it was

allowed to dry with a stream of N_2. The coated stamps were placed on the substrate (previously cleaned with O_2 plasma) and a slight pressure was applied. After removing the stamps, they were rinsed with Milli-Q water, N_2 stream was passed and the patterns were characterized by AFM. Patterns of nano- and micrometer scales were obtained. Most of the experiments were carried out in a clean room, but experiments carried out in normal laboratory conditions were also successful.

The CH_3-NVoc silanes are found to be good candidates for creating micro and nanometer patterns with micro-contact printing. Silanes synthesized and used in this work are CH_3-NVoc silanes with $-NH_2$, -COOH and -OH terminated functionalities. The micro contact printed SAMs were characterized by scanning probe microscopy. Patterns were obtained from 870 nm to 8 μm. Details of the experimental procedure of microcontact printing are given in the previous chapters.

6.2.4 Photolithography

UV crosslinker with 2.8 mW cm^{-2} (365 nm):

CH_3-NVoc silanes were photodeptotected using this crosslinker in solution as well as on surface.

Mask aligner (365 nm):

CH_3-NVoc silanes (**14a, b; 16a, b; and 18**) were irradiated through a photolithography mask with the mask aligner to create patterns of activated and non-activated areas with the shape of the mask. Benzoin silane (**22**) was not irradiated through with a mask aligner, as there was no possibility of switching the wavelength to 254 nm, which is required for the deprotection of these silanes.

UV crosslinker with 3 mW cm^{-2} (254 nm):

Benzoin silanes were photodeptotected using this crosslinker in solution, on surface (with and without the mask) for creating the patterns.

After irradiation, the substrates were rinsed with ethanol and Milli-Q water, dried with nitrogen stream and kept in the dark until labelling them with fluorescent dyes. Series of fluorescent dyes were used.

6.3 Synthesis of the Compounds

6.3.1 Synthesis of tert-butyl 11-(triethoxysilyl)undecanoate (2)

tert-Butyl undec-10-enoate (1)

(1) [240.38] 23%
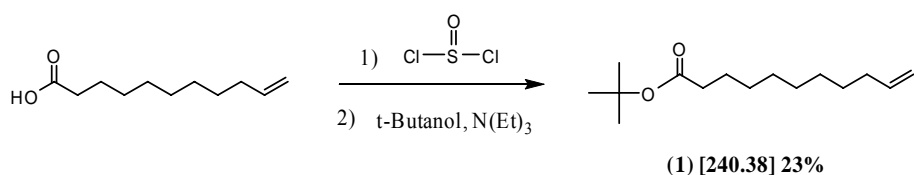
8.57g (72mmol) of thionyl chloride was added dropwise to 11.04g (60mml) of 10-undecenoic acid. The mixture was refluxed gently for 1 hour in the hood (since HCl (g) was produced), and cooled to room temperature. The mixture was added to a mixture of 2.96g of tert-butanol, 4.55g of triethylamine, and 30mL of THF at 0^oC over a period of 2 hours. After 15 hours at room temperature in Ar atmosphere, the insoluble triethylamine hydrochloride was removed by filtration. The filtrate (THF phase) was concentrated at reduced pressure, and washed by deionized water for 2 times, dried by $CaCl_2$. The crude product was distilled in vacuum and 1.12g of colourless viscous liquid **(1)** was obtained at 70~71^oC, 9.1×10^{-3}mbar. The yield was 23%.

^{1}H-NMR spectrum (250 MHz, CDCl$_3$) δ [ppm]: 1.27 (b, 10H), 1.42 (s, 9H), 1.55 (m, 2H), 2.00 (q, 2H), 2.18 (t, 2H), 4.93 (m, 2H), 5.77 (m, 1H) ppm;

^{13}C-NMR spectrum (62.5 MHz, CDCl$_3$) δ [ppm]: 25.09, 26.10, 28.88, 29.08, 29.23, 29.30, 33.79, 35.59, 79.87, 114.12, 139.18, 173.33 ppm;

IR spectrum (wavenumber): 3075cm^{-1} (alkenyl "C-H" stretches), 2977~2854cm^{-1} (alkyl "C-H" stretches), 1731cm^{-1} (ester "C=O" stretches), 1641cm^{-1} (alkenyl "C=C" stretches), 1366~1151 cm^{-1} (alkyl "C-H" bending vibrations).

FD-MS (m/z):241.6 (M^{+}).

tert-Butyl 11-(triethoxysilyl)undecanoate (2)

(1)   (2) [404.66] 31%
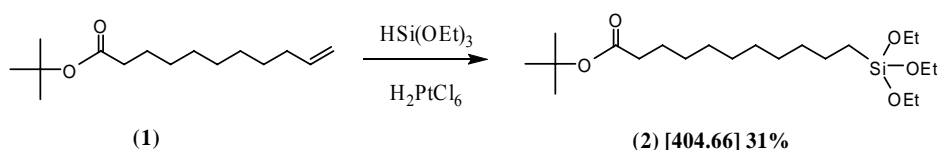
0.41g (2mmol) of tert-butyl undec-10-enoate **(1)** was dissolved in 3.29g (20mmol) of triethoxysilane followed by 8 drops of H$_2$PtCl$_6$/iso-propanol solution (20mg H$_2$PtCl$_6$ in 1mL iso-propanol). The mixture was heated to 80°C in Ar atmosphere for 14 hours and cooled down to room temperature. The excess of triethoxysilane was eliminated under vacuum. The residue was purified by column chromatography (Si-gel, eluent: dichloromethane) and 0.25g of colourless viscous liquid **(2)** was obtained (Rf = 0.6, dichloromethane). The yield was 31%.

^{1}H-NMR spectrum (250 MHz, CDCl$_3$) δ [ppm]: δ (ppm) 0.61 (t, 2H), 1.18~1.24 (m, 23H), 1.42 (s, 9H), 1.55 (m, 2H), 2.18 (t, 2H), 3.78 (q, 6H) ppm;

^{13}C-NMR spectrum (62.5 MHz, CDCl$_3$) δ [ppm]: 10.46, 18.39, 22.84, 25.21, 28.21, 29.19, 29.32, 29.39, 29.57, 33.26, 35.72, 58.38, 79.97, 173.46 ppm;

IR spectrum (wavenumber): 2973, 2925, 2854, 1731, 1366, 1076, 955, 785 cm^{-1}.

FD-MS (m/z):405.9 (M^{+}).

6.3.2 Synthesis of 2,5-dioxopyrrolidin-1-yl 11-(triethoxysilyl)undecanoate (4)

2,5-Dioxopyrrolidin-1-yl undec-10-enoate (3)

(3) [281.35] 71%
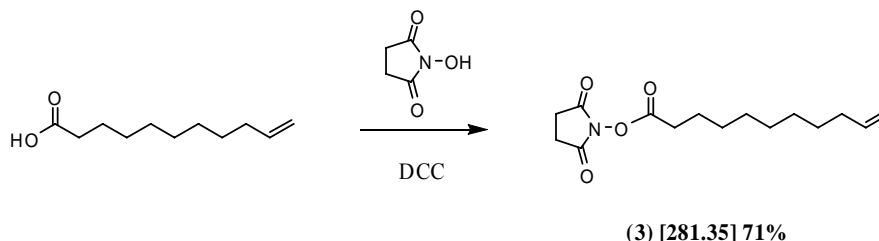
0.92g (5mmol) of 10-undecenoic acid was added to the solution of 0.58g (5mmol) of N-hydroxysuccinimide (NHS), 2.06g (10mmol) of N, N'-dicyclo hexylcarbodiimide (DCC) in 30mL of dry dichloromethane. The mixture was stirred in Ar atmosphere for 12 hours. The resulting suspension was filtrated to remove the precipitated urea (DCU). The filtrate was purified by column chromatography (Si-gel, eluent: dichloromethane), and 1.00g of white crystalline solid (3) was obtained (Rf = 0.4, dichloromethane). The yield was 71%.

Melting point: 57.4°C

^{1}H-NMR spectrum (250 MHz, CDCl$_3$) δ [ppm]: 1.29~1.26 (m, 10H), 1.73 (m, 2H), 2.01 (q, 2H), 2.59 (t, 2H), 2.82 (s, 4H), 4.94~5.01 (m, 2H), 5.78 (m, 1H) ppm;

^{13}C-NMR spectrum (62.5 MHz, CDCl$_3$) δ [ppm]: 22.48, 23.52, 26.67, 26.78, 26.92, 26.94, 27.09, 31.69, 112.08, 137.09, 166.61, 167.10 ppm;

IR spectrum (wavenumber): 3077cm^{-1} (alkenyl "C-H" stretches), 2922~2852cm^{-1} (alkyl "C-H" stretches), 1816~1786 cm^{-1} (succinimidyl "C=O" stretches), 1724cm^{-1} (ester "C=O" stretches), 1641cm^{-1} (alkenyl "C=C" stretches), 1379~1068 cm^{-1} (alkyl "C-H" bending vibrations), 863~652 cm^{-1} (succinimidyl "C-H" bending vibrations).

2,5-Dioxopyrrolidin-1-yl 11-(triethoxysilyl)undecanoate (4)

(3)   **(4) [445.62] 76%**
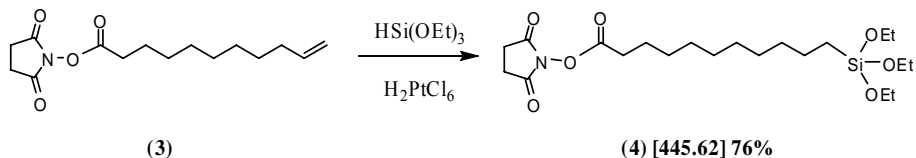
0.28g (1mmol) of 2,5-dioxopyrrolidin-1-yl undec-10-enoate **(3)** was dissolved in 1.64g (10mmol) of triethoxysilane followed by 8 drops of H_2PtCl_6/iso-propanol solution (20mg H_2PtCl_6 in 1mL iso-propanol). The mixture was heated to 80°C in Ar atmosphere for 14 hours and cooled down to room temperature. The excess of triethoxysilane was eliminated under vacuum. The residue was purified by column chromatography (Si-gel, eluent: dichloromethane) and 0.34g of colourless viscous liquid **(4)** was obtained (Rf value: 0.3, dichloromethane). The yield was 76%.

^{1}H-NMR spectrum (250 MHz, CDCl$_3$) δ [ppm]: 0.58 (t, 2H), 1.18 (t, 9H), 1.23 (b, 14H), 1.69 (m, 2H), 2.55 (t, 2H), 2.79 (s, 4H), 3.76 (q, 6H);

^{13}C-NMR spectrum (62.5 MHz, CDCl$_3$) δ [ppm]: 9.92, 17.85, 22.30, 24.12, 25.14, 28.34, 28.62, 28.76, 28.90, 28.97, 30.49, 32.72, 57.83, 166.25, 168.78 ppm;

IR spectrum (wavenumber): 2971~2854cm^{-1} (alkyl "C-H" stretches), 1814~1785 cm^{-1} (succinimidyl "C=O" stretches), 1737cm^{-1} (ester "C=O" stretches), 1365~1066 cm^{-1} (alkyl "C-H" bending vibrations), 954~644 cm^{-1} (succinimidyl "C-H" bending vibrations).

FD-MS (m/z):443.9 (M$^+$).

6.3.3 Synthesis of 3-(2,5-dioxo-2,5-dihydro-1H-pyrrol-1-yl)-N-(3-(triethoxysilyl) propyl) propanamide (6)

2,5-Dioxopyrrolidin-1-yl 3-(2,5-dioxo-2,5-dihydro-1H-pyrrol-1-yl)propanoate (5)

(5) [266.21] 46%
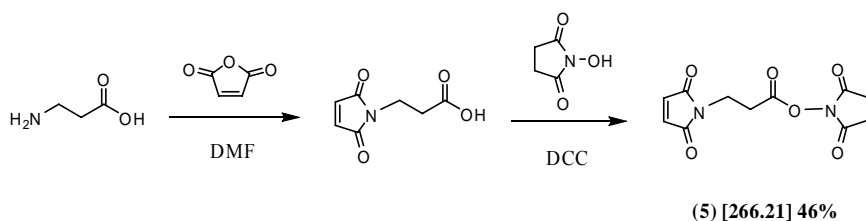
0.89g (10mmol) of 3-aminopropionic acid was added to a solution of maleic anhydride (0.98g, 10mmol) in 10mL of DMF. The suspension was stirred for 1 hour after 3-aminopropionic acid had dissolved. The resulting solution was cooled in an ice bath and 1.44g (12.5mmol) of NHS was added followed by DCC (4.12g, 20mmol). After 5 minutes, the ice bath was removed and the solution was stirred for 8 hours. The resulting suspension was filtrated to remove the precipitated DCU. The filtrate (DMF phase) was poured on 50mL of water, and this mixture was extracted with CH_2Cl_2 ($2\times$ 50mL). The CH_2Cl_2 phase was dried by Na_2CO_3. The solution was filtrated and the solvent was evaporated. The residue was redissolved in CH_2Cl_2, and the product was precipitated with petroleum ether. 1.23g of light yellow solid was obtained as (**5**). The yield was 46%.

^{1}H-NMR spectrum (250 MHz, CDCl$_3$) δ [ppm]: 2.81 (s, 4H), 3.00 (t, 2H), 3.92 (t, 2H), 6.72 (s, 2H) ppm;

^{13}C-NMR spectrum (62.5 MHz, CDCl$_3$) δ [ppm]: 25.50, 29.68, 32.94, 134.27, 165.97, 168.73, 170.06 ppm;

IR spectrum (wavenumber): 1824~1782cm^{-1} (maleic "C=O" and succinimidyl "C=O" stretches), 1716cm^{-1} (ester "C=O" stretches), 836~652cm^{-1} (maleic "C-H" bending vibrations).

Melting point: 162.3^{o}C

FD-MS (m/z):267.0 (M$^+$).

3-(2,5-Dioxo-2,5-dihydro-1H-pyrrol-1-yl)-N-(3-(triethoxysilyl)propyl)propanamide (6)

(5)   (6) [372.49] 64%
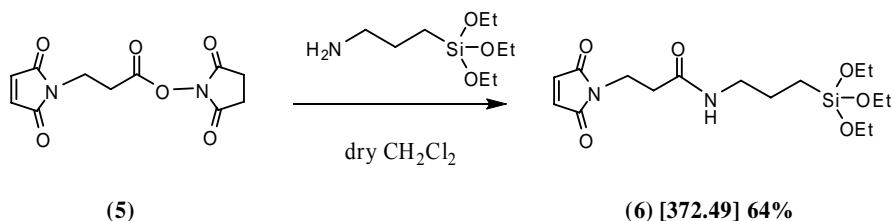
0.11 g (0.5mmol) of APTE was added to the solution of **(5)** (0.13g, o.5mmol) in 10mL of dry CH_2Cl_2. The solution was stirred in Ar atmosphere for 8 hours. The solvent was eliminated under vacuum and the residue was purified by column chromatography (Si-gel, eluent: CH_2Cl_2/acetone 9:1) and 0.12g of colourless viscous liquid as **(6)** was obtained (Rf = 0.6, CH_2Cl_2/acetone 9:1). The yield was 64%.

^{1}H-NMR spectrum (250 MHz, acetone-d6) δ [ppm]: 0.59 (t, 2H), 1.19 (t, 9H), 1.55 (m, 2H), 2.46 (t, 2H), 3.13 (q, 2H), 3.74~3.82 (m, 8H), 6.87 (s, 2H) ppm;

^{13}C-NMR spectrum (62.5 MHz, acetone-d6) δ [ppm]: 8.36, 18.82, 23.76, 29.80, 35.03, 42.46, 58.71, 135.15, 170.05, 171.33 ppm;

IR spectrum (wavenumber): 3296cm^{-1} (amide "N-H" stretches), 1701cm^{-1} (maleic "C=O" stretches), 1635cm^{-1} (amide "C=O" stretches), 695cm^{-1} (maleic "C-H" bending vibrations).

6.3.4 Synthesis of 6-(2,5-dioxo-2,5-dihydro-1H-pyrrol-1-yl)-N-(3-(triethoxysilyl) propyl) hexanamide (8)

2,5-Dioxopyrrolidin-1-yl 6-(2,5-dioxo-2,5-dihydro-1H-pyrrol-1-yl)hexanoate (7)

(7) [308.29] 19%
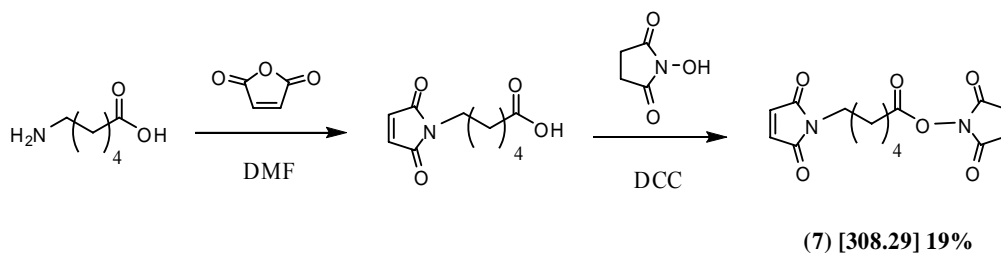
1.31g (10mmol) of 6-aminohexanoic acid was added to a solution of maleic anhydride (0.98g, 10mmol) in 15mL of DMF. The suspension was stirred for 2 hour after 6-aminohexanoic acid had dissolved. The resulting solution was cooled in an ice bath and 1.44g (12.5mmol) of NHS was added followed by DCC (4.12g, 20mmol). After 10 minutes, the ice bath was removed and the solution was stirred at room temperature for 8 hours. The resulting suspension was filtrated to remove the precipitated DCU. The filtrate (DMF phase) was poured on 50mL of water, and this mixture was extracted with CH_2Cl_2 ($2\times$ 50mL). The CH_2Cl_2 phase was dried by Na_2CO_3. The solution was filtrated and the solvent was evaporated. The residue was redissolved in small amount of CH_2Cl_2, and the crude product was purified by column chromatography (Si-gel, eluent: CH_2Cl_2/acetone 9:1). 0.60g of viscous colourless liquid was obtained as **(7)** (Rf = 0.83, CH_2Cl_2/acetone 9:1). The yield was 19%.

^{1}H-NMR spectrum (250 MHz, CDCl$_3$) δ [ppm]: 1.39 (m, 2H), 1.61 (m, 2H), 1.76 (m, 2H), 2.59 (t, 2H), 2.82 (s, 4H), 3.51 (t, 2H), 6.67 (s, 2H) ppm;

^{13}C-NMR spectrum (62.5 MHz, CDCl$_3$) δ [ppm]: 24.03, 25.55, 25.79, 28.00, 30.74, 37.41, 134.04, 168.35, 169.08, 170.79 ppm;

IR spectrum (wavenumber): 3101cm^{-1} (maleic "C-H" stretches), 2942~2866cm^{-1} (alkyl "C-H" stretches), 1812~1782cm^{-1} (maleic "C=O" and succinimidyl "C=O" stretches), 1697cm^{-1} (ester "C=O" stretches), 826~646cm^{-1} (maleic "C-H" bending

vibrations).

6-(2,5-Dioxo-2,5-dihydro-1H-pyrrol-1-yl)-N-(3-(triethoxysilyl)propyl)hexanamide (8)

(7)   (8) [414.57] 63%
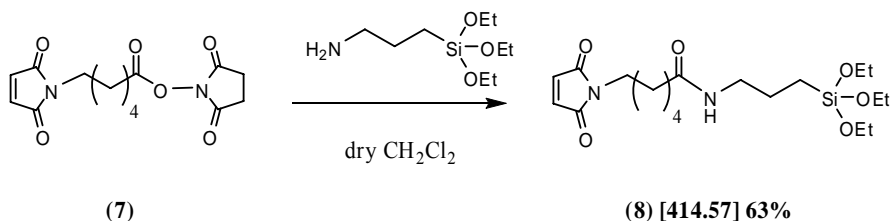
0.11 g (0.5mmol) of APTE was added to the solution of **(7)** (0.15g, o.5mmol) in 10mL of dry THF. The solution was stirred in Ar atmosphere for 8 hours. The solvent was eliminated under vacuum and the residue was purified by column chromatography (Si-gel, eluent: CH_2Cl_2/acetone 9:1) and 0.13g of colourless viscous liquid as product **(8)** was obtained (Rf: 0.7, CH_2Cl_2/acetone 9:1). The yield was 63%.

^{1}H-NMR spectrum (250 MHz, acetone-d6) δ [ppm]: 0.60 (t, 2H), 1.19 (t, 9H), 1.29 (m, 2H), 1.57 (m, 6H), 2.15 (t, 2H), 3.14 (q, 2H), 3.46 (t, 2H), 3.79 (q, 6H), 6.87 (s, 2H).

^{13}C-NMR spectrum (62.5 MHz, acetone-d6) δ [ppm]:11.19, 21.45, 26.72, 28.74, 29.80, 31.74, 39.29, 40.77, 45.23, 61.52, 137.84, 174.41, 175.49 ppm

IR spectrum (wavenumber): 3309cm^{-1} (amide "N-H" stretches), 2931cm^{-1} (alkyl "C-H" stretches), 1700cm^{-1} (maleic "C=O" stretches), 1640cm^{-1} (amide "C=O" stretches), 828~694cm^{-1} (maleic "C-H" bending vibrations).

6.3.5 Synthesis of N-(3-(triethoxysilyl)propyl)undec-10-ynamide (10)

2,5-Dioxopyrrolidin-1-yl undec-10-ynoate (9)

(9) [279.33] 74%
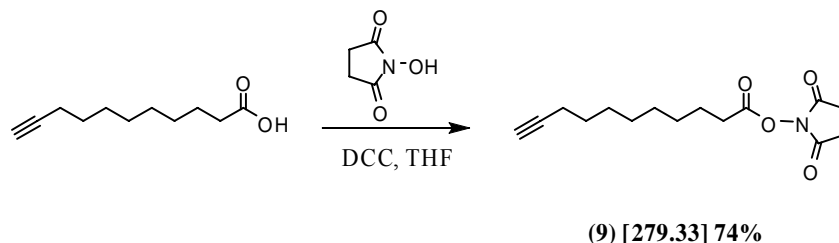
0.91g (5mmol) of undec-10-ynoic acid was added to the solution of 0.58g (5mmol) of N-hydroxysuccinimide (NHS), 2.06g (10mmol) of N, N'-dicyclo hexylcarbodiimide (DCC) in 30mL of dry THF. The mixture was stirred in Ar atmosphere for 8 hours. The resulting suspension was filtrated to remove the precipitated urea (DCU). The filtrate was purified by column chromatography (Si-gel, eluent: dichloromethane), and 1.03g of white crystalline solid **(9)** was obtained (Rf = 0.47, dichloromethane). The yield was 74%.

^{1}H-NMR spectrum (250 MHz, CDCl$_3$) δ [ppm]: 1.31 (m, ~8H), 1.50 (t, ~2H), 1.72 (m, 2.15H), 1.92 (m, 0.92H), 2.15 (m, 1.96H), 2.58 (t, 2.03H), 2.81 (s, 4H);

^{13}C-NMR spectrum (62.5 MHz, CDCl$_3$) δ [ppm]: 18.32, 24.49, 25.55, 28.35, 28.54, 28.64, 28.73, 28.87, 30.87, 68.09, 64.66, 188.62, 169.16 ppm;

FD-MS [m/z]: 280.5 (55%, M$^+$).

Melting point: 66.7^{o}C.

N-(3-(triethoxysilyl)propyl)undec-10-ynamide (10)

(9)   (10) [385.61] 52%
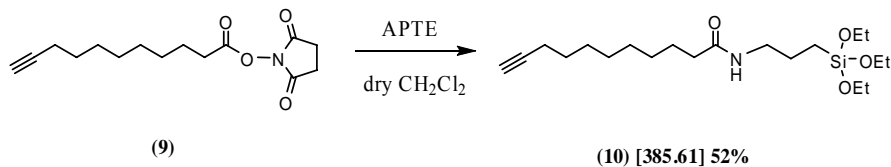
0.11 g (0.5mmol) of APTE was added to the solution of 2,5-dioxopyrrolidin-1-yl undec-10-ynoate **(9)** (0.14g, o.5mmol) in 10mL of dry THF. The solution was stirred in Ar atmosphere for 8 hours. The solvent was eliminated under vacuum and the residue was purified by column chromatography (Si-gel, eluent: hexane/ethylacetate 1:1) and 0.10g of colourless viscous liquid **(10)** was obtained (Rf = 0.58, hexane/ethylacetate 1:1). The yield was 52%.

^{1}H-NMR spectrum (250 MHz, CD$_2$Cl$_2$) δ [ppm]: 0.55 (t, 2.0H), 1.15 (t, 8.6H), 1.25 (m, 8.39H), 1.52 (m, 6.48H), 1.92 (m, 0.95H), 2.07 (m, 5.33H), 3.15 (q, 2.04H), 3.74 (q, 5.7H), 5.76 (s, 0.91H) ppm;

^{13}C-NMR spectrum (62.5 MHz, CD$_2$Cl$_2$) δ [ppm]: 8.22, 18.67, 18.82, 23.56, 26.33, 29.08, 29.25, 29.51, 29.81, 37.26, 42.27, 58.91, 88.42, 85.24 ppm;

FD-MS [m/z]: 386.9 (100%, M$^+$).

6.3.6 1-(4,5-dimethoxy-2-nitrophenyl)ethyl 3-(triethoxysilyl)propylcarbamate (14a) and 1-(4,5-dimethoxy-2-nitrophenyl)ethyl 11-(triethoxysilyl)decylcarbamate (14b)

1-(4,5-dimethoxy-2-nitrophenyl)ethanone (11):

60% yield   (11)
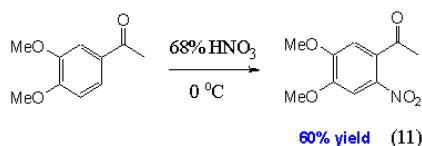
10mL of 68% HNO$_3$ was cooled to 0°C. 2g of 3,4-dimethoxy acetophenone was

slowly added to the stirring cold solution of HNO_3. The solution was stirred continuously and maintained at $0^\circ C$ throughout the addition. The mixture was allowed to stir at ambient temperature for another 2 hours and then slowly poured into an excess of crushed ice. The resulting yellow solid was collected by filtration, washed with water and cold ethanol, dried under vacuum and recrystallized from ethanol to get yellow fluffy needles of 1-(4,5-dimethoxy-2-nitrophenyl)ethanone **(11)** (R_f = 0.47, hexane/ethyl acetate = 7:3 as eluent) (1.49g, yield:60%).

^{1}H-NMR spectrum (250 MHz, CDCl$_3$) δ [ppm]: 7.58 (s, 1H), 6.72 (s, 1H), 3.91 (s, 6H), 2.417 (s, 3H) ppm;

^{13}C-NMR spectrum (62.5 MHz, CDCl$_3$) δ [ppm]: 199.85, 153.78, 149.38, 138.2, 132.57, 108.4, 106.63, 56.5, 30.15 ppm;

IR: 3019, 2939, 2849, 2400, 1703, 1567, 524, 1463, 1440, 1394, 1338, 1284, 1216, 1181, 1114, 1044, 928, 870, 756, 688 cm^{-1};

FD-MS (m/z): 225 (M$^+$).

1-(4,5-Dimethoxy-2-nitrophenyl) ethanol (12):
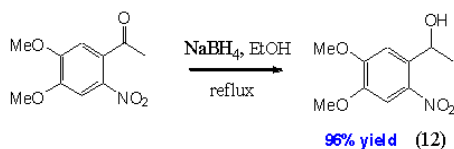
Sodium borohydride (600mg) was added to a stirring suspension of 1-(4,5-dimethoxy-2-nitrophenyl)ethanone **(11)** (4g, 8.88mmol) in 50mL of ethanol. The mixture was allowed to reflux for 1.5h. Cooled to room temperature and 1N diluted HCl was added to quench the excess NaBH$_4$. Addition of acid was done carefully by keeping it in ice. Formation of froth and precipitate was observed. The mixture was extracted with dichloromethane three times, the combined organic phase were washed with brine and dried over MgSO$_4$ and evaporated. The product **(12)** was obtained in 3.88g (R_f = 0.36,

hexane/ethyl acetate = 7:3 as eluent) (96% yield) and used without purification for further reactions.

^{1}H-NMR spectrum (250 MHz, CDCl$_3$) δ [ppm]: 7.447 (s, 1H), 7.21 (s, 1H), 5.45 (q, 1H), 3.96 (s, 6H), 2.70 (bs, 1H), 1.46 (d, 3H) ppm;

^{13}C-NMR spectrum (62.5 MHz, CDCl$_3$) δ [ppm]: 152.3, 146.2, 138.1, 135.7, 107.1, 106.2, 64.3, 55.0, 23.0 ppm;

IR spectrum: 3441, 3019, 1582, 1519, 1463, 1440, 1335, 1273, 1215, 1163, 1099, 1061, 1024, 928, 878, 850, 754, 668 cm^{-1};

FD-MS (m/z): 227 (M$^+$).

1-(4,5-Dimethoxy-2-nitrophenyl)ethyl allylcarbamate (13a) and 1-(4,5-dimethoxy-2-nitrophenyl)ethyl undec-10-enylcarbamate (13b):
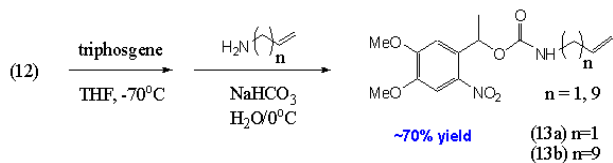
2g (8.8mmol) of 1-(4,5-dimethoxy 2-nitrophenyl) ethanol (**12**) and triphosgene (2.068g, 6.98mmol) were taken in a 100mL two-neck-flask. 25mL of dry THF was added to it with a syringe. The reaction mixture was stirred at -70°C under argon for 2 hours to form the corresponding chloroformate of (**12**) as reactive intermediate. 0.50g (8.8mmol)of allylamine (or alternatively 1.48g of undec-10-en-1-amine), sodium hydrogencarbonate (1.7g, 22mmol) and water (20mL) were placed into a round bottom flask and cooled in an ice bath. To this mixture was added dropwise the solution of the chloroformate of (**12**) (stirring at -70°C) under vigorous stirring. The mixture was allowed to stir overnight. After adding 1N HCl, the mixture was extracted three times with dichloromethane. The organic phase was dried over magnesium sulphate; the solvent was evaporated to get a yellow solid as **13a** (R$_f$ = 0.66, hexane/ethyl acetate = 7:3

as eluent) (1.99g, 73% yield), and **13b** (R_f = 0.56, hexane/ethyl acetate = 7:3 as eluent) (2.70g, 73% yield).

^{1}H-NMR spectrum (250 MHz, CDCl$_3$) δ [ppm] of (**13a**): 7.46 (s, 1H), 7.24 (s, 1H), 5.75 (m, 1H), 5.48 (q, 1H), 5.05 (q, 2H), 3.89 (s, 6H), 3.66 (d, 2H), 1.44 (d, 3H) ppm;

^{13}C-NMR spectrum (62.5 MHz, CDCl$_3$) δ [ppm] of (**13a**): 154.0, 147.9, 139.8, 137.6, 135.5, 116.1, 108.9, 107.9, 66.0, 56.7, 43.3, 24.7 ppm;

IR spectrum of (**13a**): 3447, 3020, 2400, 1585, 1597, 1518, 1463, 1440, 1335, 1273, 1215, 1163, 1099, 1061, 1018, 928, 878, 770, 668 cm^{-1}.

^{1}H-NMR spectrum (250 MHz, CDCl$_3$) δ [ppm] of (**13b**): 7.88 (bs, 1H), 7.48 (s, 1H), 7.24 (s, 1H), 5.74 (m, 1H), 5.47 (q, 1H), 4.87 (t, 2H), 3.90 (s, 6H), 3.66 (d, 2H), 1.94(q, 2H), 1.68 (m, 2H), 1.47 (d, 5H), 1.19 (m, 10H) ppm;

^{13}C-NMR spectrum (250 MHz, CDCl$_3$) δ [ppm] of (**13b**): 152.2, 146.1, 137.5, 136.0, 135.9, 107.4, 107.3, 105.9, 65.7, 64.5, 57.8, 54.8, 28.1, 24.3, 23.8, 16.6 ppm;

IR spectrum of (**13b**): 3358, 2976, 2933, 2882, 2526, 2362, 2241, 1925, 1658, 1451, 1372, 1269, 1094, 1054, 887 cm^{-1}.

1-(4,5-Dimethoxy-2-nitrophenyl)ethyl 3-(triethoxysilyl)propylcarbamate (14a) and 1-(4,5-dimethoxy-2-nitrophenyl)ethyl 11-(triethoxysilyl)undecylcarbamate (14b):
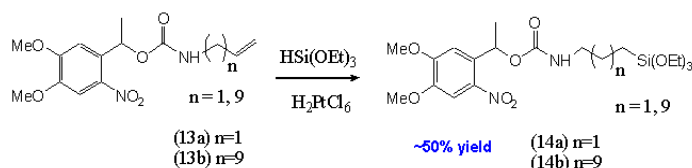
Unsaturated precursors (1g (3.22mmol) of **13a**, or alternatively 1g (2.37mmol) of **13b**) and 5.2g (32mmol) of triethoxysilane were placed into a previously HMDS-passivated dry round bottom flask and heated under argon atmosphere to 80°C. At this temperature both reactants mix homogeneously. Six drops of 1.6% H$_2$PtCl$_6$ in isopropanol

were added 3 times over the course of the reaction and the mixture was allowed to react for other 6 hours at 80°C and then stirred at room temperature overnight. Completion of the reaction was monitored by TLC. Excess of triethoxysilane was removed in vacuum and the liquid was purified by HMDS-passivated chromatography (silica gel, hexane/ethyl acetate 95:5).

The eluent was evaporated to get 1.07g of greenish liquid as **(14a)** (R_f =0.84, hexane/ethyl acetate = 95:5 as eluent) (50% yield), and 1.10g of brown colored viscous liquid as **(14b)** (R_f =0.56, hexane/ethyl acetate = 95:5 as eluent) (79.3% yield).

^{1}H-NMR spectrum (250 MHz, CDCl$_3$) δ [ppm] of **(14a)**: 7.46 (s, 1H), 7.24 (s, 1H), 5.75 (m, 1H), 4.29-3.47 (m, 12H), 2.96 (t, 2H), 1.6-1.08 (m, 14H), 0.75 (t, 2H) ppm;

IR spectrum of **(14a)**: 3355, 2973, 2885, 2541, 2256, 1925, 1707, 1685, 1455, 1380, 1380, 1331, 1274, 1090, 1049, 881, 803 cm^{-1};

UV/Vis (THF) spectrum of **(14a)**: $\lambda_{max, abs}$ = 300, 344 nm;

FD-MS (m/z):227 (M$^+$).

^{1}H-NMR spectrum (250 MHz, CDCl$_3$) δ [ppm] of **(14b)**: 7.42 (s, 1H), 7.22 (s, 1H), 5.72 (q, 1H), 4.21-3.54 (m, 14H), 1.41-1.03 (m, 30H), 0.72 (t, 2H) ppm;

IR spectrum of **(14b)**: 3358, 2976, 2891, 2738, 2526, 2368, 2235, 1925, 1925, 1652, 1524, 1452, 1379, 1336, 1282, 1094, 1050, 881, 789 cm^{-1};

UV/Vis (THF) of **(14b)**: $\lambda_{max, abs}$ = 301, 342 nm.

6.3.7 1-(4, 5-Dimethoxy-2-nitrophenyl) ethyl 3-(triethoxysilyl) propyl carbonate (16a) and 1-(4, 5-dimethoxy-2-nitrophenyl) ethyl 11-(triethoxysilyl) undecyl carbonate (16b)

Allyl 1-(4, 5-dimethoxy-2-nitrophenyl) ethyl carbonate (15a) and 1-(4, 5-dimethoxy-2-nitrophenyl) ethyl undec-10-enyl carbonate (15b):

Schotten-Baumann reaction conditions: A solution of allyl alcohol in THF (15 mL) was added slowly to a solution of N,N-carbonyldiimidazole in THF (7mL) at 0°C. The solution was stirred at 0°C for 2 hours and the formation of allyl carbonylimidazole intermediate was proven by TLC. To this mixture a solution of 1-(4,5-dimethoxy 2-nitrophenyl) ethanol **(12)** in THF (25mL) was added dropwise and the mixture was stirred at 0°C for 30 minutes and then left at room temperature. After dilution with CH_2Cl_2 and washing with sat. aq NH_4Cl, the solvents were removed and the crude product was purified by flash chromatography.

Allyl-(4,5-dimethoxy-2-nitrophenyl)ethyl carbonate (15a): allyl alcohol (0.26g, 4.4mmol) in THF (15mL), N, N-carbonyldiimidazole (0.71g, 4.4mmol) in THF (7mL), 1-(4,5-dimethoxy-2-nitrophenyl) ethanol **(12)** (1g, 4.4mmol) in THF (25mL). Flash chromatography with a mixture of petroleum ether/acetone = 8:2 (R_f = 0.58). It was further recrystallized in methanol to obtain a light yellow solid **(15a)** in 80% yield (1.096 g).

^{1}H-NMR spectrum (250 MHz, $CDCl_3$) δ [ppm]: 7.50 (s, 1H), 6.99 (s, 1H), 6.28 (q, 1H), 5.82 (m, 1H), 5.19 (q, 2H), 5.05 (q, 2H), 4.48 (d, 2H), 3.9 (s, 6H), 1.57 (d, 3H) ppm;

^{13}C-NMR spectrum (62.5 MHz, $CDCl_3$) δ [ppm]: 154.2, 148.4, 140.1, 133.0, 131.7,

119.4, 108.1, 107.9, 72.4, 68.8, 56.8, 18.0 ppm;

IR spectrum: 3450, 3018, 2399, 1597, 1522, 1428, 1217, 928, 771, 669 cm^{-1}.

1-(4,5-dimethoxy-2-nitrophenyl)ethyl undec-10-enyl carbonate (15b): undec-10-en-1-ol (0.75g, 4.4mmol) in THF (15mL), N,N-carbonyldiimidazole (0.71g, 4.4mmol) in THF (7mL), 1-(4,5-dimethoxy-2-nitrophenyl) ethanol (1g, 4.4mmol) in THF (25mL). Flash chromatography with a mixture of petroleum ether/acetone = 8:2 (R_f = 0.56) afforded 82% (1.477g) of product **(15b)**.

^{1}H-NMR spectrum (250 MHz, CDCl$_3$) δ [ppm]: 7.47 (s, 1H), 7.23 (s, 1H), 5.72 (m, 1H), 5.47 (q, 1H), 4.87 (t, 2H), 3.92 (s, 6H), 3.54 (t, 2H), 2.20 (s, 2H), 1.94(q, 2H), 1.45 (m, 5H), 1.21 (m, 10H) ppm;

^{13}C-NMR spectrum (62.5 MHz, CDCl$_3$) δ [ppm]: 154.1, 148.0, 139.6, 137.4, 114.5, 108.8, 107.9, 66.0, 63.4, 56.7, 34.1, 33.1, 29.3, 26.1, 24.7 ppm;

IR spectrum: 3423, 3019, 2930, 2855, 2400, 1638, 1519, 1464, 1640, 1335, 1273, 1215, 1020, 928, 756, 669 cm^{-1}.

1-(4, 5-Dimethoxy-2-nitrophenyl) ethyl 3-(triethoxysilyl) propyl carbonate (16a) and 1-(4, 5-dimethoxy-2-nitrophenyl) ethyl 11-(triethoxysilyl) undecyl carbonate (16b):
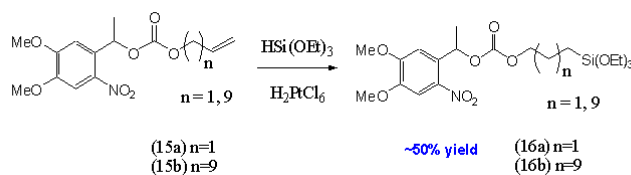
The unsaturated precursors (0.63g (2.02mmol) of **(15a)**, or alternatively 1g (2.36mmol) of **(15b)**) and 3.8g (23mmol) of triethoxysilane were placed into a previously HMDS-passivated dry round bottom flask and heated under argon atmosphere to 80$^{\text{o}}$C. At this temperature both reactants mix homogeneously. Six drops of 1.6% H$_2$PtCl$_6$ in

isopropanol were added in 3 times over the course of the reaction and the mixture was allowed to react for other 6 hours at 80°C and then stirred at room temperature overnight. Completion of the reaction was monitored by TLC. Excess of triethoxysilane was removed in vacuum and the liquid was purified by HMDS-passivated chromatography (silica gel, hexane/ethyl acetate 95:5).

Product **(16a)** (R$_f$ = 0.84, hexane/ethyl acetate 95:5) was obtained in 0.76g (50% yield), and product **(16b)** (R$_f$ = 0.82, hexane/ethyl acetate 95:5) was 0.72g (50% yield).

^{1}H-NMR spectrum (250 MHz, CDCl$_3$) δ [ppm] of **(16a)**: 7.42 (s, 1H), 6.99 (s, 1H), 5.70 (q, 1H), 4.2-3.5 (m, 14H), 1.68-1.05 (m, 14H) ppm;

IR spectrum of **(16a)**: 3490, 2974, 2236, 2082, 1885, 1750, 1639, 1578, 1639, 1578, 1521, 1465, 1382, 1336, 1274, 1220, 1166, 1166, 1105, 1051, 968, 891, 835, 786, 758 cm^{-1};

UV/Vis (THF) spectrum of **(16a)**: λ$_{max, abs}$ = 280, 341 nm.

^{1}H-NMR spectrum (250 MHz, CDCl$_3$) δ [ppm] of **(16b)**: 7.49 (s, 1H), 7.18 (s, 1H), 5.48 (q, 1H), 4.19-3.75 (m, 14H), 1.45-1.14 (m, 30H), 0.79 (t, 2H) ppm;

IR spectrum of **(16b)**: 3385, 2975, 2871, 1923, 1655, 1451, 1325, 1271, 1088, 1047, 880 cm^{-1};

UV/Vis (THF) spectrum of **(16b)**: λ$_{max, abs}$ = 301, 345 nm.

6.3.8 1-(4, 5-Dimethoxy-2-nitrophenyl) ethyl 5-(triethoxysilyl) pentanoate (18)

1-(4, 5-Dimethoxy-2-nitrophenyl) ethyl but-3-enoate (17):
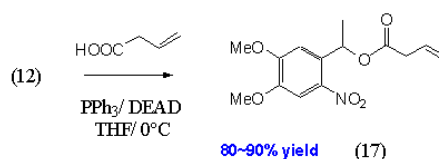
Mitsunobu reaction conditions: A solution of diethylazodicarboxylate (DEAD, 0.77g 4.4mmol), in THF (20mL) is added dropwise to a solution of triphenylphosphine (1.15g, 4.4mmol), vinyl acetic acid (0.37g, 4.4mmol), and 1g (4.4mmol) of 1-(4,5-dimethoxy-2-nitrophenyl) ethanol **(12)** in THF (30mL) at 0°C. After stirring the mixture overnight at room temperature, the solvent was removed in vacuum and 5mL of dichloromethane was added. After overnight stirring, colorless needles of diethyl hydrazinedicarboxylate precipitated. The precipitate was removed by filtration, the filtrate evaporated in vacuum and the product was purified by flash chromatography (Si-gel, dichloromethane/ethyl acetate 95:5). 1.04g of product **(17)** was obtained (R_f = 0.53, 80% yield).

^{1}H-NMR spectrum (250 MHz, CDCl$_3$) δ [ppm]: 7.51 (s, 1H), 6.93 (s, 1H), 6.42 (q, 1H), 5.85 (m, 1H), 5.10 (q, 2H), 5.05 (m, 2H), 3.88 (s, 6H), 3.05 (d, 2H), 1.55 (d, 3H) ppm;

IR spectrum: 3358, 2981, 2933, 2889, 2520, 2368, 2235, 1925, 1658, 1524, 1457, 1372, 1336, 1275, 1094, 1057, 887 cm^{-1}.

1-(4, 5-Dimethoxy-2-nitrophenyl) ethyl 5-(triethoxysilyl) pentanoate (18):

(17)   ~50% yield   (18)
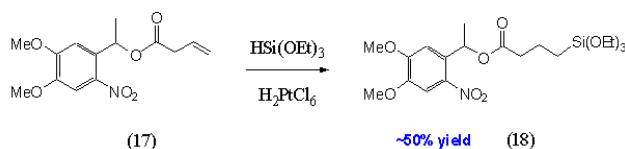
0.93g (3.15mmol) of **(17)** and 5.09g (31.5mmol) of triethoxysilane were placed into a previously HMDS-passivated dry round bottom flask and heated under argon atmosphere to 80°C. At this temperature both reactants mix homogeneously. Six drops of 1.6% H$_2$PtCl$_6$ in isopropanol were added in 3 times over the course of the reaction and the mixture was allowed to react for 6 hours at 80°C and then stirred at room temperature overnight. Completion of the reaction was monitored by TLC. Excess of triethoxysilane was removed in vacuum and the liquid was purified by passivated chromatography (silica

gel, hexane/ethyl acetate 95:5). Product **(18)** (R_f = 0.8, hexane/ethyl acetate 95:5) was obtained in 0.78g (50% yield).

^{1}H-NMR spectrum (250 MHz, CDCl$_3$) δ [ppm]: 7.50 (s, 1H), 7.19 (s, 1H), 5.65 (m, 1H), 4.14-3.70 (m, 12H), 1.46-1.11 (m, 16H), 0.77 (t, 2H) ppm;

IR spectrum: 3423, 2971, 2934, 1736, 1618, 1583, 1522, 1463, 1370, 1336, 1274, 1274, 1220, 1169, 1103, 1081, 1052, 955, 873, 794, 758 cm^{-1};

UV/Vis (THF) spectrum: $\lambda_{max, abs}$ = 296, 340 nm.

6.3.9 1-(3,5-Dimethoxyphenyl)-2-oxo-2-phenylethyl 3-(triethoxysilyl) propyl carbamate (22)

1-(Ethoxy (phenyl) methyl)-1H-benzotriazole (19):
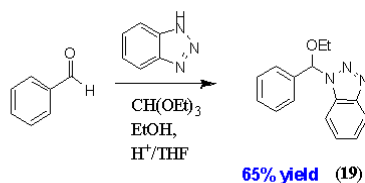
A mixture of benzaldehyde (2.12g, 20mmol), benzotriazole (2.98g, 25mmol), absolute EtOH (1.84g, 40mmol), triethyl orthoformate (8.88g 60mmol), and a catalytic amount of sulfuric acid (6 drops) was stirred in THF (30mL) for 2 hours at room temperature and followed by refluxing for 3 hours. Diethylether (200mL) was then added, and the solution was washed with saturated Na$_2$CO$_3$ solution (2×100mL) and water (100mL). The solvent was dehydrated by dry CaCl$_2$. Evaporation of the solvents gave a residue, which was chromatographed on silica gel (hexane/ethylacetate=15:4). 3.29g of colorless viscous liquid **(19)** was obtained (R_f = 0.59, hexane/ethylacetate=15:4). The yield was 65%.

^{1}H-NMR spectrum (250MHz, acetone-d6) δ [ppm]: 1.26 (t, 3H); 3.48 (m, 1H); 3.84 (m, 1H); 7.33-7.43 (m, 9H); 8.04 (m, 1H) ppm;

^{13}C-NMR spectrum (62.5MHz, acetone-d6) δ [ppm]:14.95; 65.53; 90.13; 112.35; 120.47; 124.95; 126.80; 128.26; 129.36; 129.75; 132.16; 137.93; 147.69 ppm;

FD-MS [m/z]: 253.0 (100%, M[+]).

2-(3,5-Dimethoxyphenyl)-2-hydroxy-1-phenylethanone (20)
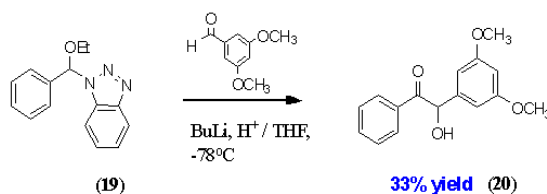
To a solution of 1-(ethoxy (phenyl) methyl)-1H-benzotriazole **(19)** (0.51g, 2.0mmol) in dry THF (30mL) was added n-BuLi (1.6M in cyclohexane, 1.25mL, 2.0mmol) at -78°C. The solution was stirred at this temperature for 15-120 seconds. Then 3,5-dimethoxylbenzaldehyde (0.50g, 3.0mmol) was added and the solution was kept at this temperature for 1-2 minutes. The mixture was quenched at this temperature with water (30mL), diluted HCl (4mL concd HCl in 10mL water) was added, and the solution was stirred at room temperature for 30-60 minutes. The solution was then extracted with diethyl ether (100mL), washed with saturated Na_2CO_3 solution (2×50mL) and water (50mL), and dried over $MgSO_4$. The solution was evaporated and the residue was purified by column chromatography on silica gel (hexane/ ethylacetate=15:4). The fraction with R_f=0.27 was chromatographed on silica gel again (hexane/ethylacetate=1:1). 0.18g of yellow colored viscous liquid (**20**, R_f = 0.76) was obtained. The yield was 33%.
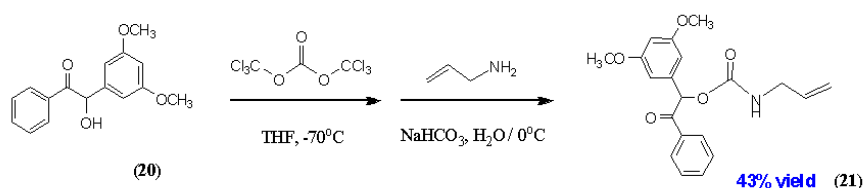
^{1}H-NMR spectrum (250MHz, CD_2Cl_2) δ [ppm]: 3.69 (s, 6H); 5.80 (s, 1H); 6.31 (s, 1H); 6.42 (s, 2H); 7.39 (m, 2H); 7.49 (m, 1H); 7.87 (d, 2H) ppm;

^{13}C-NMR spectrum (62.5MHz, CD_2Cl_2) δ [ppm]: 55.83; 76.65; 100.64; 106.27;

129.20; 129.52; 134.19; 134.43; 142.4; 161.85; 199.41ppm;

FD-MS [m/z]: 272.4 (100%, M$^+$).

1-(3, 5-Dimethoxyphenyl)-2-oxo-2-phenylethyl allyl carbamate (21)

To a solution of 2-(3, 5-dimethoxyphenyl)-2-hydroxy-1-phenylethanone **(20)** (0.16g, 0.59mmol) in dry THF (10mL) was added triethylamine (0.18g, 1.8mmol) at -78°C. The reaction mixture was stirred under argon atmosphere for 6 hours. Allylamine (0.034g, 0.59mmol) was dissolved in 5mL of dry THF. This solution was added dropwise to the reaction mixture at -78°C. After 2 hours, the mixture was allowed to stir overnight at room temperature. 100mL of diethylether was added to the mixture. The organic phase was washed to neutral with Milli-Q water and dehydrated with dry MgSO$_4$. The solvent was evaporated and gave a residue which was chramatographed on silica gel (hexane/ethylacetate 15:4). 0.09g of yellow colored viscous liquid (**21**, R$_f$ = 0.2) was obtained. The yield was 43%.

^{1}H-NMR spectrum (250MHz, CDCl$_3$) δ [ppm]: 3.73 (s, 6H); 3.74-3.81 (m, 2H); 4.50 (m, 1H); 5.10 (m, 1H); 5.83 (m, 1H); 6.34 (s, 1H); 6.46 (s, 1H); 6.58 (s, 1H); 7.40 (m, 2H); 7.53 (m, 1H); 7.91 (m, 2H) ppm;

^{13}C-NMR spectrum (62.5MHz, CDCl$_3$) δ [ppm]: 43.51; 55.30; 76.11; 100.39; 105.76; 116.24; 128.63; 129.05; 133.44; 133.90; 135.86; 140.99; 155.35; 161.20; 198.69 ppm;

FD-MS [m/z]: 355.3 (45%, M$^+$);

UV/Vis (THF) spectrum: λ$_{max, abs}$ = 247nm.

110

1-(3,5-Dimethoxyphenyl)-2-oxo-2-phenylethyl 3-(triethoxysilyl) propylcarbamate (22)
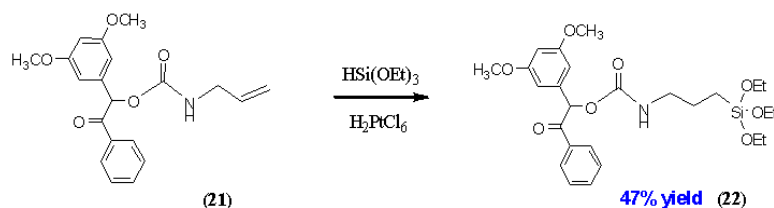
0.36g (1mmol) of allyl-carbamic acid 1-(3,5-dimethoxy-phenyl)-2-oxo-2-phenyl-ethyl ester **(21)** was dissolved in 1.64g (10mmol) of triethoxysilane followed by 8 drops of H_2PtCl_6/iso-propanol solution (20mg H_2PtCl_6 in 1mL iso-propanol). The mixture was heated to 80°C in Ar atmosphere for 14 hours and cooled down to room temperature.

The excess of triethoxysilane was eliminated under vacuum. The residue was purified by HMDS-passivated column chromatography (Si-gel, eluent: dichloromethane) and 0.23g of colourless viscous liquid **(22)** was obtained ($R_f = 0.24$). The yield was 47%.

^{1}H-NMR spectrum (250MHz, CD_2Cl_2) δ [ppm]: 0.55 (t, 2H); 1.15 (t, 9H); 1.60 (m, 2H); 2.40 (m, 2H); 3.70 (s, 6H); 3.75 (q, 6H); 6.37 (s, 1H); 6.52 (s, 2H); 6.67 (s,1H); 7.39 (m, 2H); 7.51 (m, 1H); 7.88 (m, 2H) ppm;

^{13}C-NMR spectrum (62.5MHz, CD_2Cl_2) δ [ppm]: 10.87; 18.70; 23.34; 44.50; 55.96; 58.73; 77.95; 101.30; 107.08; 129.20; 134.04; 135.29; 136.36; 161.84; 173.61; 194.18 ppm;

FD-MS [m/z]: 521.1 (100%, M$^+$);

UV/Vis (THF) spectrum: $\lambda_{max,\ abs} = 246$nm.

Chapter 7

Summary

The aim of this thesis was to investigate novel techniques to create complex hierarchical chemical patterns on silica or quartz surfaces with micro to nanometer sized features. These modified surfaces were used for functional group-selective surface reactions and site-selective assembly of colloidal particles. For this purpose, novel functionalized triethoxysilanes were synthesized by a modular convergent approache, coupling 3-aminopropyltriethoxysilane and an amino-reactive fragment. After deposition of these silanes as molecular layers onto planar silica and quartz surfaces, the functional groups of these silanes form new functional surfaces (by liquid- or vapor phase silanization) or even lateral functional patterns (by micro-contact printing or photolithography) that allow further chemical reactions at these surfaces.

By the above mentioned modular approach triethoxysilanes with terminal t-butyl-, maleimide-, succinimidyl-, and alkyne moieties were synthesized and surface layers were prepared with them. Kinetic experiments with varying hydrolysis- and incubation times were performed while monitoring changes in hydrophilicity of the functional surfaces and the layer thickness to study the efficiency of silanization process. From these results the hydrolysis conditions could be optimized in order to form uniform and well defined self-assembled surface layers. In model reactions it was shown that their head groups can further bind appropriate molecules due to their characteristic chemical reactivities.

Furthermore, a series of novel photosensitive silanes with 1-(4,5-dimethoxy-2-nitrophenyl)ethanol (CH$_3$-NVoc)-protected -OH, -COOH and -NH$_2$ functionalities, and 3,5-dimethoxybenzoin (Bzn)-protected -NH$_2$ group were synthesized and characterized. UV-Vis spectra of both CH$_3$-NVoc and Bzn silanes were recorded in solution phase and as SAMs on quartz surfaces for different irradiation times at the respective deprotection wavelengths to optimize the photodeprotection step. By irradiation through a gold mask in a UV mask aligner (365 nm) or a crosslinker (254 nm), both CH$_3$-NVoc and Bzn SAMs could be patterned with functional (photodeprotected / irradiated) and protected (unirradiated) regions, respectively. The obtained functional pattern could be visualized by site-selective staining with fluorescent probes. Furthermore, site-selective colloid absorption could be observed on the photosensitive silane layer patterns after local deprotection with light.

Bibliography

[Becker 1991] H.G.O Becker. Einfuehrung in die Photochemie. Deutscher Verlag d. Wissenschaften, Berlin (1991).

[Bochet 2000] C. G. Bochet: Wavelength-Selective Cleavage of Photolabile Protecting Groups, *Tetrahedron Lett.*, 41, 6341-6346 (2000).

[Bochet 2002] Ch. G. Bochet: Photolabile Protecting Groups and Linkers, *J. Chem. Soc., Perkin Trans*. 1, 67, 125-162 (2002).

[Boos 2004] Diana Boos: Synthesis and Characterization of photoreactive Silanes for the Self-Assembly on Functionalised Silica Surfaces, dissertation (2004), University of Mainz.

[Braun 2003] F. Braun, L. Eng, S. Trogisch, B. Voit: Novel Labile Protected Amine Terpolymers for the Preparation of Patterned Functionalized Surfaces: Synthesis and Characterization, *Macromolecular Chemistry and Physics*, 204, 1486-1496 (2003).

[Burmeister 1999] F. Burmeister, W. Badowsky, T. Braun, W. Wieperich, J. Boneberg, P. Leiderer, Colloidal Monolayer Lithography: A Flexible Approach for Nanostructuring of Surfaces, *Appl. Surf. Sci.*, 144, 461-466 (1999).

[Cameron 1991] J. F. Cameron, J. M. J. Frechet: Photogeneration of Organic Bases from

o-Nitrophenyl-Derived Carbamates, *J. Am. Chem. Soc.*, 113, 4303-4313 (1991).

[Chamberlin 1966] J. W. Chamberlin: Use of the 3,5-Dimethoxybenzyloxycarbonyl Group as a Photosensitive N-Protecting Group. *J. Org. Chem.*, 31, 1658-1660 (1966).

[Chen 2000] K. M. Chen, X. Jiang, L. C. Kimerling, P. T. Hammond: Selectivity Self-organization of Colloids on Patterned Polyelectrolyte Templates, *Langmuir* 16, 7825-7834 (2000).

[Cheng 2006] W. Cheng, J. Wang, U. Jonas, G. Fytas, N. Stefanou, Observation and Tuning of Hypersonic Bandgaps in Colloidal Crystals, *Nat. Mater.*, 5, 830-836 (2006).

[Corey 1965] E. J. Corey, D. Seebach: Carbanions of 1,3-Dithianes. Reagents for C-C Bond Formation by Nucleophilic Displacement and Carbonyl Addition, *Angew. Chem. Int. Ed. Engl.*, 4, 1075-1077 (1965).

[Davidson 1999] M. W. Davidson, M. Abramowitz, "Optical Microscopy", Internet article, http://micro.magnet.fsu.edu/primer/opticalmicroscopy.html, © 1998-2007 by M. W. Davidson, M. Abramowitz, Olympus America Inc., and the Florida State University.

[del Campo 2005] A. Del Campo, D. Boos, H. W. Spiess, U. Jonas: Surface Modification with Orthogonal Photosensitive Silanes for Sequential Chemical Lithography and Site-selective Particle Deposition, *Angew. Chem. Int. Ed. Engl.* 44, 4707-4712 (2005).

[Dobkin web resource] D. M. Dobkin, "Silicon Dioxide: Properties and Applications", http://www.batnet.com/enigmatics/semiconductor_processing/CVD_Fundamentals/films/SiO2_properties.html

[Dziomkina 2006] N. V. Dziomkina, M. A. Hempenius, G. J. Vancso: Synthesis of Cationic Core-Shell Latex Particles, *European Polymer Journal*, 42, 81-91 (2006).

[Eckert 1987] H. Eckert, B. Forster: Triphosgene, a Crystalline Phosgene Substitute, *Angew. Chem. Int. Ed. Engl.*, 26, 984-985 (1987).

[Elender 1996] G.Elender, M.Kuener, E.Sackmann: Functionalisation of Si/SiO$_2$ and Glass Surfaces with Ultrathin Dextran Films and Deposition of Lipid Bilayers, *Biosensensors and Bioelectronics*, 11, 565-577 (1996).

[Fadeev 1999] A. Y. Fadeev, T. J. McCarthy: Trialkylsilane Monolayers Covalently Attached to Silicon Surfaces: Wettability Studies Indicating that Molecular Topography Contributes to Contact Angle Hysteresis, *Langmuir* 15, 3759-3766 (1999).

[Fustin 2003] C. A. Fustin, G. Glasser, H. W. Spiess, U. Jonas: Site-Selective Growth of Colloid Crystals with Photonic Properties on Chemically Patterned Surfaces, *Adv. Mater.*, 15, 1025-1028 (2003).

[Fustin 2004] Charles-André Fustin, Gunnar Glasser, Hans W. Spiess, Ulrich Jonas: Parameters Influencing the Templated Growth of Colloidal Crystals on Chemically Patterned Surfaces, *Langmuir*, 20, 9114-9123 (2004).

[Gates 2005] B. D. Gates, Q. Xu, M. Stewart, D. Ryan, C. G. Willson, G. M. Whitesides: New Approaches to Nanofabrication: Molding, Printing, and Other Techniques, *Chem. Rev.* 105, 1171-1196 (2005).

[Greene 1999] Theodora W. Green, Peter G. M. Wuts: Protective Groups in Organic Synthesis (Third Edition); page 404-408, Wiley-Interscience Publication 1999.

[Hayashi 1999] Tamio Hayashi: Comprehensive Asymmetric Catalysis; page 319-333, Springer 1999.

[Houseman 2003] Benjamin T. Houseman, Ellen S. Gawalt, Milan Mrksich: Maleimid-Functionalized Self-Assembled Monolayers for the Preparation of Peptide and

Carbohydrate Biochips, *Langmuir*, 19, 1552-1531 (2003).

[Howland 1996] R. Howland, L. Benatar, "A Practical Guide to Scanning Probe Microscopy", Thermomicroscopes, Inc., Sunnyvale, CA, 1996, p73.

[Im 2002] S. H. Im, Y. T. Lim, D. J. Suh, O. O. Park: Three Dimensional Self-Assembly of Colloids at a Water-Air Interface: A Novel Technique for the Fabrication of Photonic Bandgap Crystals, *Adv. Mater.*, 14, 1367-1369 (2002).

[Ishida 1984] H. Ishida, J. D. Miller: Substrate Effects of the Chemisorbed and Physisorbed Layers of Methacryl Silane Modified Particulate Minerals, *Macromolecules*, 17, 1659-1666 (1984).

[Israelachvili 2002] Jacob Israelachvili: Intermolecular & Surfae Forces, Academic Press (2002), London, UK

[Jonas 2002a] U. Jonas, A. del Campo, C. Kruger, G. Glasser, D. Boos: Colloidal Assemblies on Patterned Silane Layers, *Proc. Nat. Acad. Sci.*, 99, 5034-5039 (2002).

[Jonas 2002b] U. Jonas, C. Krueger: The Effect of Polar, Nonpolar, and Electrostatic Interactions and Wetting Behaviour on the Particle Assembly at Patterned Surfaces, *J. Supramol. Chem.*, 2, 255-270 (2002).

[Katritzky 1995] A. R. Katritzky, H. Lang, Z. Wang, Z, Zhang, H. Song: Benzotriazole-Mediated Conversions of Aromatic and Heteroaromatic Aldehydes to Functionalized Ketones, *J. Org. Chem.*, 60, 7619-7624 (1995).

[Kolb 2001] Hartmuth C. Kolb, M. G. Finn, K. Barry Sharpless: Click Chemistry: Diverse Chemical Function from a Few Good Reactions. *Angew. Chem. Int. Ed*, 40, 2004-2021 (2001).

[Krüger 2001] Christian Krüger: Kolloidale Organisation auf lithographisch hergestellten Silanschichten: Neue Möglichkeiten der Strukturbildung auf Oberflächen, dissertation (2001), University of Mainz.

[Lee 2002] I. Lee, H. Zheng, M. F. Rubner, P. T. Hammond: Controlled Cluster Size in Patterned Particle Arrays via Directed Adsorption on Confined Surfaces, *Adv. Mater.*, 14, 572-577 (2002).

[Lewis 1975] F. D. Lewis, R. T. Lauterbach, H. G. Heine, W. Hartmann, H. Rudolph: Photochemical α Cleavage of Benzoin Derivatives. Polar Transition States for Free-Radical Formation, *J. Am. Chem. Soc.*, 97, 1519-1525 (1975).

[Lipson 1996] M. Lipson, N. J. Turro: Picosecond Investigation of the Effect of Solvent on the Photochemistry of Benzoin, *J. Photochem. Photobiol. A. Chem.*, 99, 93-96 (1996).

[Lummerstorfer 2004] Thomas Lummerstorfer, Helmuth Hoffmann: Click Chemistry on Surfaces: 1, 3-Dipolar Cycloaddition Reactions of Azide-Terminated Monolayers on Silica. *J. Phys. Chem. B*, 108, 3963-3966 (2004).

[MacBeath 1999] Gavin MacBeath, Angela N. Koehler, Stuart L. Schreiber: Printing Samll Molecules as Microarrays and Detecting Protein-Ligand Interactions en Mass. *J. Am. Chem. Soc.*, 121, 7967-7968 (1999).

[McGall 1997] G. H. McGall, A. D. Barone, M. Diggelmann, S. P. A. Fodor, E. Gentalen, N. Ngo: The Efficiency of Light-Directed Synthesis of DNA Arrays on Glass Substrates, *J. Am.Chem.Soc.*, 119, 5081-5090 (1997).

[Min 2005]. S. Min, K. Ahn, J. Kim: Patterned Fluorescence Images Using a Photocleavable NVOC-Protected Quinizarin, *Bulletin of Korean Chemical Society*, 26, (9), 1437-1439 (2005).

[Oener 2000] D. Oener, T. J. McCarthy: Ultrahydrophobic Surfaces. Effects of Topography Length Scales on Wettability, *Langmuir* 16, 7777-7782 (2000).

[Olympus Web Resouce] http://www.olympusfluoview.com/theory/index.html

[Ottl 1998] J. Ottl, D. Gabriel, G. Marriott: Preparation and Photoactivation of Caged Fluorophores and Caged Proteins Using a New Class of Heterobifunctional, Photocleavable Cross-Linking Reagents, *Bioconjugate Chemistry*, 9, 143-151 (1998).

[Pillai 1980] V. N. R. Pillai: Photoremovable Protecting Groups in Organic Synthesis, *Synthesis*, 1, 1-26 (1980).

[Ramrus 2004] D. A. Ramrus, J. C. Berg: Characterization and Adhesion Testing of Mixed Silane-treated Surface, *J. Adhesion Sci. Technol.*, 18, 1395-1414 (2004).

[Sheehan 1964] J. C. Sheehan, R. M.Wilson: Photolysis of Desyl Compounds. A New Photolytic Cyclization, *J. Am. Chem. Soc.*, 86, 5277-5281 (1964).

[Sheehan 1971] J. C. Sheehan, R. M. Wilson, A. W. Oxford: The Photolysis of Methoxy-Substituted Benzoin Esters. A Photosensitive Protecting Group for Carboxylic Acids, *J. Am. Chem. Soc.*, 93, 7222-7228 (1971).

[Stenger 1992] D. Stenger, J. H. Georger, C. S. Dulcey, J. J. Hickman, A. S. Rudolph, T. B. Nielsen, S. M. McCort, J. M. Calvert: Coplanar Molecular Assemblies of Amino- and Perfluorinated Alkylsilanes: Characterization and Geometric Definition of Mammalian Cell Adhesion and Growth, *J. Am. Chem. Soc.*, 114, 8435-8442 (1992).

[Stowell 1996] M. Stowell, R. S. Rock, D. C. Rees, S. I. Chan, A. A. Noyes: Efficient Synthesis of Photolabile Alkoxy Benzoin Protecting Groups, *Tetrahedron Lett.*, 37, 307-310 (1996).

[Tadmor 2004] R. Tadmor: Line Energy and the Relation between Advancing, Receding, and Young Contact Angles, *Langmuir* 20, 7659-7664 (2004).

[Taniguchi 1974] N. Taniguchi: On the Basic Concept of Nano-Technology, Proc. Intl. Conf. Prod. Eng. Tokyo, Part II, Japan Society of Precision Engineering, 1974.

[Tieke 2001] B. Tieke, K.-F. Fulda, A. Kampes, Mono- and Multilayers of Spherical Polymer Particles Prepared by Langmuir-Blodgett and Self-Assembly Techniques. In M. Rosoff (eds.), Nano-Surface Chemistry, pp. 213-242. Marcl Dekker, New York (2001).

[Ulman 1991] A. Ulman, A Introduction to Ultrathin Organic Films from Langmuir-Blodgett to Self-Assembly, Academic Press, London, UK (1991).

[Vossmeyer 1997] T. Vossmeyer, E. DeIonno, J. R. Heat: Light-Directed Assembly of Nanoparticles, *Angew. Chem. Int. Ed. Engl.*, 36, 1080-1084 (1997).

[Vossmeyer 1998] T. Vossmeyer, S. Jia, E. DeIonno, M. R. Diehl, S. H. Kim, X. Peng, A. P. Alivisatos, J. R.Heath: Combinatorial Approaches Toward Patterning Nanocrystals, *J. Appl. Phy.* 84, 3664-3670 (1998).

[Whitesides 2001] G. M. Whitesides, J. C. Love, "The Art of Building Small", Scientific American 285, 38-47(2001).

[Wilhelm 1998] S. Wilhelm, B. Groeber, M. Gluch, H. Heinz, "Confocal Laser Scanning Microscopy: Principles", Internet article, www.zeiss.de, Carl Zeiss Jena (1998).

[Wojtyk 2002] J. T. C. Wojtyk, K. A. Morin, R. Boukherroub, D. D. M. Wayner: Modification of Porous Silicon Surfaces with Activated Ester Monolayers. *Langmuir*, 18, 6081-6087 (2002).

[Xia 1998] Y. Xia, G. M. Whitesides: Soft Lithography, *Angew. Chem. Int. Ed. Engl.*, 37, 550-575 (1998).

[Xia 1999] Y. Xia, J. A. Rogers, K. E. Paul, G. M. Whitesides: Unconventional Methods for Fabricating and Patterning Nanostructures, *Chem. Rev.*, 99, 1823-1848 (1999).

[Xia 2000] Y. Xia, B.Gates, Y. Yin, Y. Lu: Monodispersed Colloidal Spheres: Old Materials with New Applications, *Adv. Mater.*, 12, 693-713 (2000).

[Zhuravlev 1987] L. T. Zhuravlev: Concentration of Hydroxyl Groups on the Surface of Amorphous Silicas, *Langmuir*, 3, 316-318 (1987).

Curriculum Vitae

Xiaosong Li

Personal Details:

Date of Birth: 15-02-1979

Place of Birth: Peking, China

Nationality: China

University Education:

01/2005-01/2008	Ph.D. Studies
	Max Planck Institute for Polymer Research &
	Johannes Gutenberg-University of Mainz
03/2003-12/2004	Master of Science
	Max Planck Institute for Polymer Research &
	Johannes Gutenberg-University of Mainz
09/1997-07/2001	Bachelor of Science
	Peking University

School Education:

09/1994-07/1997	Beijing No. 22 Middle School (Senior High School)
09/1991-07/1994	Beijing No. 22 Middle School (Junior High School)
09/1985-07/1991	Beijing He-Ping-Li No. 9 Elementary School